3D air-liquid interface culture of Cystic Fibrosis bronchial epithelia, macrophages and *P. aeruginosa* to assess host-pathogen interaction and drug efficacy

Dissertation

zur Erlangung des Grades

des Doktors der Naturwissenschaften

der Naturwissenschaftlich-Technischen Fakultät

der Universität des Saarlandes

from

Carlos Victor Montefusco Pereira

Saarbrucken

2020

Tag des Kolloquiums:	14.07.2020
Dekan:	Prof. Dr. Guido Kickelbick
Berichterstatter	Prof. Dr. Claus-Michael Lehr
	Prof. Dr. Rolf W. Hartmann
Vorsitz:	Prof. Dr. Marc Schneider
Akad. Mitarbeiter:	Dr. Jessica Hoppstädter

"If you can't love yourself,

how the hell you're gonna love somebody else?"

RuPaul Charles, Drag Queen Diva

"七転び八起き"

Japanese proverb

Table of Contents

Abstract

To establish a predictive human infected *in vitro* system for Cystic fibrosis (CF) lung infection, we set-up a *P. aeruginosa*-infected model at the air-liquid interface (ALI), constituted by the human cystic fibrosis bronchial epithelial cells (CFBE41o⁻) in the apical side of a transwell and human macrophages (THP-1) in the basolateral side.

Planktonic *P. aeruginosa* infection of CFBE41o⁻ cells led to an earlier biofilm formation after 6 hours. Macrophages migrated towards the infection side, on the apical compartment already after 3 hours of infection, and were able to internalize the bacteria. Upon tobramycin treatment, the bacterial killing was higher on an abiotic surface (plastic plates) than on cell surface, which suggests an overestimation of the drug efficacy in cell-free assays.

Perspectively, this model can be used to further investigate the immune system. Here, we present the characterization of a neutrophil-like cell, HL-60, and its potential to be a platform to use neutrophils as delivery methods of internalized nanoparticle therapy. Aiming for therapy, we assessed the potential of quaternary ammonium surfactant-liposomes to inhibit bacterial adherence. That was the first step to develop a particle to simultaneously inhibit adhesion and provide encapsulation of antibiotic drugs as combination drug delivery.

Zusammenfassung

Um ein prediktives infiziertes humanes in-vitro System für eine Lungeninfektion im Rahmen einer ZF zu etablieren, haben wir ein mit *P. aeruginosa* infiziertes Modell, welches über eine Grenzfläche Luft/Flüssigkeit verfügt, erstellt. Dieses Modell besteht aus humanen zystisch-fibrotischen Bronchalepithelzellen (CFBE41o⁻) auf der apikalen Seite und humanen Makrophagen (THP-1) auf der basolateralen Seite.

Die Infektion von CFBE41o⁻ Zellen mit planktonischen *P. aeruginosa* führte nach 6 Stunden zu einer früheren Biofilmentwicklung. Makrophagen migrierten bereits nach 3 Stunden zur infizierten Seite und waren, Bakterien in sich aufzunehmen. Bei der Behandlung mit Tobramycin fand eine stärkere Abtötung auf einer abiotischen Oberfläche statt als auf einer Zelloberfläche, was eine Überschätzung der Wirkstoffeffektivität bei zellfreien Tests nahelegt.

Hierbei stellen wir die Charakterisierung einer Neutrophilen-ähnlichen Zelle, HL-60, vor sowie deren Potential als Platform zu dienen, an dem Arzneistofftransportmethoden der internalisierten Nanopartikeltherapie getestet werden können. Wir haben die Fähigkeit von quartäre oberflächenaktive Ammoniumverbindung-Liposomen, bakerielle Anhaftung zu verhindern, untersucht. Dies war der erste Schritt bei der Entwicklung eines Partikels, das die Adhäsion hemmt und gleichzeitig dazu dienen kann, mit Antibiotika - im Sinne eines kombinierten Arzneistofftransports – beladen zu werden.

Chapter 1: Establishment of CFBE41o- and THP-1 infected co-culture

1. Introduction

1.1. Respiratory system

The respiratory tree branches out into several bifurcations directly from the trachea. Although the trachea does not take part in gas exchange, it is from the trachea that the bronchi start with two branches that are followed by the bronchial and bronchiolar bifurcations. Those branches will progressively decrease to give rise to peripheral branches and the alveolar region. In there, the alveoli are the main stations responsible for the gas exchange.[1]

The lung and the respiratory branches are protected by an epithelial barrier that has important roles like i) avoids insults, ii) can self-repair and modulate airways response, and iii) release defensive fluids as the mucus, surfactant and lining fluid that contains antimicrobial peptides.[2]

Among the epithelial cells, fifty cell types compose the respiratory system with unique functions, according to its location. The lower airways include the bronchial region, and it is composed by a pseudo-stratified epithelium of columnar cell to secretory goblet cells, basal and ciliated cells that are important on the mucociliary clearance mechanism; while cuboid and Clara cells are the ones located at the terminal bronchioles. The deep lung or distal airways are composed of type I and II alveolar cells. Moreover, macrophages are the first-encounter immune cells that can be located on top of the alveolar epithelium or in between the layers of the bronchial airways as interstitial macrophages.[3]

1.1.1. Airways epithelium

The airway epithelium is the main biological barrier of the lung and is responsible for the strategies around mucociliary clearance, the maintenance of levels in ion content and

surface fluid, plus the release of mucus containing anti-inflammatory, antiinfectives and antioxidant defenses.[4]

However, the airway cellular structure provides a line of defense itself that is promoted by cell-to-cell connections as a barrier (Figure 1). When this barrier faces challenges, like the exposure to allergens or microbes, it becomes compromised, resulting in cytotoxicity and inflammation[5].
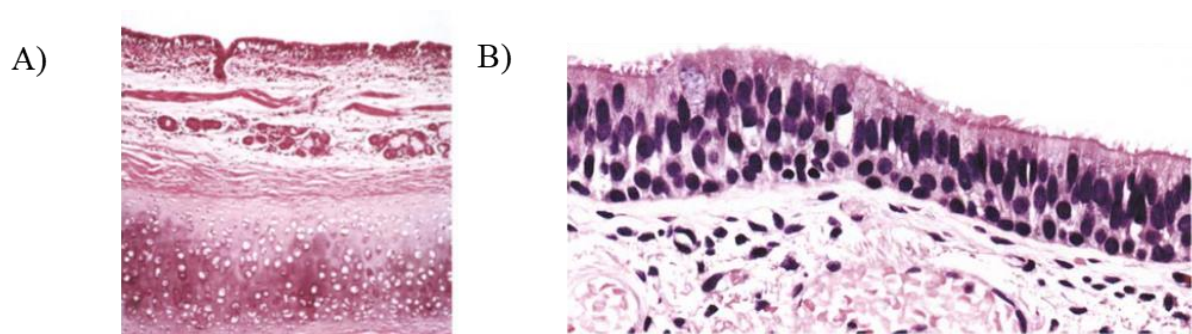
Figure 1. Light micrographs of bronchial airways histology. A) Low magnification of the bronchial wall for orientation. B) bronchial mucosa showing the ciliated cells, rare goblet cells, and basal bronchial cells resting on a thin basement membrane. Adapted with permission from [6].

The integrity of the epithelial barrier is promoted by the tight junctions proteins (claudins, occludin, zona occludens-1, E-cadherins), and it separates the transport of molecules, particles, and other cells in compartments: the apical and basolateral[7]. These proteins are master regulators of the molecules' flow, including the maintenance of the surface lining fluid and the release of antimicrobial molecules. The epithelial barrier is also the entrance point of control for inhaled microbes towards the bloodstream, so its integrity is a demanded line of defense.[8]

Alterations as cell damage, cell lesions, loss of permeability, cell reprogramming are main consequences from pathological modifications caused by diseases as lung cancer,

COPD, or cystic fibrosis.[9] Such alterations can be either triggered or worsened by the inhalation of particulates as environmental pollutants and microbes[10].

The above mentioned-lung alterations raise the need for suitable models in which such modifications could be emulated. For instance, the development of the model towards the features of how regeneration, pathology, lung exacerbation, and therapeutics pose the strategies to avoid or treat insults to the lung. While animal models have significantly been used to study CF disease, they fail to reproduce the spontaneous CF lung disease, most likely due to inter-species differences [11,12].

1.1.2. Models of the human lung

To be instrumental for the comprehension of alterations during the developed or diseased lung, animal models are a valid option. When functional studies were performed towards molecular lung alterations, animal models present a different outcome when comparing genetic gain- and loss-of-function, mostly due to differences as i) fast development of the mouse lung with increased branching of the airways tree before the actual development of the alveoli, ii) development of alveoli only post-birth and iii) residence of progenitor cells different to humans. These, among others, represent a failure in recapitulating the human lung.[13]

When mimicking disease, lung injuries on rodents can trigger fibrosis and emphysema, an advantage for uncovering the complex mechanisms of these diseases[14]. Also, entire processes involving the physiology of branch morphogenesis can be studied with the mice arborized tree[15]. Nonetheless, on preclinical tests using animal models, most new molecules are effective, and about 80% of the approved molecules end up as false positives when translated to human clinical trials[16]. Therefore suitable human *in vitro* models are needed for a better prediction of drug efficacy. Moreover, *in vitro* models can provide

screening platforms of large-scale, assessment of specific cell-to-cell molecular differences and the opportunities to understand lung disorders while, at the same time, offer personalized medicine[13].

Ex vivo models are remarkably useful in the sense that one uses part of the whole lung, in which it can be reconnected for artificial input (drugs, particles, pathogens) to increase the model complexity; alternatively, slices of the lung can be cultivated[17]. These approaches preserve not only the *in vivo* architecture but also the cell types enclosed to it. In fact, models as the embryonic chicken trachea had shown independent of particle size or shape, the activity of mucociliary clearance is still effective. Alternatively, models as the porcine lung show a spatial availability very close to the human lung. [18]

Sakagami[17] reviewed different lung models towards the testing of inhaled drugs and addresses the choice of model is intrinsic to the scientific question. On the modeling of complex interaction from a living organism, the *in vivo* model will provide the level of complexity; however, to address the lung barrier or cell interaction with other cells or particles or pathogens the *in vitro* model might be a better choice for studying this interplay.

Direct cultivation of cells from the trachea, bronchi, and alveoli is possible with the advances in cell culture and the access to primary cells. However, the approximate cultivation of primary cells needs to mimic the lung environment, including the air-to-lung interface[19]. In fact, the use of cultures at the air-liquid interface (ALI) on permeable membranes is a valid and commonly used method in respiratory research. This is validated with the profiling of mRNA expression of cultures in ALI versus direct human airways derived from bronchoscopy or bronchial brushing.[19]

From the sampling of human lungs, recent progress has allowed the expansion of patient-specific cells on the development of inducible pluripotent stem cells (iPSC)[20]. This

cellular model brings the opportunity for a full genetic background related to disease, in which personalized medicine and research on gene targets and repair can be used, including mutations derived from cystic fibrosis.[21] Nonetheless, to create iPSC, one needs a batch of samples obtained from different patients and this individuality could result in increased differences regarding age, sex, disease severity and other pathophysiological variables.[22]

By providing a three-dimensional environment, cells will take this as biological cues to behave as an *in vivo* scenario, including in modes of self-assembly. For that, bronchial cells, lung fibroblasts or endothelial cells can be cultivated as airway organoids.[23] 3D models can, for instance, i) make use of extracellular matrix, ii) generate bronchospheres, and ii) establish bronchial cells with fibroblasts to stimulate plasticity with proximal cell interaction and microenvironment of a co-culture. This evolution is represented in fig. 2 from monolayers to the use of microfluidic chips to show influence of shear stress.
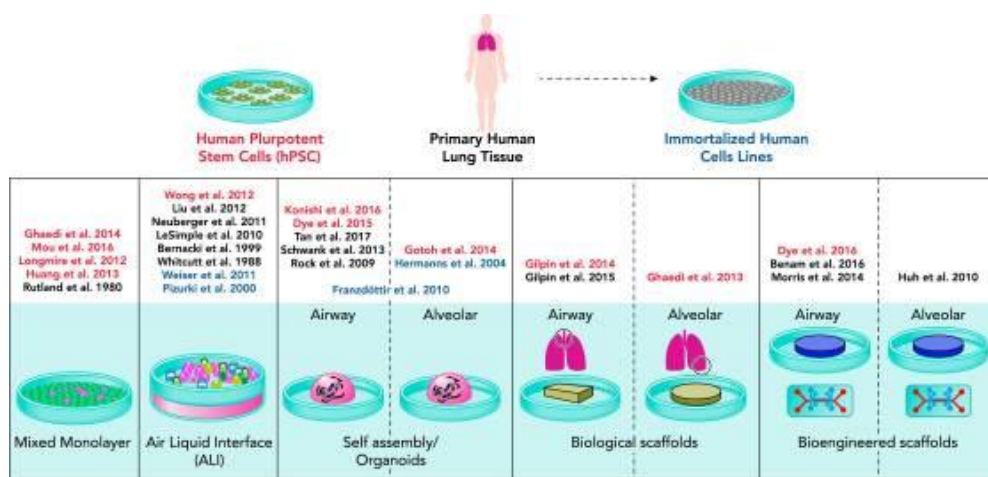
Figure 2. Evolution of *in vitro* models of the human lung. Adapted with permission from [13.]

Although primary cell culture is available, it is more demanding and expensive than expected, so, the use of immortalized cell lines has prevailed. Those cells derived from well-defined diseases or from specific parts of the lung bring the stability of infinite proliferation

with the advantages to preserve cell morphology and functionality. Some of the most recent

models recapitulate the lung with cell lines or the combination of those, as shown in figure 3.

Figure 3. Lung constructs of the human bronchial epithelium. Calu-3: human airway epithelial cells, representative of airway submucosal glands; 16HBE14o−: human bronchial epithelial cell line; NHBE: primary

Cell model	Derivation	Pros	Cons	Micrographs
Calu-3	Carcinoma of the bronchus	Immortalised Form confluent mono-layers Develop Cilia Express mucin genes	Variation in tight junction (TJ) formation	
BEAS-2B	Transformed bronchial epithelium	Immortalised Form confluent mono-layers Secrete cytokines Express antioxidants	No mucin secretion Lack TJs	
16HBE14o−	Transformed bronchial epithelium	Immortalised Differentiated & multi-layered Develop cilia & microvilli Secrete cytokines	No mucin secretion	
NHBE	Normal human bronchial epithelium (primary cells)	Long lifespan & not transformed Differentiated & multi-layered Form cilia, TJs, secrete mucus Serum-free medium	Not immortal Labour intensive	
aMatTek Epiairway™	Human tracheal/bronchial epithelium (primary cells)	Long lifespan & not transformed Differentiated & multi-layered Form cilia, TJs, secrete mucus Serum-free medium	Not immortal Cost to purchase	
aEpithelix MucilAir™	Human respiratory tract (primary cells)	Long lifespan & not transformed Differentiated & multi-layered Form cilia, TJs, secrete mucus Serum-free medium	Not immortal Cost to purchase	
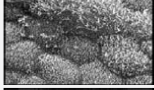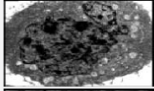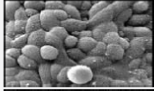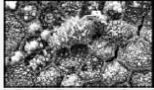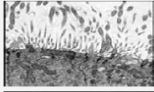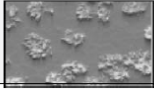
human bronchial epithelial cells; BEAS-2B: human bronchial epithelial cell line. Reproduced with permission from [3]

On a transwell system or on a chip, advanced models as co-cultures have successfully

mimicked the interaction of lung cells, as shown in figure 4. The airway epithelium,

bronchial or alveolar, is always present as the main barrier, which can be complemented by

other cellular components like immune cells. To mention a few, the combination of bronchial

cells/fibroblasts, endothelia/eosinophils, bronchial cells/alveolar macrophages is already

reported. Even commercialized models as MucilAir™ with immune cells can provide the

reliability to understand pathology, inflammation, and host response (as for instance,

mucociliary clearance).[24]

Epithelial cells	Combined cell type	Experimental setup/characteristics
A549	MDM (MDDC)	Polystyrene particle interaction; cells grown on Transwell® filter
16HBE14o−	HUVEC	Barrier properties; cells grown on Transwell® filter
A549/NCI-H441	HPMEC	Barrier properties; cells grown on Transwell® filter
NCI-H441	ISO-HAS-1	Toxicity of cadmium exposition; pro-inflammatory markers and TEER; cells grown on Transwell® filter
NCI-H441	ISO-HAS-1	Cytotoxicity, inflammatory response and investigation of apoptosis markers
NCI-H441	HPMEC or ISO-HAS-1	Study adsorption, uptake and trafficking of novel nanosized carriers under different physiological conditions; cells grown on Transwell® filter
HBECs	Monocytes	Cytokine release after rhinovirus infection
Calu-3 or A549	Peripheral blood mononuclear cells	Regulation of inflammatory pathway
16HBE14o−	MDM and MDDC	Barrier properties and particle uptake; cells grown on Transwell® filter
Primary AT I	MDM and MDDC	Primary *in vitro* models for transport studies; cells grown on Transwell® filters
16HBE14o− or A549	MDM and MDDC	Particle uptake and inflammatory responses; cells grown on Transwell® filter
A549	MDM and MDDC	Particle uptake and inflammatory responses; cells grown on cell culture inserts
A549	HFL-1	Toxicity of cigarette smoke extract
A549	Human lung fibroblasts	Squamous metaplasia (SM) and airway obstruction; cells grown on Transwell® filter
A549	Human lung fibroblasts	Toxicity of cigarette smoke extract
HBECs and 16HBE14o−	Wi-38	Cellular differentiation, cytokine stimulation and barrier properties
A549 and endothelial cells (EAHY926)	THP-1 and HMC-1	Evaluation of the interaction and contributions of different cell types; response to particles, cytokine release; cells grown on Transwell® filter
A549 and endothelial cells (EA.hy 926)	THP-1 and HMC-1	Alveolar barrier and properties and particle toxicity; cells grown on Transwell® filter
A549, NCI-H441 or E10	HMVEC-	Particle uptake, toxicity and inflammatory responses, infection; cells grown on a "chip"

Figure 4. Examples and applications of advanced lung co-culture models. A549: human alveolar type II cell; MDM: human blood monocyte-derived macrophages; MDDC: human blood monocyte-derived dendritic cells; 16HBE14o−: human bronchial epithelial cell line; HUVEC: human umbilical vein endothelial cells; Wi-38: human lung fibroblast cells line; NCI-H441: human lung adenocarcinoma cell line; HPMEC: primary human pulmonary microvascular endothelial cells; ISO-HAS-1: human hemangiosarcoma cell line, HBECs: primary human bronchial epithelial cells; Calu-3: human airway epithelial cells, representative of airway submucosal glands; HFL-1: human fetal lung fibroblasts; EA.hy 926: human umbilical vein cells; THP1: human monocytic cell line; HMC-1: human mast cell line; E10: nontumorigenic alveolar type II cells; HMVEC-L: human pulmonary microvascular endothelial cells.[25]

From the efficiency of particle/drug delivery to the toxicity of this material, a triple co-culture of alveoli, macrophages, and dendritic cells provide better information on toxicological reactions to therapy.[26] The access to cells can be mimicked on co-cultures producing an alveolar-capillary barrier and acknowledging the intensity of toxicity derived from materials as silica nanoparticles.[27]

On that note, the access of nanoparticle formulation can take a different view, since the co-culture cell interaction can show an increased expression of tight junction (versus monoculture). With this, Chowdhury *et al.*[28] observed increased mRNA of Occludin once bronchial epithelial and endothelial cells are cultured together. Even without immune cells, the advantages of co-culture can reflect how particle influence inflammation. A co-culture of alveolar epithelia with pulmonary endothelial shows increased barrier but also increased IL-6 and IL-8 during the exposure to the environmental pollutant, cadmium (Cd^{2+}).[29]

1.2. Lung Cystic fibrosis

Cystic Fibrosis (CF) is a genetic autosomal recessive disorder caused by mutations in the cystic fibrosis transmembrane conductance regulator (CFTR), an ABC ion channel transporter of chloride regulated via cyclic amp (cAMP). This disease is followed by cardinal traits affecting organs like pancreas, liver, intestine, and the lungs with significant airway obstruction and *P. aeruginosa* infection.[30]

Mutations in the CFTR or Cystic Fibrosis transmembrane conductance regulator can impair the transport of chloride and water transport on epithelial cells, especially in the lungs; such conditions make CF a genetic, life-threating disease[31]. F508del is the predominant mutation (70% patients) from the 5 mutation classes of CF, and it brings translational alteration issues to this receptor protein. By removing a single amino acid on CFTR, it does not allow the protein to maintain its 3D shape, which triggers the cell's mechanisms of error

and disposal of this protein[32]. The mutations are defined as classes in which I) no CFTR synthesis, II) process blockage of CFTR, III) regulation blockage of CFTR, IV) differential CFTR conductance, and V) reduced CFTR production[33].

Chloride and combined sodium hyper-absorption in the airway surface liquid alters mucus viscosity, allowing more adherence to the epithelial layer that consequently stops the regular ciliary function[34]. This results in bacteria not being cleared, adhering to thick mucus, and indirectly on the epithelia, settling persistent infections. Those infections will then trigger inflammation and immune response to be excessive, leading to tissue damage [35].

The molecular role of CFTR impairment is still to be confirmed, and mechanisms to explain the alterations are being investigated. Smith *et al*[36] observed CF lung epithelia does not secrete antibacterial components anymore. Instead, the antibacterial activity was only recovered by the supplementation with sodium chloride. This created a high salt hypothesis in which the impairment of CFTR in controlling ion affects salt levels, and this would decrease the activity of defensins, natural antimicrobial peptides.

The low volume hypothesis comprises sodium flow and inhibition of the epithelial sodium channel (ENaC)[37] by CFTR mutations. This consequently alters the flow of chloride ions with resulting surface dehydration and thickening of mucus[38]. The last explanation of the role of CFTR involves the cultivation of airways gland cells. Those cells release specific secretions containing antimicrobial proteins; however, the production of this secretion only occurs when CFTR is well-functioning[39].

1.2.1. Interactions with the immune system: inflammation versus infection

When a pathogen enters the respiratory tract, there is the airway epithelium with a tight cell-to-cell barrier and the presence of mucus/lining fluid with antimicrobials. At the

basis of this defense, the epithelium detects the presence of foreign DNA with Toll-like receptors, pattern recognition receptors, etc[40].

The first checkpoints of microbes are a subset of immune cells but also dendritic cells and alveolar macrophages[41]. An array of lipid mediators and chemokines start the recruitment of effector immune cells. In this communication, CXC chemokines and cytokines (IL-1α and IL-1β, IL-10, IL-17, IL-23, IL-25, IL-33, and thymic stromal lymphopoietin) control the regulation of inflammation[42].

Dendritic cells (DCs) and macrophages can engulf bacteria via interferon-γ, but those cells will also present antigens to start activation of T lymphocytes (CD4$^+$ and CD8$^+$) and release cytokines (for instance, IL-6) to mature B lymphocytes, integrating the adaptive immune system[43].

The regulation of inflammation is tightly attached to context and time. Similarly, enzymes like neutrophil elastase or MMP can destroy bacterial proteins, but its excess can degrade the extracellular matrix and harm the lung tissue[44]. In respiratory diseases, it is common that immune cells fail to resolve infection leading to chronic state and excessive inflammation, as in the cases of cystic fibrosis and COPD[45].

The main issues the CF patient has to deal with are:

- Defective CFTR leading in impairment of water and chloride transport,[46]

- thickening of mucus with abnormal elasticity[47],

- airways blockage[48],

- slowing towards ineffective mucociliary clearance,

- inactivation of antimicrobial molecules on mucus/surface lining fluid[49] and

- opportunistic bacterial and fungal infections that evolute to biofilm formation[50].

In consequence, these manifestations will alter host immunity, especially the innate immune system. This exposure to pathogenic organisms demands a warning system, but a system that acknowledges what a threat is and how much response is required before inducting tissue destruction. For that, the pathogen-associated molecular patterns (PAMPs) are the critical signals for microbes to be recognized as foreign. From that concept, the family of Toll-like receptors started to be uncovered as the first stage on using microbe patterns, bind to those and initiate the response.[51]

CFTR coordinates the functionality of the nuclear factor kappa-light-chain-enhancer of activated B cells (NF-κB), and its lack of regulation will lead to an increase in IL-8 in the consequent neutrophil invasion, lung injury and allow for bacteria development into biofilms (see figure 5). Because of one of the primary mutations in CF, CFTR does not transcend to the cell membrane and to its lipid rafts, where it starts the control of inflammation via NF-κB. [52]
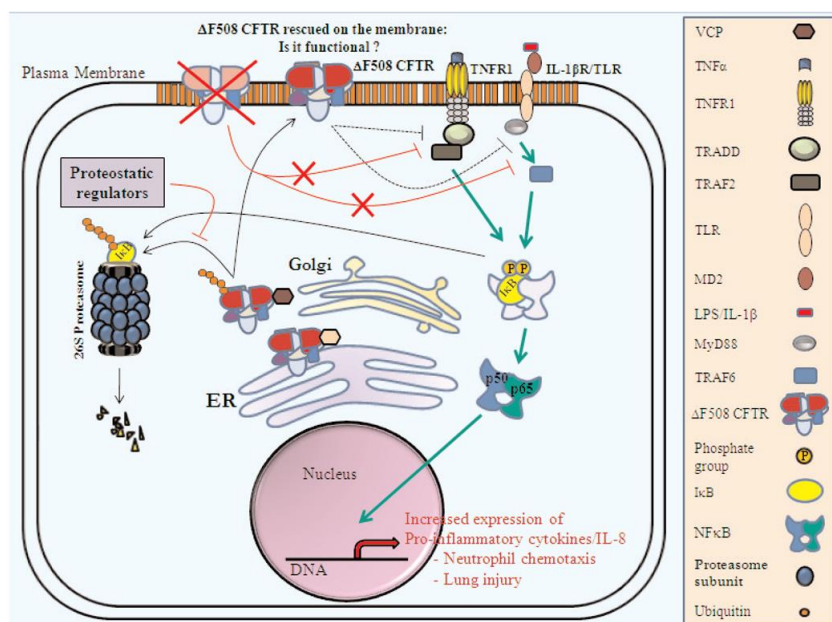
Figure 5. Impairment of CFTR functionality provokes inflammation triggering excessive inflammation. Reproduced with permission from [52].

If inflammation is not controlled during CF mutations of CFTR, the molecular events must be uncovered. For immune cells, when facing an antigen, there is either direct uptake or extraction of some of the antigen components. The outer core oligosaccharide of the lipopolysaccharide (LPS) in the outer membrane of *Pseudomonas aeruginosa* initiates an immune response, and its endocytosis leads to NF-κB translocation. On the lung epithelium, CFTR is a non-classical site for attern recognition molecules to extract and internalize LPS. This regulation is wholly altered during the failure to produce a complete and translocated CFTR.[53]

If CFTR recognizes *P. aeruginosa*, it starts the production of other signals as IL-1β, so alterations of this receptor, as in CF, can bring dysregulation also of this main cytokine. This cytokine influences transcription factor as MyD88 and, once more, NF-κB. Polymorphisms on this cytokine's gene have been associated with loss of control of inflammation and lung disease severity in CF patients[54].

If the release of cytokines is disrupted during CF, the recruitment of immune cells is also influenced. CFTR in primary monocytes was shown to increase calcium on levels that would alter gene expression, and for that, in the view that neutrophils, macrophages, and T cells are recruited, there is a reduction in the activation of those immune cells.[55] One of the main consequences of this inactivation is also leading to influence on cell homeostasis in which the production of glutathione is decreased (the main issue on the control of reactive oxygen species)[56] and on the increase of prostaglandins[57]. Finally, incomplete CFTR culminates on hyper inflammation that will be worsened by chronic infection, summarized in figure 6.
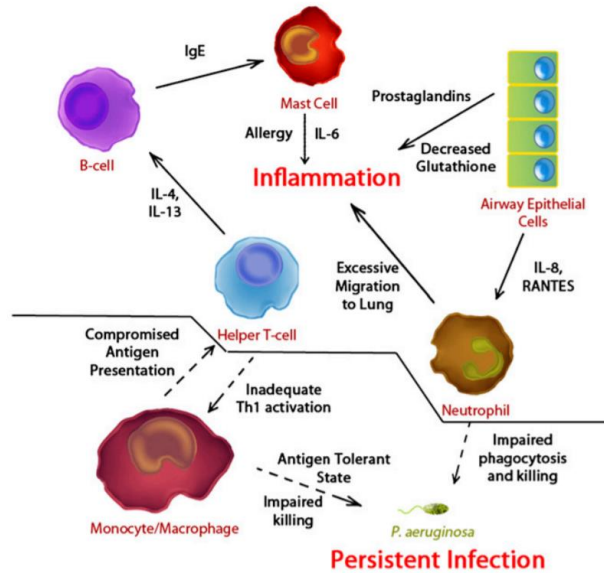
Figure 6. Alterations of the immune system due to mutant CFTR. Reproduced from [55].

1.2.2. Predominant infections in cystic fibrosis

The CFTR alterations result in the formation of obstructive airway plugs and impaired cilia beating. Those alterations over time create a new lung microenvironment, one that fosters the infection by *S. aureus,* followed by *P. aeruginosa.* [58]

Age does influence the type of infection, and microbiological identification methods like agar plating are not enough to distinguish the infection. For that, studies on the CF lung microbiome are progressively seen as more suitable. Fig. 7 shows the 16S microbiome results of one patient along a decade of CF, with infection and antibiotic exposure[59]. This extends CF infections to be dominated by *P. aeruginosa*, but never exclusive of it. It includes *Haemophilus influenzae* (a cause of exacerbations in children), *Burkholderia cepacia*, *Stenotrophomonas maltophilia* and non-pathogenic bacteria as *Prevotella sp*.
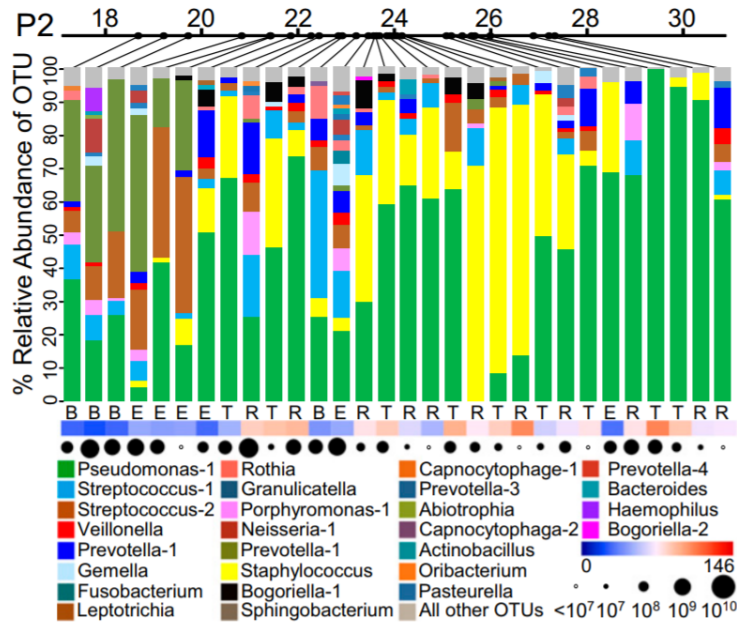
Figure 7. The bacterial community of a cystic fibrosis patient along one decade. 16S microbiome from 18 to 28 years of age showing the abundance of operational taxonomic units (OTUs) with a scale of BETR (baseline, exacerbation, treatment, recovering) and heat map of the antibiotic load. Reproduced from [59]

As observed, the CF lung is colonized by many microbes and the airways epithelial cells are infected continuously by bacteria, viruses, fungi, and virulence factors. Those organisms become part of the lung, forming an ecological community of natural microbes, the microbiome[60]. From the beginning with real-time polymerase chain reactions, passing by pyrosequencing and mRNA sequencing, the methods to define the microbiome have changed, and with those, it is possible to advance the stratification and understanding of healthy and diseased patients (along time, along with treatment, along with exposure, etc.)[61]

Already in asthma and COPD, the lung microbiome presents insights into the mechanisms along with disease progression, and this can be further investigated with *in vivo* models of, for instance, the influence of other microbes on allergen tolerance.[62] For CF, the lung microbiome brings the complexity of the polymicrobial infection that has altered the way we understand infection, and for that, we can observe this dynamics[63]. The airways might maintain its homeostasis precisely because of its interaction with the microbiome, including in properties as barrier formation; counting with the note that all inhaled particle

and microbes are fastly uptaken to be killed, but also, in the end, to stimulate and build the memory of our immune system. [64]

1.3. *Pseudomonas aeruginosa* lung infection

Pseudomonas aeruginosa is an opportunistic and ubiquitous Gram-negative bacillus colonizing multiple environmental niches, but acute infection comes with fragile immune response, for instance, in patients from intensive care units. Nonetheless, it is the chronical bacterial lung infection that accounts for the majority of the morbidity and mortality seen in the disease. This state is governed by the production of polysaccharide as alginate and mucoid exopolysaccharide leading to bacterial adherence to host cells and in evasion of the host immune response.[65]

The alterations derived from CFTR mutations bring severe issues for the respiratory system, but it is the infection with *P. aeruginosa* that worsens the clinical symptoms. With that, respiratory failure occurs in 80% of CF patients because of the chronicity and disease evolution.[66]

Gene expression and the virulence factors of *P. aeruginosa* are the needed machinery for this bacterium to adapt[67], and as seen in figure 8, there are many tools to influence the host and improvement the microenvironment for better bacterial adherence and survival.
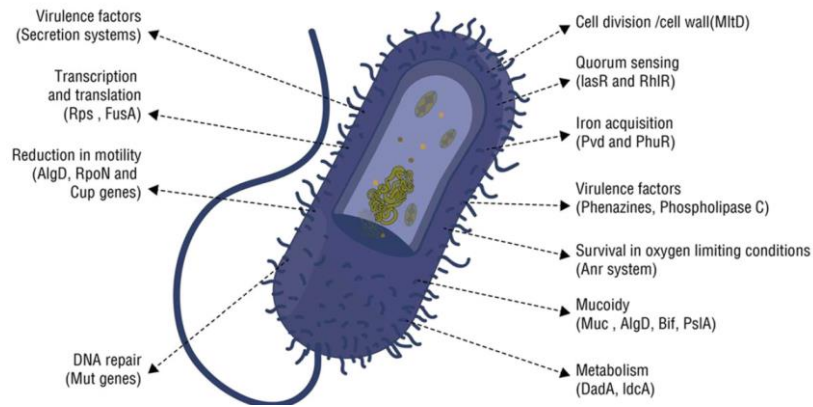
Figure 8. *P. aeruginosa* has an array of strategies fights against host defenses to promote bacterial adaptation, including these virulence factors. Reproduced from [58]

P. aeruginosa infection demands several factors for bacterial adaptation, but to reach chronic disease some changes are required as: gene exchange for antibiotic resistance, slowing metabolism with consequent decreased growth, restrain of motility with adherence on the epithelial layer, hinder of bacterium communication (quorum-sensing) and production of its own matrix, based on alginate.[68]

The fluctuations in gene expression are required to promote the transition from planktonic to biofilm[69]. For that, the network or kinases are regulators of this transition when the RetS-Gac-RsmA system regulates the interaction with the host (by coordinating the release of toxins from the type III secretion system (TTSS) and the production of the extracellular polysaccharide matrix, producing *P. aeruginosa*-specific polymers *psl* and *pel*, leading to the pellicles, or bacterial aggregates in air-liquid interface.[70] Studies on the chemical nature of those systems can bring an understanding of how to control this transition.

Not always, *P. aeruginosa* succeeds in establishing an infection in humans because the pressure from our immune system can be sufficient; however, this pressure can activate the expression profile of hyper-mutator strains. Because of the establishment of infection, neutrophils, for instance, release oxidative stress, via ROS or reactive nitrogens. This is a

valid strategy to alter bacterial lipids, but for the surviving bacteria, those variants are now selected to maintain guard facing the host challenges.[71]

When pressure from the host is on, regulation of virulence and motility is needed. For that, mutation on the *mucA* gene will produce mucoid strains or mutations on *psl,* and *pel* will creat small-colony variants; moreover, the glycosylation of LPS will hinder recognition by immune cells or mutations on *lasR* and homoserine lactone system will stop production of elastase, pyocyanin and etc[72–75].

Our immediate reaction to infections is antibiotic treatment, and this does create another pressure for bacterial killing. However, the resistance to antibiotic therapy is a known trait for *P. aeruginosa*[68]. In reports, systems as MuxABC-OpmB are essential genes on avoiding the efficacy of novobiocin, aztreonam, macrolides, and tetracycline, as well as MexXY efflux system on aminoglycoside efficacy[76,77]. Surprisingly, acquired antibiotic resistance is linked to mutations of regulatory genes from virulence functions in *P. aeruginosa*[76], which shows that heterogeneity is a must.

1.4. Current treatment for lung CF infections

People living with Cystic Fibrosis (CF) account for 70,000 worldwide[32] that require hospitalization and efforts on drug development toward pulmonary and nutritional therapies. In the pipeline of drug development, researchers have contributed to the restoration of CFTR function, mucociliary clearance, anti-inflammatories, anti-infective (including inhaled Tobramycin powder), and nutritional supplements. However, this same pipeline shows only 4 approved anti-infectives out of the 11 drugs on development[78]. Besides the approval of new drugs, the discovery of new antibiotics has suffered a decrease along decades and this is not only the case for Cystic Fibrosis.

Antimicrobial discovery had golden times in the 1960s with natural products from Actinomycetes in which we obtained tetracyclines, aminoglycosides, and other non-beta-lactams drugs[79]. Nonetheless, microbes have their resources to prevent drug penetration, and mainly, the development of resistance and resistance-acquiring mechanisms have dampened drug discovery. Still, the search for natural compounds has changed with the collaboration with genomic sciences: an evolution towards the detection of metabolites. Besides metabolomics, new screening methods have led to new compounds[80], showing only increased complexity brought further advantages.

With the advent of ESKAPE organisms (*Enterococcus*, *Staphylococcus aureus*, *Klebsiella* species, *Acinetobacter baumannii*, *Pseudomonas aeruginosa*, *Enterobacter*)[81], the resistance problem gets worsen by persister cells and biofilm formation allied with absent metabolism that is the main target of antibiotics. New research towards adjuvant drugs been developed on account of the understanding of virulence pathways with pathoblockers and quorum-sensing inhibitors being revealed[82].

On the treatment of CF lung disease, progress was made on innovation and drug delivery. On fig. 9A, the recommended antibiotics in CF therapy are currently commercialized in formulations focusing on pulmonary drug delivery. Through lung application, the drug can reach the site of infection, and thereby being more active against the bacteria while avoiding the development of bacterial resistance. On figure 9B, we observe that besides antibiotics, other options of treatment have been explored, either targeting bacterial biofilm, the excessive inflammation in the lungs, or the correction of CFTR defects. Nanotechnology offers the possibility to improve CF lung treatment, through the on drug protection/retention, the access to the core of biofilms, the uptake by the host cell and control of particle deposition. All those advantages are described in Figure 9C and aim to prevent antibiotic failure by delivery of new molecules.

A)

	Formulation	Product name	Drug	Development status
Pharmaceutical aerosols	Inhalation solution	Tobi®, Bramitob®	Tobramycin	Marketed
		Pulmozyme®	Dornase alfa	Marketed
		Aeroquin® (formerly MP-376)	Levofloxacin	Phase III (NCT01270347, NCT01180634)[a]
	Lyophilized powder for inhalation solution	Cayston®	Aztreonam lysine	Marketed
		Promixin®	Colistimethate sodium	Marketed
Dry powder for inhalations	Inhalable lipid particles (Pulmosphere™)	Tobi® Podhaler™	Tobramycin	Marketed
	Excipient-free spray-dried powders	Colobreathe®	Colistimethate sodium	Marketed
		Bronchitol®	Mannitol	Marketed

[a] Further information on the status of clinical trials can be found at http://clinicaltrials.gov.

B)

Type of therapy	Name of the therapy	Benefits of the therapy
Airway clearance therapy	Dornase-alfa	Breakdown of excess DNA in cell debris and mucous of chronically inflamed airways
	Nebulization of hypertonic saline	Increases airway hydration and mucociliary clearance
Antibiotics therapy	Tobramycin	Helpful in chronic stages of cystic fibrosis
	Aztreonam lysinate	Improves lung function and reduces incidences of pulmonary exacerbations
	Colistin (colistimethate sodium)	Improves lung function
Anti-Inflammatory therapy	Azithromycin	Macrolide antibiotic. Long term usage in CF reduces neutrophilic inflammation and pulmonary exacerbations. Improves lung function
	Ibuprofen	Reduces the decline in lung function. Especially effective in pediatric patients
Gene therapy	1.Zinc finger nucleases 2.Transcription activator –like effector nucleases (TALENs) 3.RNA guide engineered nucleases (derived from CRISPR)	These nucleases cleave the DNA at a specific site of interest and allow genomic modifications
CFTR modulation	1.Potentiators (VX-770, VX661 Ivacaftor, Lumacaftor, Riociguat, QBW251). 2.PTC therapeutics or ataluren	Aimed at correcting the dysfunction of CFTR like nonsense, frameshift, splice mutations and non-functional CFTR mutations.

C)
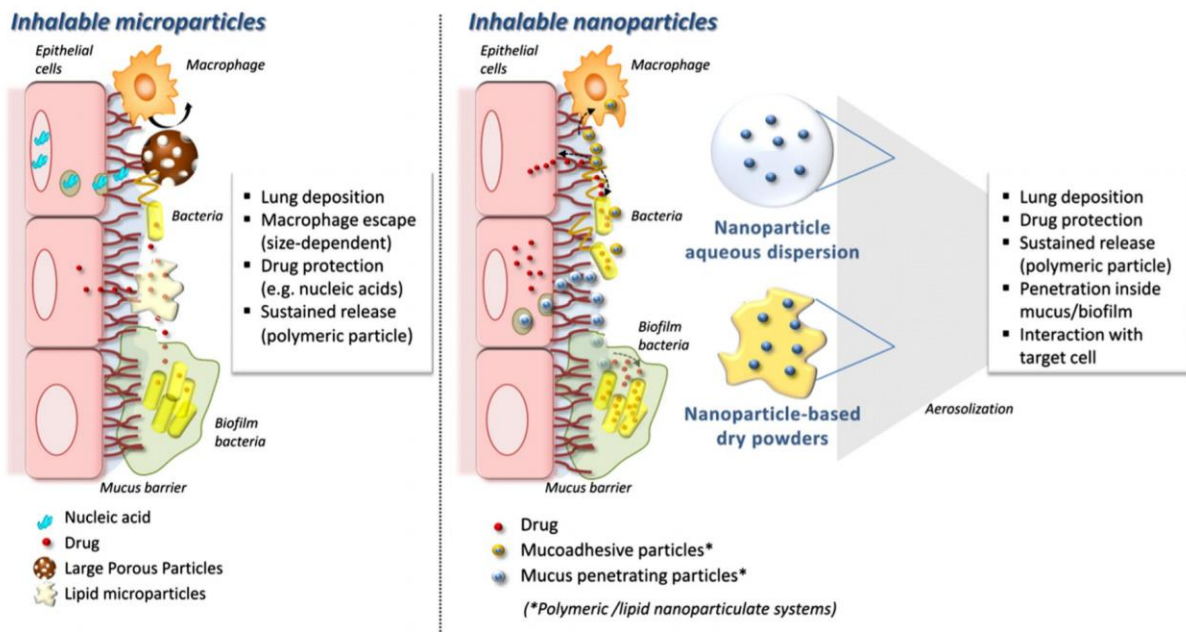
Figure 9. CF therapy: from inhaled antibiotics to CF correctors. A) Current commercially available inhaled antibiotic formulations. B) Summary of novel agents in the pipeline for CF treatment. C) Engineering of nanoformulations for inhalation pulmonary delivery to the lung of CF patients. Adapted with permission from [58,83]

1.5. Models for *P. aeruginosa* infection in cystic fibrosis

Testing platforms of new, old, and improved drugs have changed from bacteria alone to bacteria growing on the presence of cells. It was clear that microbes were not alone and were influenced by other bacteria in the environment[84] or bacteria-derived molecules and the presence of the host[85]. Interestingly, microbes as *P. aeruginosa* have been outed as saboteurs of new drugs or beneficial molecules (e.g., Cif factor blocking a CFTR corrector[86] and bacterial hydrolases stopping resolving lipid mediators[87]), but, most importantly, those discoveries were only possible by integrating bacteria and human cells to then proceed with treatment.

1.5.1 *In vivo*

One of the most accessible models of CF is the mouse; however, the introduction of CF-related mutations has not provided spontaneous disease. Nonetheless, this model can be altered with the stimulation by bacteria, creating an infection/inflammation scenario.[88]

CFTR deletion is one approach. However, other receptors mimic CF disease progression. On mice, the overexpression of the epithelial sodium channel (β-ENaC) influences in the volume of airway surface fluid, on producing blockage by mucus with lung injury and chronic inflammation.[61]

The mice model requires special attention as it shows a failure to thrive, mortality and excessive responsive to infection that is not reflected by human CF[89]. For that, other models are presented, in an attempt to overcome some of those issues, but also to provide disease progression in the lung.

Besides mice, large animals have also been used in CF research. Lung pathology, excessive responsive of the airways and alterations on surfactant started to be investigated on the pig CF model, due to its comparative anatomy[90]. CFTR deficiency presented changes in

tracheal development and gastrointestinal blockage, but only the aging pig gave similar lung problems in its function that are found in CF infants (although there is the question if those were exclusive of the introduced defects on CFTR)[91]. It is an exciting model that demands high costs for husbandry with extended reproduction cycle[92].

Although other animals have been described for CF models, as monkey[93] and sheep[94], the ferret is the third most used animal. The knockout of CFTR in the ferret brought neonates with defects on chloride transport and alterations on submucosal glands. Yet an improvement on animal models, biological tools against ferrets antigens are scarce.[95]

1.5.2 *In vitro*

Using *in vitro* models and cell lines is a relatively new concept to mimic different aspects of CF and to develop new platforms for drug discovery and drug testing[11].

Notably, the lung from the trachea to the alveolar region encloses more than 10 cell types and especially the bronchial area, or upper airways count with ciliary structures, mucus, and surfactant fluids [96]. Considering such *in vivo* complexity, the establishment of an *in vitro* cell system that could minimally mimick the diseased airway is instead a not simple task. Therefore several groups, including us have established several co-cultures models, constituted minimally by two cell types (usually epithelial and immune cells)[97,98]. This combination goes beyond the traditional classical cultivation of cells as monocultures, while allowing to access parameters like increase inflammation, excessive immune cells recruiting, tissue damage due to matrix-breaking molecules and failure of bacteria control[99].

The bronchial region can benefit from the rolling of alveolar macrophages through the air interface nearby the terminal bronchioles[100]; however, the majority of the bronchial epithelium relies on the transmigration of immune cells (macrophages and neutrophils) from the basal sub-epithelial space across the epithelium to the airways following infection[101–103].

Transmigration models have been developed[104,105], though still lacking focus on Cystic Fibrosis specific issues, including the use of proper diseased bronchial epithelial cells.

The pulmonary system is comprised of the upper airways, trachea, and primary bronchi for lower airways and alveolar for the distal/small airways. This division is useful because it demonstrates cell composition being completely different among these regions. As well as, cell susceptibility to infection and content of antimicrobial molecules. Besides, for CF disease, the lower lung is the area prone to infection with consequent lung re-structure and excessive inflammation.[106]

Human primary bronchial epithelia can be obtained through biopsies, explants, and some factors as cell´s yield, bacteria colonization from the host, and lung injuries turn the procurement of primary cells a fair challenge. Other options as airway brushings or use of content from bronchoalveolar lavage and nasal swabs are being used, although cell counts are lower even more scarce in CF patients.[107] New technologies gave us access to the development of patient-specific cells as basal stem cells, transdifferentiation from type-II alveolar into type-I cells, inducible pluripotent and embryonic stem cells.[108,109]

From primary cells to immortalization, bronchial cell alveolar models, have brought the needed requirements for long-term cell culture with the advantages of cell differentiation and possibilities to develop scenarios of disease progression, including acute to chronic infection.[106] By growing cells on plastic dishes/wells or the permeable porous membrane, it is possible to mimic such scenarios. The figure 10A shows that cell models of the bronchial area can now be cultivated at air-liquid interface, in double to triple cell-culture, besides also the possibility to include extracellular matrices and shear stress (either of air and liquid). That has provides insights into the characterization of CF immortalized cells, as CFBE41o- cell,

which express mature receptors as TLR1-5 and 9 as well as healthy bronchial cells 16HBE14o[110].

Advancing on the models (fig. 10B), the inclusion of immune cells has now provided differences in between non-CF versus CF cells (NuLi versus CuLi-1 with F508 CF mutation) on increases inflammation in the presence of CFTR defects, including increased neutrophil migration[111]. This co-culture with immune cells has been used not only for the analysis of drug delivery methods but also on CF infection as the inclusion of *S. aureus*.[104,112,113]

Besides the influence of the host, the outcome in CF disease will also be influenced by the bacteria growth, more specifically by the transition from planktonic to biofilm form. Marquis-Moreau *et al*[114] has demonstrated the use of co-cultures to observe early biofilm formation on top of CFB41o cells after 6 hours of *P. aeruginosa* infection (fig. 10C) and this model has now led to increased understanding of biofilm control, drug efficacy, and antibiotic resistance[115].

If early *P. aeruginosa* colonization of lung can now be mimicked *in vitro*, the establishment of a mature biofilm on epithelial cells is still a challenge. The infection itself is highly toxic to epithelial cells – no longer than 6 hours, the epithelia is not viable anymore, remaining, therefore, only the bacteria. This limit further studies on bacteria-host cell responses in the long term infection. Thus, different strategies are being used since the external growth of biofilm and transfer of its content[116] as well and biofilm growth into gels in the separated compartment but still the same well with airway epithelial cells (fig. 10D)[117].

The increase of *in vitro* cell complexity has demanded the development of new models that explore lung regions, cell types, cell differentiation, cell source, diseases versus healthy scenarios[118].
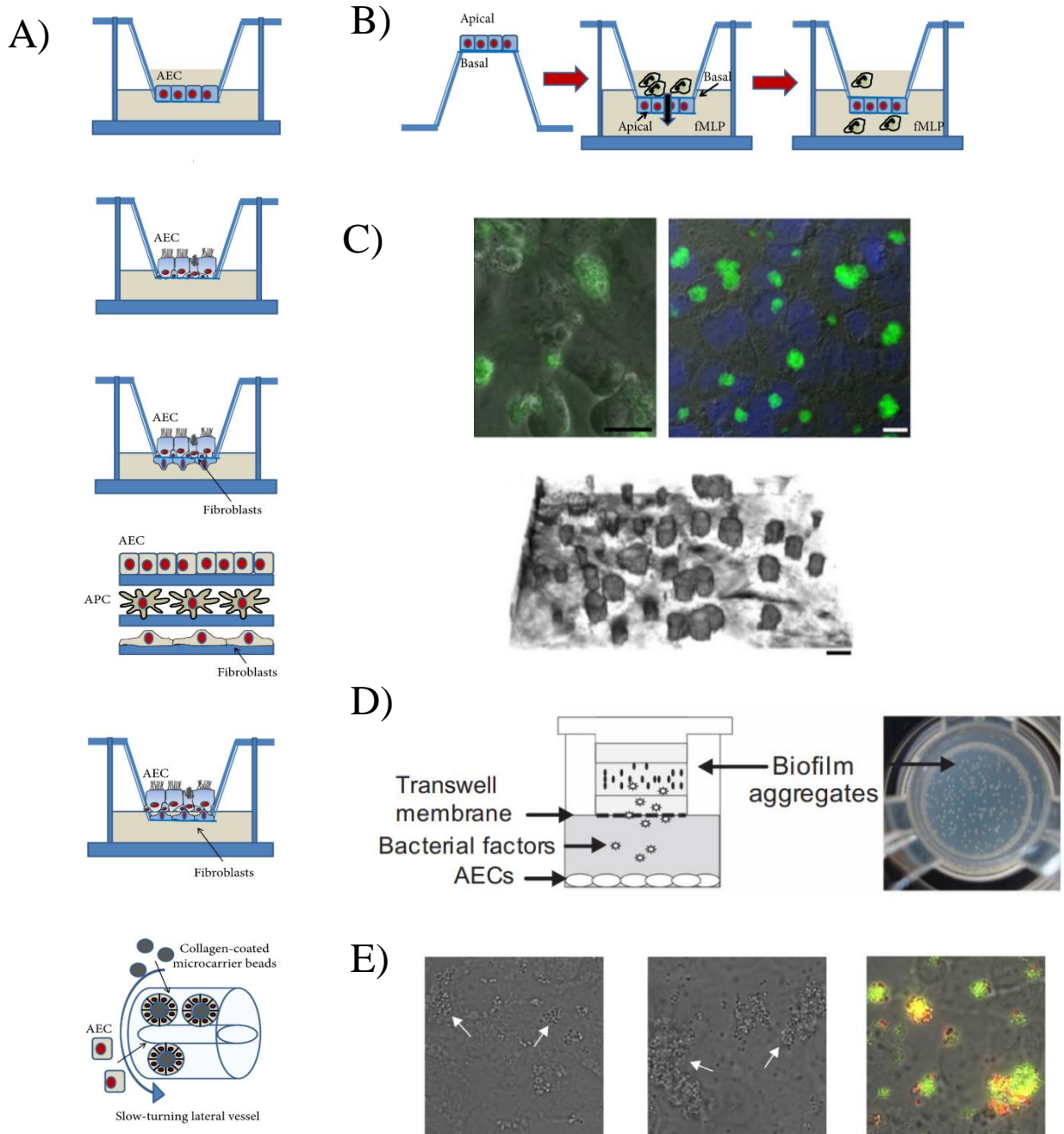
Figure 10. Summary of in vitro of CF and its inclusion of bacteria. A) Airway epithelial cells (AEC) and its variation, from monoculture to polarization with ALI, the addition of fibroblasts, co-culture with antigen-presenting cells, the inclusion of collagen matrix and shear stress. B) Co-culture for neutrophil transmigration. C) Growth of *P. aeruginosa* early biofilm (6 hpi) on CFBE41o- cells in a flow cell. D) Inclusion of mature biofilm aggregates. E) Dual microbial infection of *P. aeruginosa* and *S. aureus* on top of CFBE41o- cells. Adapted from [114,117–119].

2. Aim of this work

In this study, we have developed a new air-liquid interface 3D *in vitro* cell co-culture constituted by CF bronchial epithelial cells (CFBE41o-) and differentiated macrophages (THP-1), infected with *P. aeruginosa*.

This model approaches the manner we think on drug discovery towards new antibiotics because it challenges that an analogical view on kill versus not killing bacteria. This drug testing should be recommended to test bacteria that are grown on live substrates. First, to understand how bacterial adaptation could protect them from antibiotic action and second, to comprehend the dynamics of lung cells in the battle of drugs and bacteria.

If a bacteria can grow on a live surface as the lung epithelia, a second important feature is the role of immunity. With the potential to include inflammation as a third component, we want to evolve the co-culture for inflammation-producing cells like the macrophages. This integration will increase complexity, but it will challenge our capacity to understand why antibiotics might not work and how to start thinking of new strategies.

By uncovering the issues of adherence of these two chosen lung cells in different compartments of a transwell membrane, we bring forward the role of macrophage migration, inflammatory stimulation/response, while a diseased epithelium presents the formation of early biofilm aggregates from *P. aeruginosa*. Monocultures in comparison to the double co-cultures were characterized in terms of its features, e.g., morphology/viability of the cells, integrity of the epithelial layer, use of cells as substrate for bacterial growth and biofilm formation, cell collaboration on induction of inflammation, tobramycin response on bacteria survival and host response in a more complex system mimicking the *in vivo* situation. The interplay between epithelial cells and macrophages and bacteria uptake was investigated with Confocal Laser Scanning Microscopy (CLSM).

3. Establishment of co-culture with CF bronchial epithelial and macrophage-like cells

3.1. Materials and Methods

3.1.1 Cells

3.1.1.1. CFBE41o- Cystic Fibrosis Bronchial Epithelial cell culture

CFBE41o-, derived from a cystic fibrosis patient and homozygous for ΔF508 mutation,[120,121] was received as a kind gift from Dr. Dieter C. Gruenert (University of California, San Francisco, CA, USA). The cells (passage number 4.60 - 4.80) were maintained in MEM (Gibco™ Thermo Fisher Scientific Inc., Waltham, MA, USA) supplemented with 10% FCS (Lonza, Basel, Switzerland), 1% non-essential amino acids (NEAA, Gibco™) and 600 mg/L glucose (Sigma-Aldrich) at 5% CO_2 atmosphere and 37°C, respectively. Cells were fed every 2-3 days. For co-culture experiments, cells were seeded with a density of 200,000/well in 12 well Transwell® plates (500 µL MEM apical side, 1.5mL MEM basolateral side) with a PET membrane of pore size of 3 µM (Corning, Amsterdam, Netherlands). Cells were lifted to the air-liquid interface (ALI), 3 days after seeding, and fed every 2 days until cells formed a confluent monolayer and barrier properties exceeded 300 Ω*cm² (typically 7 days after seeding).

3.1.1.2. Macrophage culture and differentiation

The THP-1 cells (No. ACC-16), a monocyte-derived cell line[122], was obtained from the *Deutsche Sammlung von Mikroorganismen und Zellkulturen* (DSMZ; Braunschweig, Germany). The cells were grown in T75 culture flasks using Roswell Park Memorial Institute (RPMI) 1640 medium (Gibco® by Lifetechnologies™, Paisley, UK) supplemented with 10% FBS. Before using them in experiments, the suspension cells were differentiated by adding 10 ng/mL PMA (Sigma, Germany) to cell culture medium[123] and further incubated for 48 h [124]. Accutase® (0.5 mM EDTA•4Na, Sigma, Germany) was used to remove cells from flasks.

For cell number optimization, we used ImageJ to count cells using different cell density and incubation together with CFBE41o- grown on transwells. After obtaining

imaging with confocal microscopy, we used the transferred image and opened it with Fiji. By converting to RGB, we can then adjust threshold and observe the structures we will count. By subtracting the background and using the watershed program, we can adequately define the edges of the particles. We then use "Analyze particles," setting size 0-Infinity and circularity 0-1, then each particle is numbered and counted.

3.1.1.3. QuasiVivo® flow system

A bioreactor (Quasi-Vivo, QV600, Kirkstall, United Kingdom) that is also a perfusion chamber with a peristaltic pump is commercially used and was used for the testing of CFBE41o- differential growth. The cells were cultivated on 0.33 cm^2/0.4 µm pore size transwells for 1 day on adherence in liquid-covered conditions. On the next day, transwell upper rings were manually cut to fit the flow chamber, then transferred to the flow chamber or remained as static. Importantly, transwells were installed, so only the basolateral side has contact with the medium and the flow, therefore maintain the air-liquid interface. Using CFBE41o- cell medium on reservoir bottles, we tested 0.5 and 1 ml/min as flow rates compared to static conditions along 6 days using a cell incubator (37ºC, 5% CO_2), with measurements of TEER everyday and cytotoxicity assays (MTS, Promega, Germany and LDH, Roche, Switzerland), according to the manufacturer's recommendations.

3.1.2. *P. aeruginosa* (PAO1-GFP and PA14) cultures

P. aeruginosa strain PAO1, its fluorescent-labeled strain ATCC® 10145GFP™, and PA14 were grown in LB broth (Sigma-Aldrich, Germany). For the GFP expressing strain, the LB medium was supplemented with 300 μg/ml ampicillin (Carl Roth, Germany). Overnight cultures were grown by inoculating 15-20 ml of LB broth with a single colony of bacteria and incubating for 16-18 hours at 37°C and 180 rpm. For cell infection, an overnight culture of PAO1 in exponential growth phase was PBS-washed and diluted to a final OD600 0.1 (~ $1x10^7$ CFU/mL) in MEM cell medium.

3.1.3. Set-up of the 3D co-culture model

3.1.3.1. Uninfected 3D co-culture

Setting-up the co-culture was performed based on Ding *et al*[104] with modifications. To visualize the mono and co-cultures, CFBE41o- cells were labeled one day before the set-up of co-culture with CellTracer Far Red (1µM, Sigma, Germany) and when needed THP-1 cells with 10 µM CellTracker. The medium from CFBE41o- monolayers was removed (from both apical and basolateral chamber), and the inserts with the established epithelial layer were turned upside down. The cells that overgrown through the membrane pores in the basal side were removed with a cell scraper. Then the transwells were deposited in sterile glass Petri dishes (50 x 200 mm, Normax, Portugal).

Differentiated THP-1 macrophages were harvested, suspended in RPMI 1640, and 200 µl of the cell suspension ($2x10^5$ cells/well, which corresponds to 1 macrophage:1 epithelium ratio[125]) was added to the basal side of the inserts turned upside down. The Petri dishes were closed and incubated for 2 h at 37°C/5% CO_2. Afterward, the Transwell inserts were placed back into the plates and 0.5 ml CFBE41o- cell medium was added to the lower chamber to maintain the air-liquid interface.

Cystic Fibrosis Bronchial Epithelial cells

Seed (2×10^5 cells) on transwell of 3 µM pore size membrane

8-10 days

Prestain with CellTracer

P. aeruginosa GFP

Overnight bacteria culture of *P. aeruginosa* PAO1 strain

Bacteria preparation MOI from 1:1 to 20:1

THP1 monocytes into macrophages

THP1 differentiation with phorbol myristate acetate (10ng/mL **PMA)**

2 days

Pre-staining with Cell Trace

Ratio 1:1

Leave for adherence for 2h inside the cell incubator
Turn the transwell back inside the well, let it interact for 1 hour
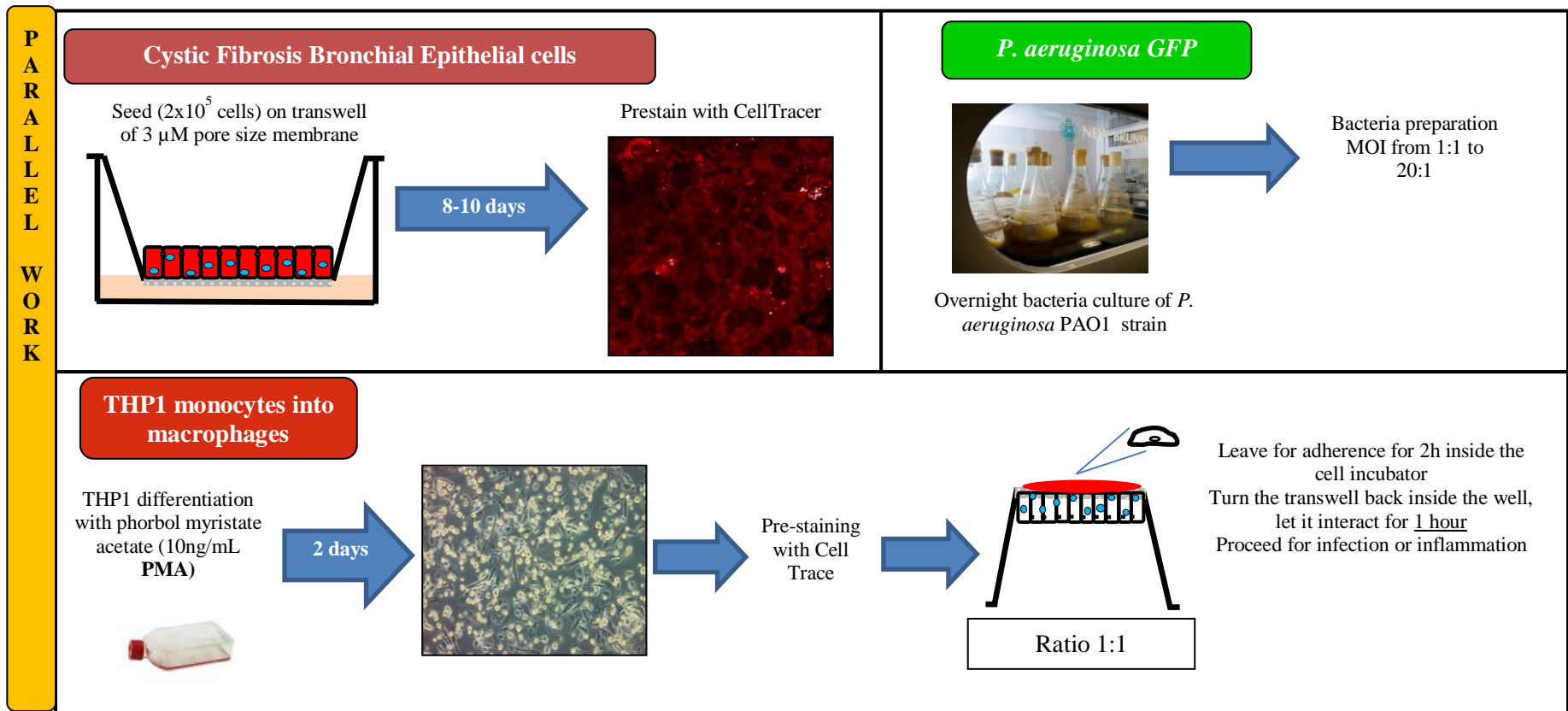Proceed for infection or inflammation

Figure 11. The workflow of establishing co-culture and its infection.

3.1.3.2. Infected 3D co-culture

Double cell co-cultures were either infected with *P. aeruginosa* PAO1-GFP (ATCC® 10145GFP™) or incubated with LPS *E. coli* 10µg/mL for testing potential inflammatory response.

Overnight culture of PAO1-GFP in exponential growth phase was PBS-washed and diluted to an OD600 for a final concentration of $2x10^5$ PAO1 cells (Multiplicity of infection MOI 1:1) of bacterial suspension in 100 µl of MEM medium for 1h on the apical side to infect wells; afterward the apical medium was removed and the bacteria on top of epithelial cells were exposed to the air.

A stock of tobramycin sulfate salt (1mg/mL in PBS, Sigma, Germany) was diluted on Phosphate Buffer Solution (PBS, pH 7.4). A volume of 500 µl of the drug solution was applied on the apical side of the corresponding wells 1 h after the infection.
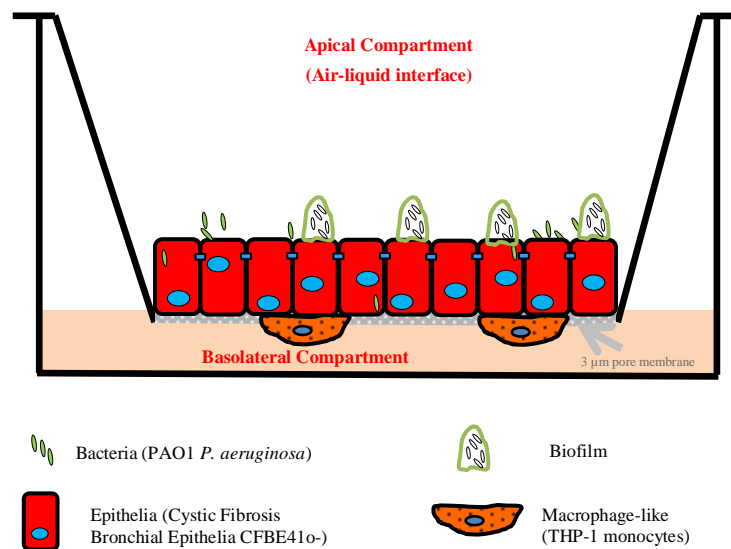

Figure 12. Scheme of elements on the establishment of co-culture on transwell.

3.1.4. Transepithelial Electrical Resistance Measurements (TEER)

To assess the epithelial barrier properties, CFBE41o- mono and co-cultures were incubated with cell medium (500 µl apical and 1500 µl basolateral) for 1 hour, and TEER was measured with an epithelial volt-ohm meter (EVOM, World Precision Instruments, Sarasota, FL, USA) equipped with STX2 chopstick electrodes. The TEER was calculated by subtracting the resistance value of blank inserts containing only medium (120 Ω for 1.12 cm²) from all samples, with further multiplication by the cultivation area of the inserts.

3.1.5. Confocal Laser Scanning Microscopy

3D and cross-section images were obtained by CLSM (Leica TCS SP 8; Leica, Mannheim, Germany), using lasers at 405 nm (DAPI), 488 nm (GFP), 505 nm (Yellow) and 633 nm (Far Red). Microscopic images were acquired at 1024×1024 resolution, using a 25x or 63x water-immersion objective. Zeta-stack mode (10-15 stacks) was used to build a three-dimensional model of the co-culture, in which cross and orthogonal sections were used to observe macrophage transmigration and bacteria phagocytosis. Confocal images were analyzed using Analysis was performed using LAS X software (Leica Application Suite X; Leica, Mannheim, Germany).

3.1.6. Fixation and Immunostaining of zona occludens (ZO-1)

Immunohistochemical staining for the TJ protein ZO-1 was performed as previously described[109,126] with minor modifications. Briefly, system the cells were fixed with 3% methanol PFA (stock 16%; 15710-S, Electron Microscopy Sciences, USA) in PBS from apical and basolateral side for 1 hour. The following steps, including quenching, blocking, permeabilizing, and staining were then performed from the apical compartment of cocultures and monocultures. In brief, the samples were quenched with 150 µL of 50 mM NH_4Cl in PBS for 1h, followed by a blocking and permeabilizing step using a mixture of 0.5% BSA / 0.025% Saponin in PBS for 1h min at room temperature (RT). The primary antibody against

ZO-1 (Purified Mouse Anti-Human ZO-1 Clone 1/ZO-1 (RUO), Catalog No. 610966, BD Biosciences) was diluted 1:200 in 0.5% BSA / 0.025% Saponin/PBS-solution; 200 µL was then added apically, followed by incubation at 4°C overnight. The secondary antibody (polyclonal Alexa-Fluor 633 conjugated rabbit anti-mouse, Catalog No. A11059, Invitrogen) was diluted 1:2000 in 0.025% Saponin/PBS-solution and incubated for 2h at RT. The samples were washed with PBS and counterstained with DAPI (1:10000, 0.5 µg/mL; 30 minutes) and/or rhodamine-phalloidin for staining of F-actin (Invitrogen, Germany; 20 µM in methanol for 2 hours). Transwell® membranes were then cut out of the filter insert structure, mounted in between two glass coverslips and a drop of DAKO mounting medium (Product No. 85 S302380-2, DAKO, USA), then analyzed by CLSM.

3.1.7. Cytotoxicity assay: the release of lactate dehydrogenase (LDH)

LDH was calculated about negative (medium only, 0% cytotoxicity), and positive controls (1% Triton-X100, ICN, Eschwege, Germany, positive control, 100% of cytotoxicity). The supernatant of cells infected or not infected was placed in a new 96-well plate and centrifuged (5000 RPM for 10 minutes), then 100 µL of supernatant was separated for LDH assay (Roche Cytotoxicity LDH kit, Germany). LDH kit mix was incubated with the supernatants for 5 minutes in the dark at room temperature, according to manufacturer instructions. The absorbance was read by a Tecan microplate reader (Germany) at 492 nm.

3.1.8. Colony-forming units (CFU) assay

After the specific time points of infection, supernatants were removed, sterile MilliQ water was added on the wells for cell lysis (15 minutes) then samples were stored at -20°C. The supernatant was centrifuged to separate the pellet of bacteria, then stored at -20°C. For plating, samples were re-suspended in PBS, serially diluted in PBS/Tween80 0.05%, and drop-plated (3x 20µL drops per dilution) on agar plates to determine the CFU. Adherent/internalized bacteria on transwells were scraped using a pipette, then serially

diluted and drop-plated. LB-Agar plates were incubated at 30°C overnight for 24-76 hours, colonies were counted, and CFU calculated accordingly.

3.1.9. Enzyme-linked immunosorbent assay (ELISA) of cytokines

Pro-inflammatory cytokines were detected on the supernatant of infected cultures with the Cytokines ELISA Ready-SET-Go kits (Affymetrix eBioscience, USA). Briefly, Nunc Maxisorp® 96-well plates were coated with capture antibody of the respective cytokine and incubated overnight at 4°C. A series of washes were performed with Wash Buffer (PBS/Tween20 0.05%) then wells were blocked by incubation with ELISA/ELISPOT Diluent for 1 hour. Samples were applied (or previously diluted, in the case of IL-8 plates) together with kit cytokine standards, and plates were incubated overnight at 4°C. Plates were washed then received detection antibody of the respective cytokine for 1 hour RT incubation. Another series of washes were performed and plates received Avidin-HRP for detection of biotinylated antibodies for 30 minutes. The last series of washes were performed and the TMB solution was applied as enzymatic/color inductor from the kit. The reaction was stopped with 1M H_3PO_4 solution and absorbance (Spectrophotometer; MultiskanGo 1510, Germany) was read at 450nm for detection and 570nm as background. Values were paired with an internal calibration curve from the cytokine standards well and then properly calculated to the sample wells.

3.1.10. Multiplex cytokine panel with Flow Cytometry

In order to quantify the cytokines Panel I (IL-2, IL-4, IL-5, IL-6, IL-9, IL-10, IL-13, IL-17A, IL-17F, IL-21, IL-22, IFN-γ and TNF-α) and Panel II (TSLP, IL-1α, IL-1β, GM-CSF, IFN-α2, IL-23, IL-12p40, IL-12p70, IL-15, IL-18, IL-11, IL-27, and IL-33) secreted by uninfected, infected not treated and infected tobramycin-treated, we used LEGENDplex™ Immunoassay according to the manufacturer's instructions (Biolegend, USA).

3.1.11. Measurement of *P. aeruginosa* virulence factors: pyocyanin and pyoverdine

CFBE41o- mono and co-culture (200,000 cells/well) were cultivated on 24-well microplates until 80% confluence (3 days of growth). *P. aeruginosa* PA14 strain was cultivated for 18h in 200ml-Erlenmeyer, incubated at 37ºC, 200rpm, 75% humidity. On the next day, the content was transferred to a 50mL-Falcon and centrifuged at 5000 RPM for 10 minutes. The content was then PBS-washed and its optical density (λ=600nm) was measured at the spectrophotometer. Bacteria suspension was adjusted to a final OD of 0.02.

PPGAS medium or medium with candidate compounds was filled in each well of 1.5mL, then for each well 15 µL of the bacterial suspension was given to have a multiplicity of infection of 1:40 (cell to bacteria). The cells were infected, infected treated or non-infected for 18 hours in which the plates were covered with a BreathSeal cover (Greiner, Germany). After incubation, the seal was removed, and the content of each well was transferred to a plastic tube. The following methods were validated and described by Thomann *et al*[82].

Before the extraction of pyocyanin, 100 µL of each sample transferred to a black transparent 96-well plates (Greiner BioOne, Germany) and pyoverdine was measured through Fluorimeter (Excitation 400/Emission 460nm; TECAN Infinite M200Pro, Austria).

For pyocyanin, the method has been previously described by Kurachi (1958). Thomann *et al*.[82] used 900 µL 100% chloroform per plastic tube, then proceed to centrifugation at 14K RPM for 15 minutes. Each tube formed 3 phases, we transferred the organic phase into a new plastic tube, followed by the addition of 250 µL of 0.2M HCl and centrifugation of 14K RPM for 10 minutes. Pyocyanin was measured from the aqueous phase at the spectrophotometer (520nm).

3.1.12. Statistical analysis

Data represent 3 independent experiments and are shown as mean ± standard deviation (SD). One or Two-Way ANOVA with Tukey´s posthoc test was performed using GraphPad Prism 5 software (GraphPad).

3.2. Results

3.2.1. Optimization

Three-dimensional models require advanced cell culture methods to comprise different cell types, induce cell polarization, create compartments that mimic biological barriers or access to the systemic blood network. These and other requirements demand the use of a platform that provides a connection between the created compartments. Most of the available 3D in vitro models were established on permeable filters (Transwell® system).

Different surface area, material, thickness, different pore size, and density are some of the few variables when choosing a transwell. Although this system has been extensively used, an adaptation of new cell lines requires attention on growth rate, cell attachment, differentiation and growth area. Optimization of cell number, method of cultivation, cell medium, and time of incubation is presented here for CFBE41o- in comparison to another bronchial epithelial cell, Calu-3.

When the cell adheres and differentiates on the apical side of the transwell, the communication between cells increases and gives space for the formation of tight junctions. This is constantly monitored and characterized here via measurement of the transepithelial electrical resistance. After defining differentiation, it was necessary to understand and test the adaptation of *P. aeruginosa* on top of the newly formed epithelial layer. However, our challenge was the integration of macrophage-like cells, derived from the activation of THP-1

monocytic cells, in the basolateral side of the transwell that contains the grown epithelial layer.

A subsequent optimization was required on macrophage number and time of incubation for adherence, plus an observation of how epithelial cells behave and grow in contact with medium from another cell. Once the co-culture is established, cell overgrowth was observed and demanded changes in the protocol. As we are in demand for a model that mimics excessive inflammation, LPS was firstly used as a stimulant antigen, while key cytokines were measured to start the characterization of the co-culture. Finally, the infection of the co-culture using *P. aeruginosa* required further elaboration to then provide us the *in vitro* model that can predict host-response and drug efficacy.

3.2.1.1. Growing CFBE41o- cells on transwell pore 3µm

Between all factors that can influence the growth of a cell, the substrate is one crucial physical aspect that can affect cell growth and differentiation. For conventional assay as viability or scratch assay, cells can be easily cultivated on plastic bottoms or coverslips (covered with agents to alter adherence, e.g., poly-L-lysine). For more complex systems, one can consider the permeable systems, so-called Transwells®. In our model, we used the transwell systems for the following reasons: i) possibility to expose the cells in the apical side to the air, which is close to the lung physiology, and ii) the porous membrane mimics a barrier that dependent on the comprised cells.

Cell growth on transwell demands direct visualization with light microscopy to control cell confluence and early qualitative cell differentiation. For that, CFBE41o- cells were grown on a polystyrene membrane transwell with pore size 0.4 µm (figure 13A). Due to cell density number (200,000 cells per well) on the second day, an epithelial layer started to

be formed, until the fourth day it shows increased cell density, cell packing and lining fluid is observed. This configuration is useful for modeling CFBE41o- as a monoculture.

Figure 13A shows the growth of bronchial epithelial cells, Calu-3, followed for 8 days in a transwell system that has a pore size of 3 µm. This pore size is a critical factor for our co-culture model that also intends to follow the transepithelial migration of immune cells. Using CFBE41o-, these cells were grown on two transwells of the same material, similar surface area, but different pore density distribution along its surface. However, the transwell with lower pore density did not provide visualization under the microscope, which leads to an issue when monitoring cell growth.

A comparison between transwell 3462 and 353181 is observed in figure 13B that shows that the same cell type and density, being observed in better quality for the lower pore density transwell. Through the use of transwell 353181, the cells can easily be visualized and monitored. Moreover, this transwell allows the observation of characteristic signs of layer confluence and differentiation.
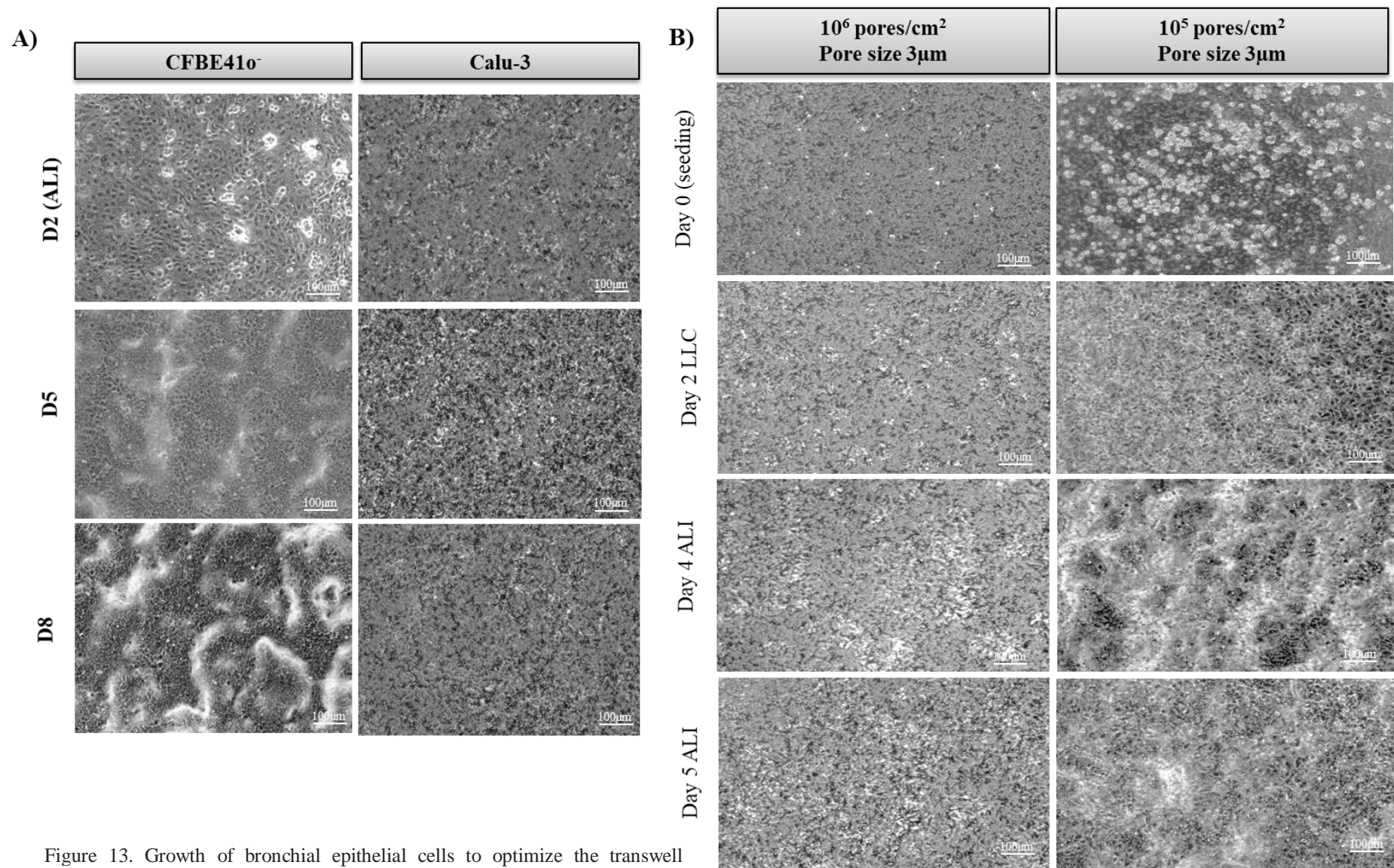
Figure 13. Growth of bronchial epithelial cells to optimize the transwell system. A) CFBE41o- and Calu-3 growth on 0.4 µm transwell. B) Growth comparison of CFBE41o- cells on transwell of different pore density. Representative images of 2 independent observations.

On the assessment of functional cell epithelial barrier, the use of measurement of transepithelial electrical resistance (TEER) reflects how pore density and size influences on the formation of the epithelial layer. CFBE41o- being a bronchial cell line from a diseased condition, can be compared to the standard bronchial cell line, Calu-3. With this comparison, we observe the establishment of TEER and the barrier of these two bronchial cells to find a specific day then for CFBE41o- to be used as model. For that, in figure 14 we observed stable high TEER for CFBE41o- in the transwell with 3 µm pore size, which shows the disposition of this cell line to adapt to different transwell pore sizes.
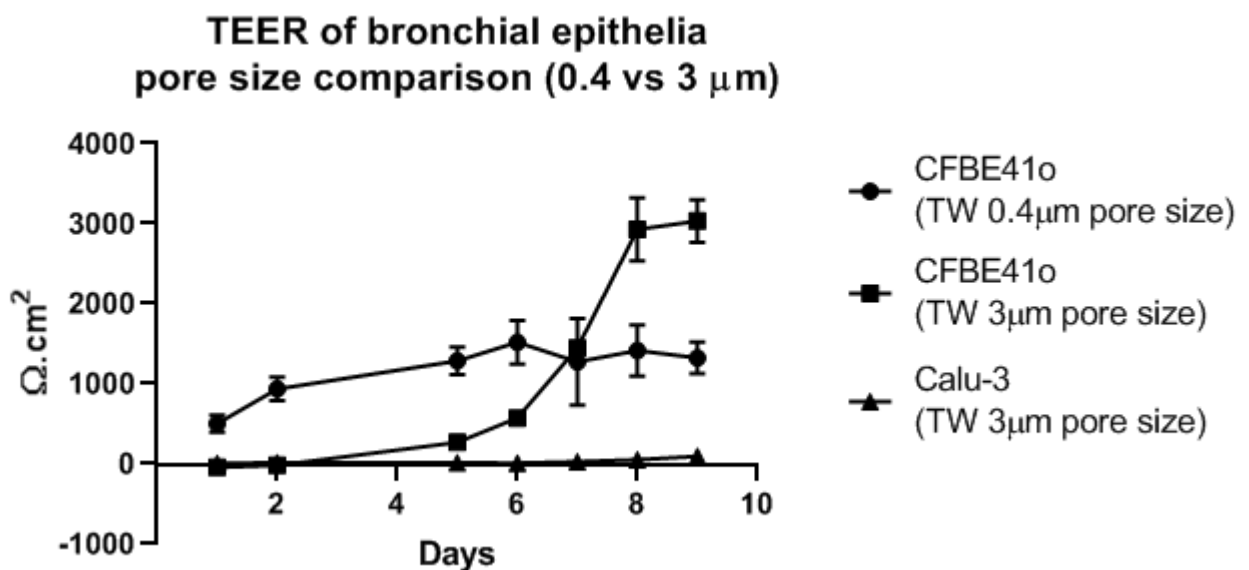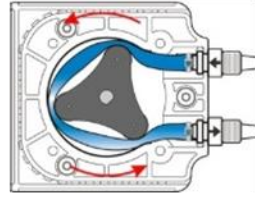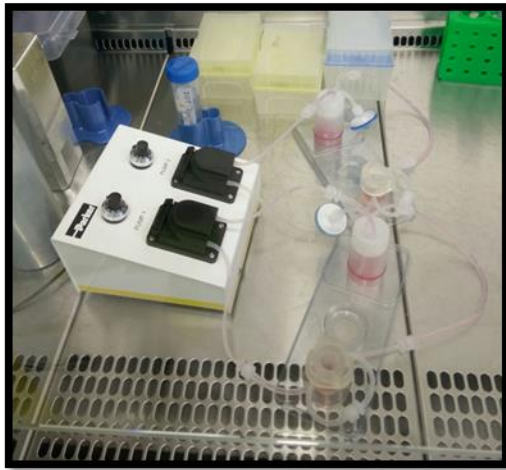

Figure 14. TEER comparison of Calu-3 and CFBE41o- on different transwells. N= 2 experiments.

A flow system can improve and speed the cell differentiation, and with primary lung cells has improved barrier function and increase the production of cilia and mucus when compared to static culture[127]. For us, a CF cell line has ideal growth after 10 days on transwell, and we would like to observe faster confluence and barrier formation with the use of a flow system.

The available model is a bioreactor, together with a peristaltic pump. The system has a silicone chamber with connector tubes attached to reservoir bottles for continuous feeding. We used two flow rates (0.5 and 1 mL/min) and adapted the transwells to fit inside the flow chambers and at a height to continue to mimic the air-liquid interface. We could then monitor TEER development and at day 6 of cultivation to compare cytotoxicity.

Figure 15A shows the setting-up for the system, the position where the transwell sat inside the flow chamber and micrographs of day 6 of culture to compare flow versus static. In this, we observe 1ml/min may interfere with the formation of CFBE41o- lining fluid, but flow rate 0.5 mL/min provides apparently increased cell differentiation. Even so there were no alterations on cytotoxicity levels on the addition of flow (fig. 15C); stable TEER was reached similarly (fig. 15B). In conclusion, this approach is more useful for specific questions around flow, while we needed a more stable platform in a facile method with more capacity for screening.
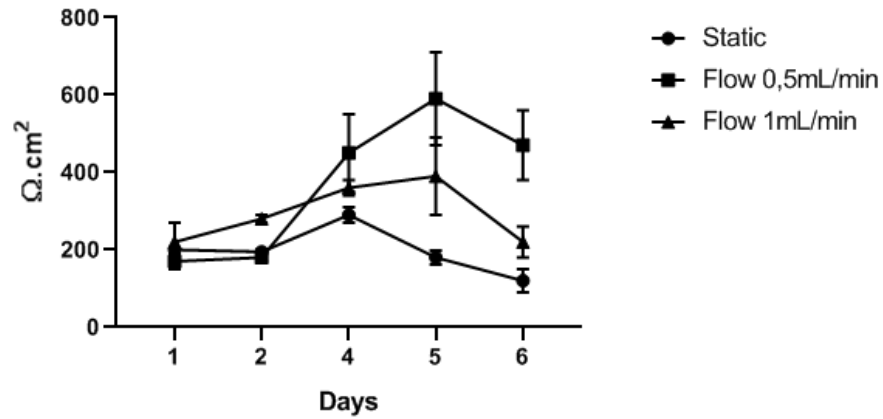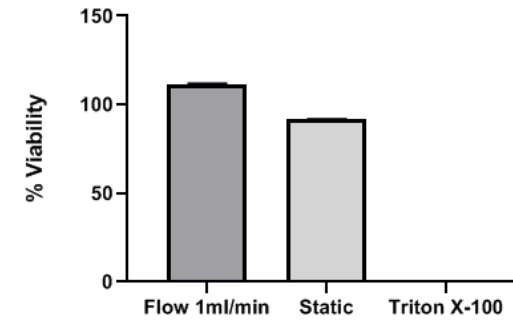
A)

QV600
Kirkstall®
Flow system

Static

Flow 0.5 ml/min

Flow 1 ml/min

100 μm

100 μm

100 μm

Day 6 in culture
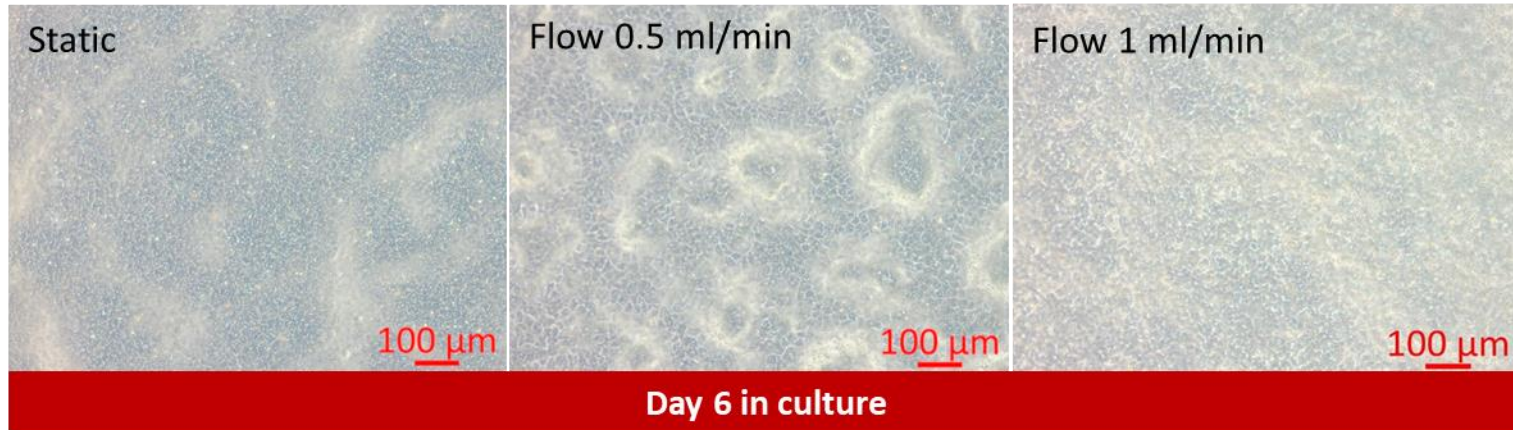
B)

TEER of CFBE41o- on static vs. flow
(transwell 0.33 cm^2/0.4μm pore size)

Legend:
- Static
- Flow 0,5mL/min
- Flow 1mL/min

Y-axis: Ω.cm^2
X-axis: Days

C)

CFBE41o- viability on QuasiVivo Flow (MTS assay)

Y-axis: % Viability
X-axis: Flow 1ml/min, Static, Triton X-100

CFBE41o- cytotoxicity on QuasiVivo Flow

Y-axis: % LDH release
X-axis: Apical, Basolateral

Legend:
- Flow 1ml/min
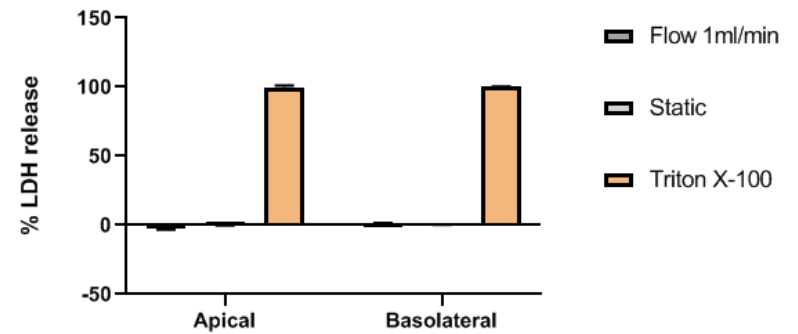- Static
- Triton X-100

Figure 15. Testing of CFBE41o- growth, differentiation and layer formation on a flow system. A) QuasiVivo® flow system inside the flow bench with light micrographs of CFBE41o- cells (static and flow). B) TEER results from flow testing. C) Viability (MTS assay) and cytotoxicity of flow on CFBE41o- cells. N= 2 experiments.

3.2.1.2. CFBE41o- cells overgrow through the 3 µm membrane pores over the basolateral side

One limitation to set-up a co-culture model in a **3 µm membrane pores** transwell is that the cells seeded in the apical side can migrate through the pores of the filter to the basolateral side. As observed in figure 16, a CFDA pre-stained CFBE41o- grown through the transwell pores already after day 4 of seeding. To seed the macrophages on the basolateral side of this membrane, the overgrown epithelia were removed from the basolateral side using a cell scraper. This step was crucial for the macrophages seeding and epithelial barrier formation.
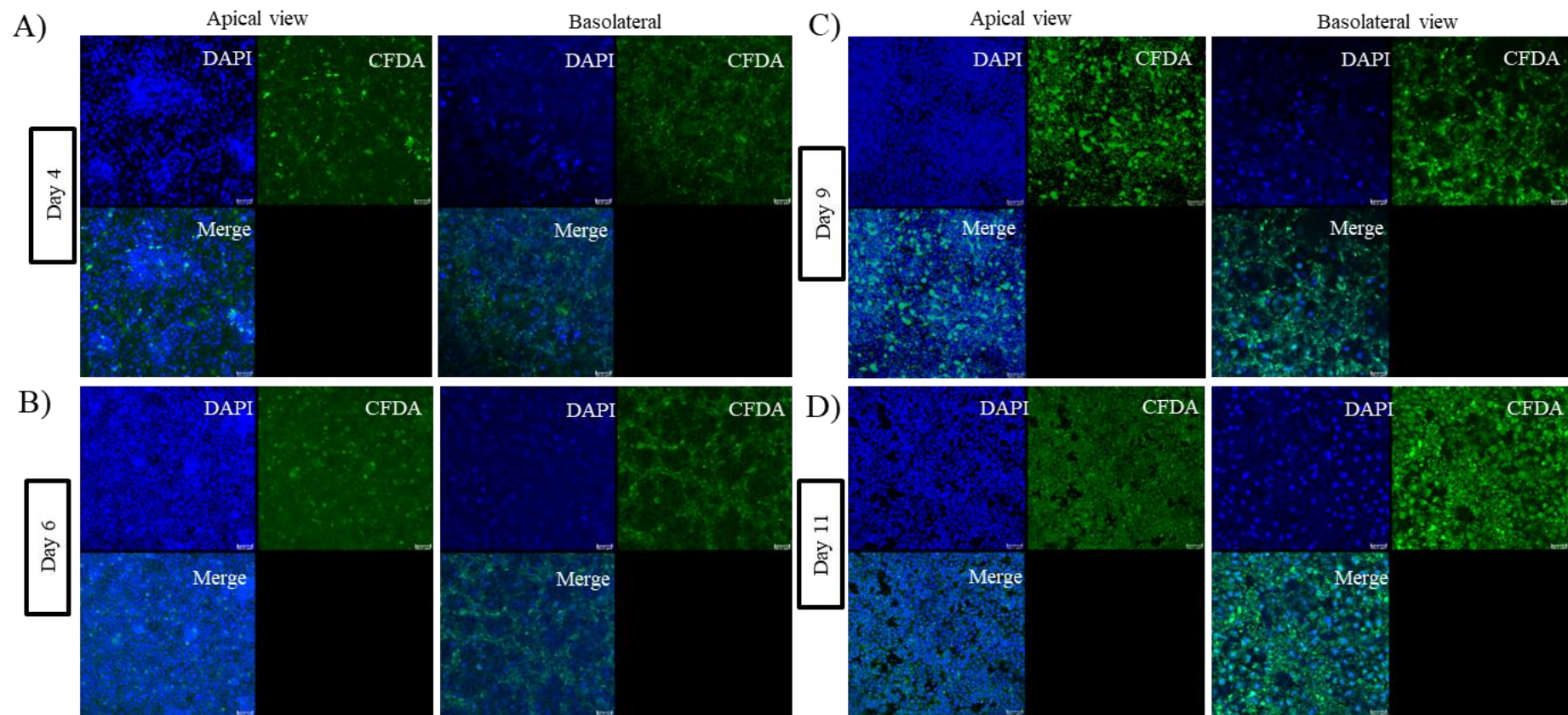
Figure 16. Overgrowth of CFBE41o- cells on 3 µm transwell stained with DAPI (nuclei) and CFDA (cytoplasm). Day 4 (A), 6 (b), 9 (C) and 11 (D). Kinetics of apical and basolateral view of CFBE41o- monoculture growth near the transwell membrane. N= 2 independent experiments.

3.2.1.3. Optimization THP1-macrophages on the variation of cell density, time of adherence and interaction with CFBE41o- epithelia

The inclusion of THP-1 cells on the double cell co-culture requires the seeding on an inverted transwell that already contains a CFBE41o- layer. We looked into cell density and model incubation to observe the maintenance of cell number after adherence and which combination keep more macrophages in a shorter time of incubation. This is because, for us, the model establishment is only one of the steps for the full infected model, so cells should be interacting and ready to be infected.

We further optimize the seeding of THP-1 macrophages on transwell, by following the cell viability of THP-1 with CFDA Cell Tracer®. At least three images per sample were obtained, then a counting protocol was applied using ImageJ (as described in Methods).

Figure 17 shows the data compilation from macrophages seeded on the bottom of a 3µm transwells in the presence of the CFBE41o- epithelial layer. Using these co-cultures, we vary density number of macrophages, the incubation time for the adherence on the transwell (1 or 2 hours) and the cell-to-cell incubation time in which the transwell with the 2 cells is placed back into microplate for rest and interaction (1, 6 and 18 hours).

Our focus was to have the shortest time of adherence to be able to go for the next step: the infection. So observing adherence and cell-to-cell incubation time, a combination that guarantees a high number but with a time that will safely promote adherence was to use 200,000 cells in 2 hours of adherence and 1 hour of cell-to-cell incubation.

With fig. 18 shows a sample of the collected images as an example of how the image analysis took place. The imaging of 3 fields per sample (in which one area is represented on this figure) versus the variations of macrophage integration is presented, and the use of DAPI as a fluorescent nuclei marker was used. The nuclei marker was quantified as the edges of

nuclei can be defined and counted as one cell, then this number was compared to the initial seeding number.

The initial number of macrophages was chosen based on Ding *et al* [104]. From the graph, when using 2 hours of adherence and then 6 or 18hours of incubation, there is a lower number of macrophages, considering the epithelia can shed vesicles that can activate the role of macrophages, but yet to be proven here. In the seeding of 200,000 macrophage cells, shorter adherence time (2 hours) and 1 hour of incubation right after that provides the presence of approximately 120,000 cells. This is an initial step to use the model with a significant number of macrophages that are not aged cells in the model and that are still fresh waiting for activation via the subsequent infection.
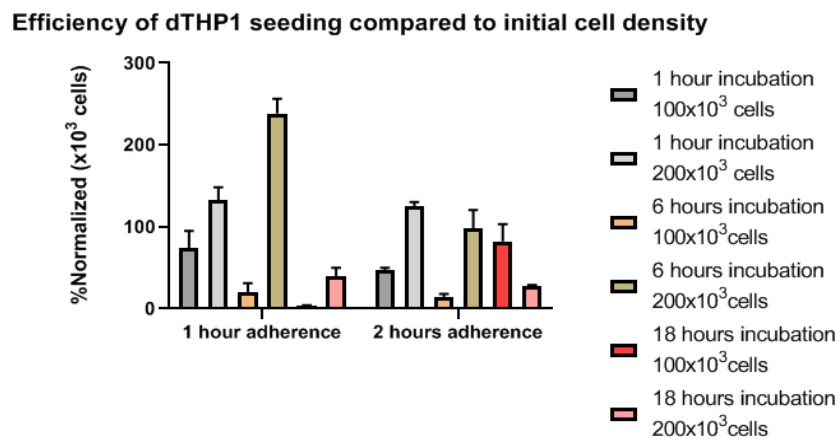

Figure 17. Variation of THP1: cell density, time of adherence and interaction with CFBE41o- cells. Quantification of THP1 adhesion along time (adherence and communication with epithelia) and 100,000 versus 200,000 cells/well.
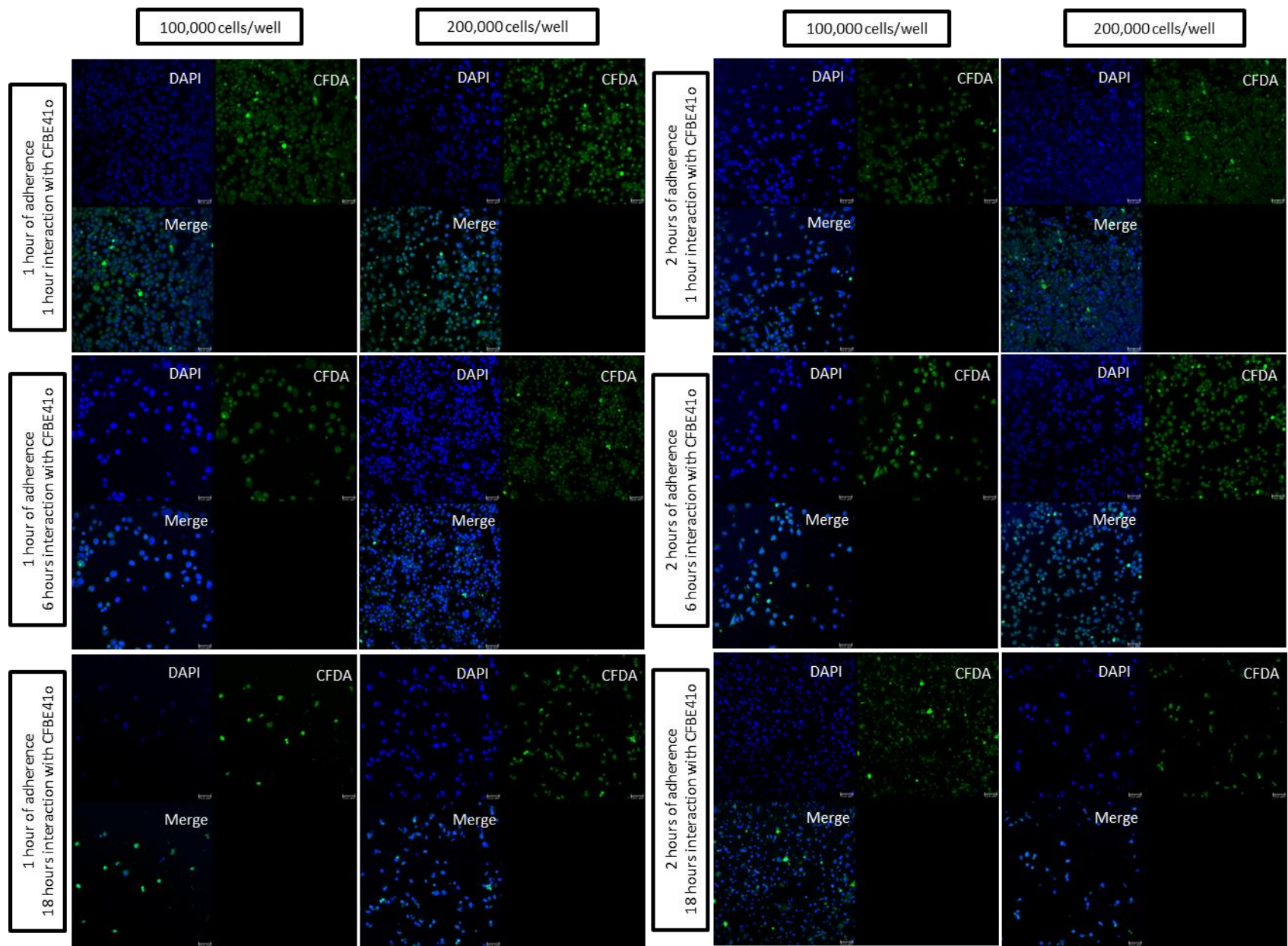
Figure 18. Variation of THP1: cell density, time of adherence and interaction with CFBE41o- cells. Basolateral views of THP1 adherence: 3 images per sample. N= 2 independent experiments.

3.2.1.4. Establishment of non-infected co-culture of bronchial epithelial and THP1 cells

The addition of macrophages could finally take place after i) adjustment on cell adaptation on the transwell and ii) variation of conditions for optimal adherence of macrophages. When putting two cells together, one needs to observe which medium suits better for cultivation if its interaction account for cell stress/toxicity and if the barrier from the epithelial layer is affected by the other cell inclusion.

Figure 19 comprises results on Calu-3 that it was used as a starting point and to provide a future model of the non-CF bronchial co-culture model. No significant differences were founded on cell proliferation with the different media (Fig. 19A) nor on barrier integrity (Fig. 19C). Plus, no significant cytotoxic effect (Fig. 19B) was observed upon the co-culture establishment: even if the borderline level of 20% LDH release from Calu3+THP1. At last, using confocal microscopy and focusing on the basolateral side, we could find the THP1-macrophages (Fig. 19D). The use of cross-sections helped verify macrophage presence and start of cell-to-cell interactions (Fig.19E).

These interactions, even without any external stimuli, could reveal a protrusion of macrophages on the basolateral side, but no transmigration. On fig. 20A, macrophages are limited to the transwell membrane or below, but specific formations of cell pseudopods and possible cell-derived vesicles could be observed. Fig. 20B shows that macrophage behavior is different when not interacting with other cells, and it takes a flat conformation.
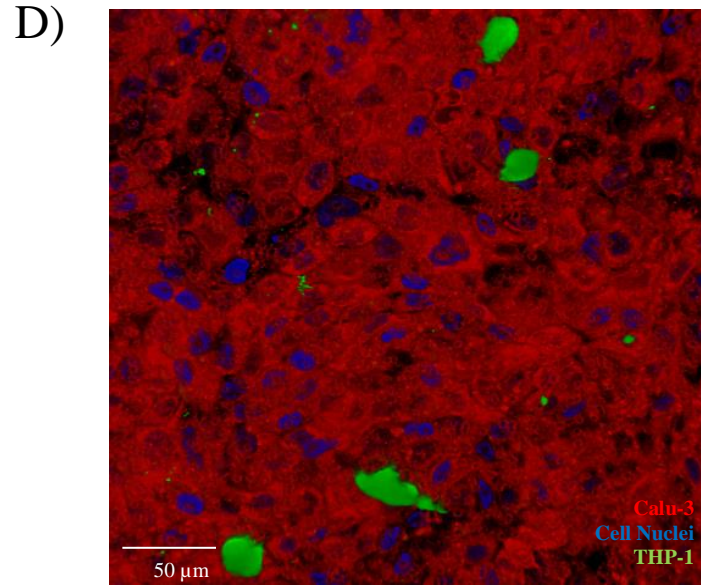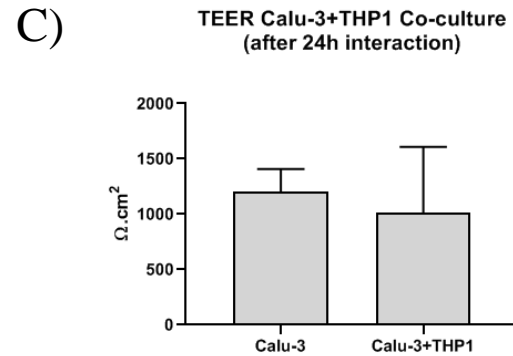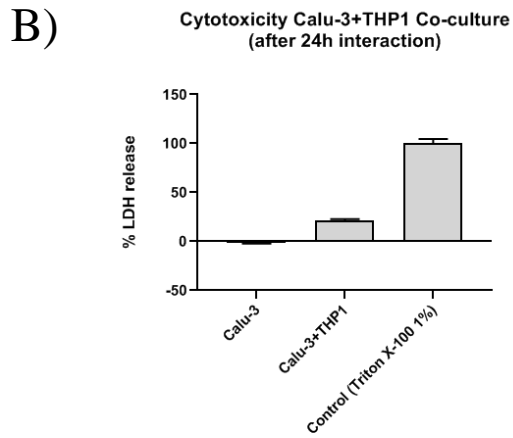
A)

B)

C)

D)

E)
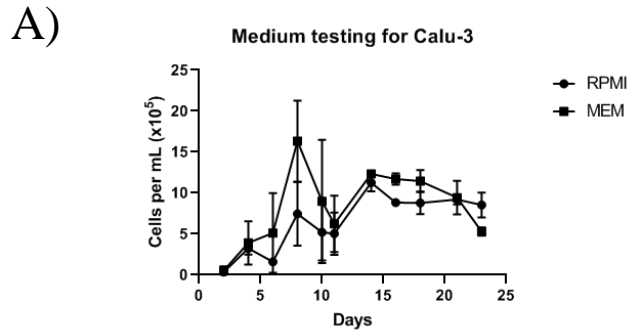
Figure 19. Testing the establishment of co-culture in Calu-3 + THP1 cells. A) Calu-3 growth kinetics with epithelia and macrophage cell media. B) LDH cytotoxicity release of integrating THP1 cells to Calu-3 Day 10 on transwell. C) TEER measurements comparing mono versus co-culture after 24 hours of establishment. D) Confocal micrograph of basolateral side of co-culture on transwell confirming THP1 and Calu-3 presence. E) Cross-sections of transwell membrane from co-culture showing macrophage state and migration after 24 hours of interaction with Calu-3 epithelia. N= 2 independent experiments.

60

A)

Co-culture Calu 3 + THP1

apical

basolateral

apical

basolateral

apical

basolateral

B)

Monoculture THP1

apical

basolateral

No membrane channel
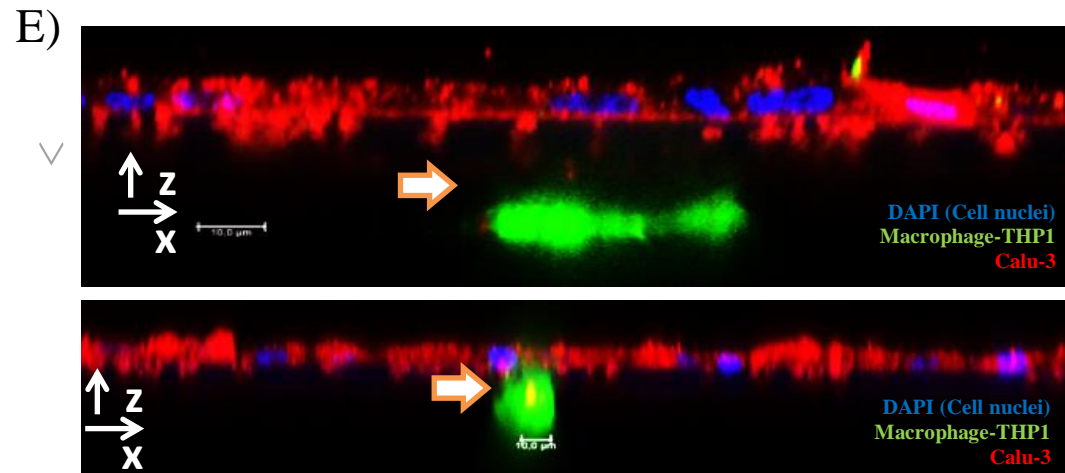
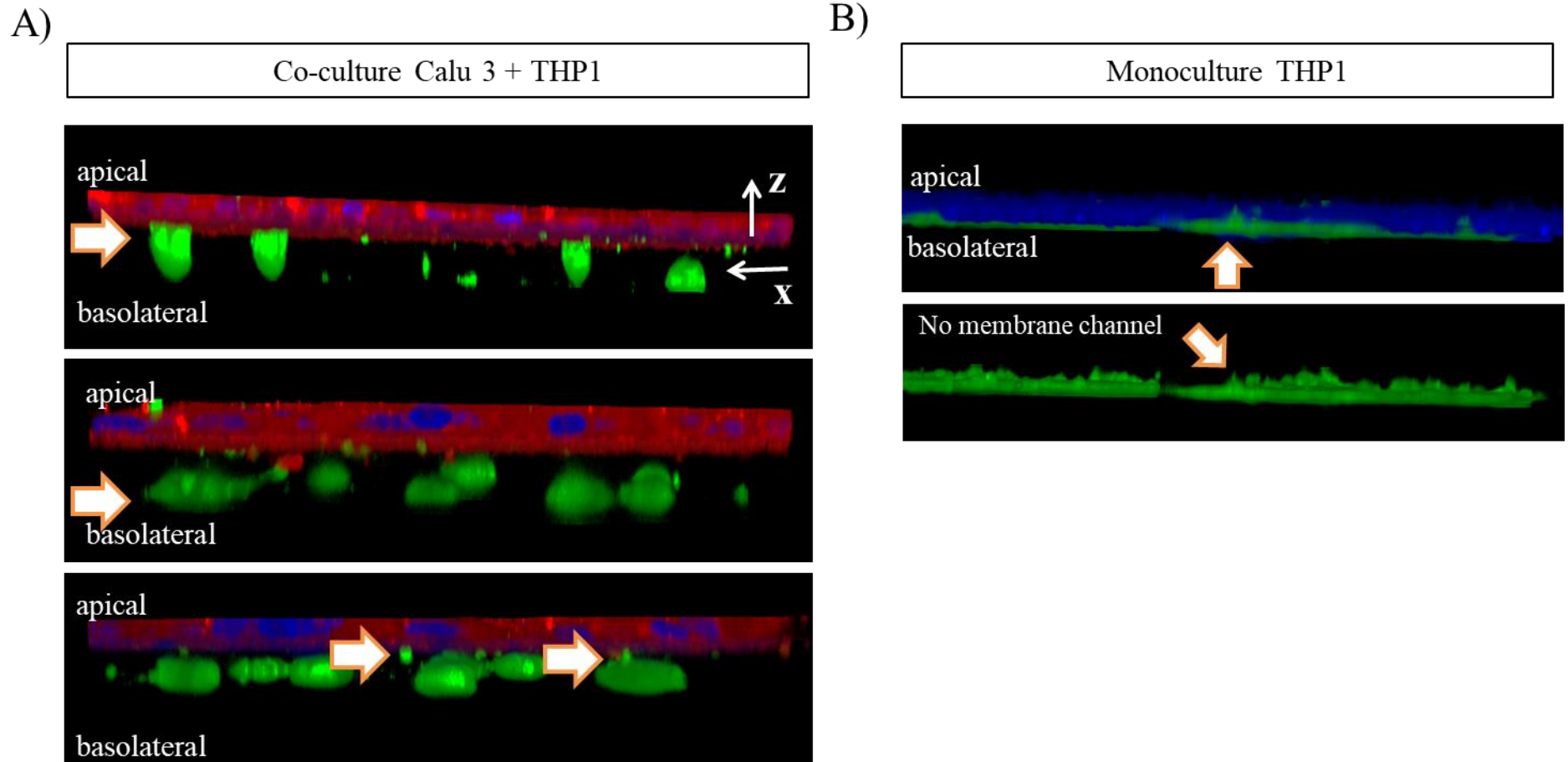Figure 20. THP1-macrophage behavior and morphology. In co-culture (A) with Calu-3 epithelia after 24h, macrophage on co-culture takes globular and horizontal shape with or without cell protrusions towards the Calu-3 layer. In monoculture (B), macrophage morphology is wholly flattened, showing the interaction with Calu-3 alters macrophages. N= 2 independent experiments.

Aiming for cystic fibrosis *in vitro* model we used the established CFBE41o- cell line, which was immortalized from a CF patient with a mutation ΔF508. This mutation accounts for 70% of CF patients, and it does not allow CFTR protein to be transported[128]. Medium testing, with 10% fetal calf serum for both cell media, started this characterization and incubation of CFBE41o- cells in RPMI THP1-medium led to early cell proliferation, so the regular medium was used for the co-culture (fig.21). On microscopy, the viability dye used did not correctly stain CFBE41o- cells, which might be due to cell turnover and proliferation instead of actual cell death. Even so, macrophages adhered to the transwell already containing stable CFBE41o- epithelial layer.

Focus on macrophage behavior had shown the movement of these cells and an evident change of morphology towards macrophage activation when the co-culture was maintained for longer time (36 hours post macrophage seeding, fig . 21C). This could be from cell debris of the needed cell turnover on the epithelial layer that would bring influence on the establishment of inflammation of this model.

A)

Medium testing for CFBE41o-

- RPMI
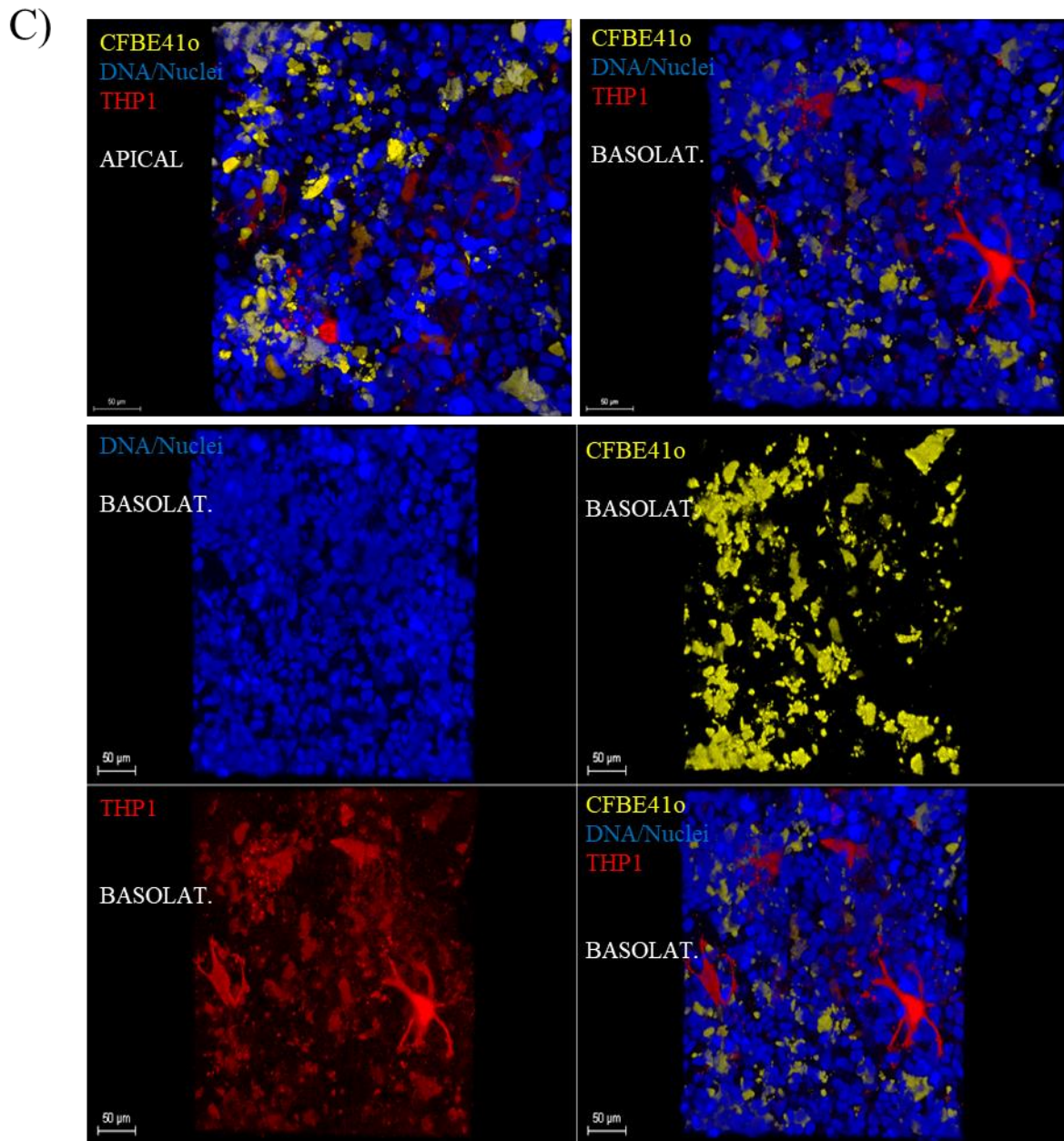- MEM
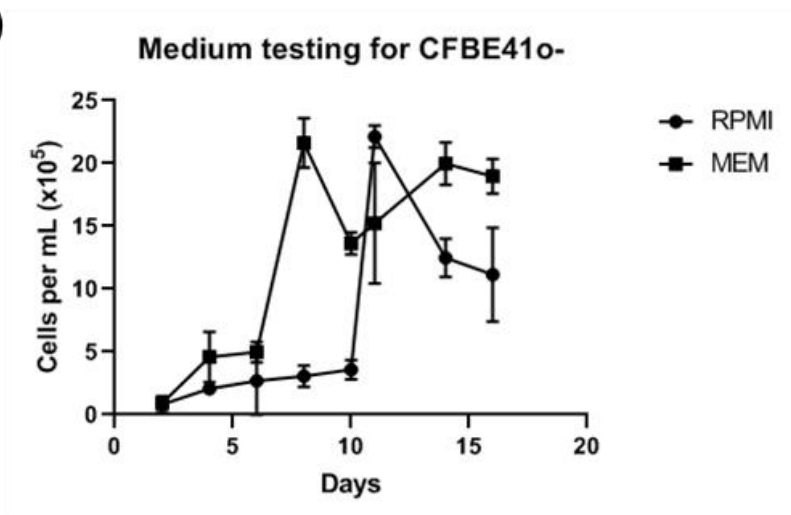
B)
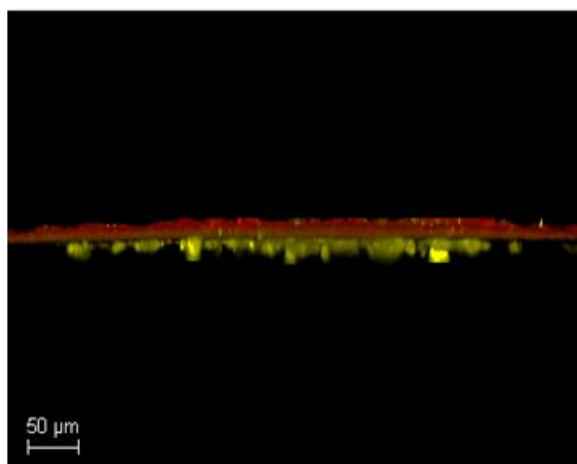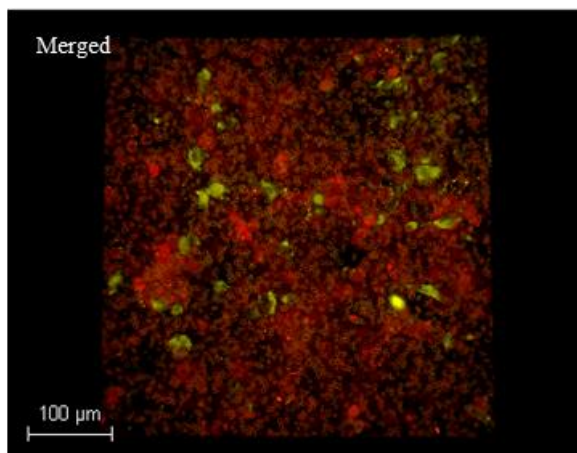
Figure 21. Establishment of co-culture CFBE41o- epithelia with THP1-macrophage. A) Medium testing via cell growth kinetics of CFBE41o- cells, using a CASY automated cell counter. B) Confocal micrographs showing apical and cross-sections of uninfected co-culture. C) Uninfected co-culture after 36h of cell interaction changes macrophage morphology — N= 2 independent experiments.

3.2.1.5. LPS-triggered inflammation on the co-culture

Once the 3D co-culture was established investigated, we assessed the potential to trigger inflammation with Lipopolysaccharide extract from *E. coli* (LPS). For that, mono and co-cultures were treated with 10µg/ml of LPS in CFBE41o- cell medium and measured the followings parameters: cytotoxicity, TEER, and the release of interleukins.

Figure 22A and B demonstrates that for the timepoint required of analysis (6 hours), even though LPS itself is not disrupting the epithelial barrier even after 20h of incubation. However, co-culture leads to a decrease in TEER. There are no differences in TEER values or cytotoxic levels from the samples.

By placing an immune cell with an epithelial layer, we can activate this system. This activation is the possible start of inflammation. If we consider that drug testing should understand the organ's complexity, the addition of infection and inflammation are essential variables to be found on drug efficacy. With the co-culture, we expect to have a higher release of cytokines due to cell-cell crosstalking[129,130].

LPS from *E. coli* at that specific concentration was not able to stimulation CFBE41o-monoculture on interleukin-8 (IL-8) release (Fig. 22C). However, it stimulated THP-1 to release around 2500 pg/mL of IL-8 after 6 hours of exposure. This was then translated to contribute to the release of this cytokine from the co-culture, an advantage on modeling of excessive inflammation. Interleukin-1β was stimulated with LPS on mono and co-culture, although at lower release than expected, showing the need for a full stimulation with the whole bacterium or different amount of LPS.
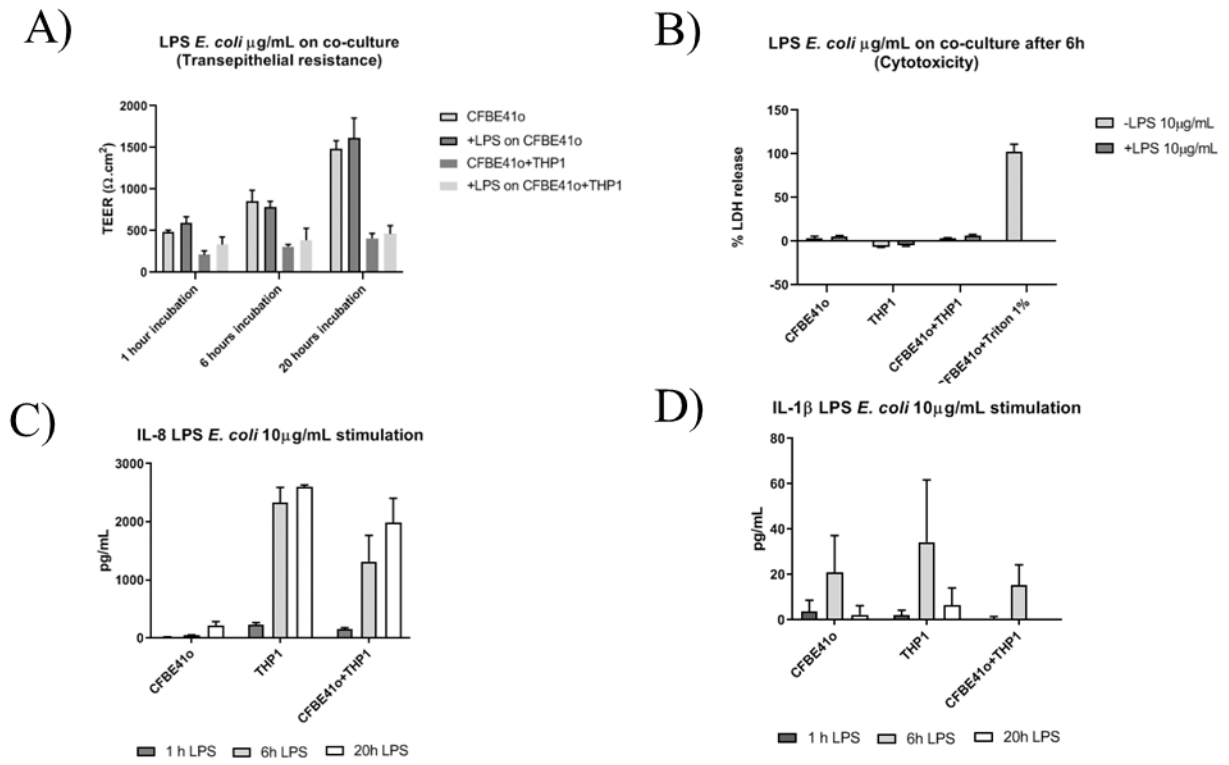
Figure 22. LPS stimulation (10μg/mL) on co-culture establishment. A) TEER measurements of 10 LPS stimulation on mono and co-cultures after 1, 6 and 20 hours. B) LDH release after 6 hours of LPS stimulation. C) IL-8 release after 6h of LPS stimulation. D) IL-1β after 6h of LPS stimulation. N= 2 independent experiments.

3.2.1.6. Optimization of bacterial growth on cell infection

With wild type strain of *P. aeruginosa* we can monitor bacteria growth alterations, however the host-pathogen interaction requires detailed visualization of microbe adherence, maturation and possible formation of communities; this work is facilitated with the use of fluorescent probes for cell nuclei, cytoplasm, membrane and a constitutively fluorescent bacteria (our case using PAO1-GFP).

An initial step is to monitor growth via optical density, and figure 23 shows no significant differences in PAO1 wild type versus PAO1-GFP during the time interval of the proposed infection (1-20 hours). Also, bacteria proliferation was compared via CFU assay, and incubation of bacteria alone for 6 or 20 hours did not show differences between the strains.
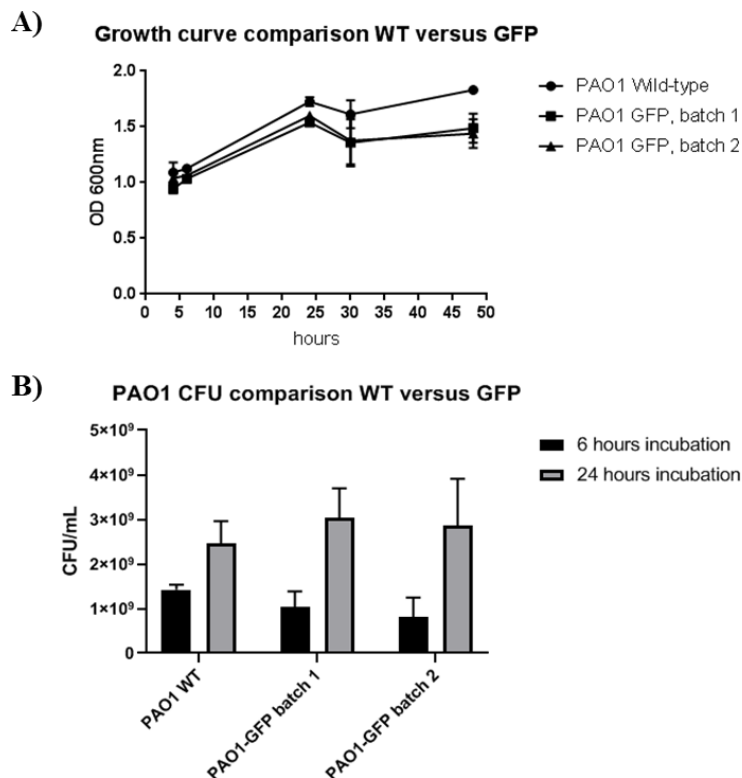

Figure 23. Growth curve and proliferation of *P. aeruginosa* strains wild type and GFP, respectively, via optical density (600nm) (A) and colony-forming units assay (CFU) (B). N= 2 experiments.

Once defined the balanced growth of the strains, the following work was performed only with PAO1-GFP. Following the literature search[87,114,118,131], the use of the ratio of 20 bacteria to 1 cell is the most common adopted multiplicity of infection (MOI).

Variation of MOI must be assessed beforehand to observe the development of infection, but, at that same time, the cell model is alive in the easy-to-work experimental window of 1 to 12 hours post-infection. By experimenting with lower MOI's, we assessed these differences and adaptations.

After 1 hour of bacteria adherence, the bacteria suspension is removed, and the infected monoculture model (for initial observations) is incubated for different time points. Instead of using the entire sample, we can separate the "type of bacteria" via the ones that did not adherence to the suspended ones. Those are then named planktonic for the suspended individual bacteria versus biofilm for the adhered ones and lysate for the membrane-associated and intracellular bacteria. We then proceeded with a stratification of the same well/sample: on figure 24A, first wash obtained planktonic bacteria, while the cell lysate was another fraction analyzed.
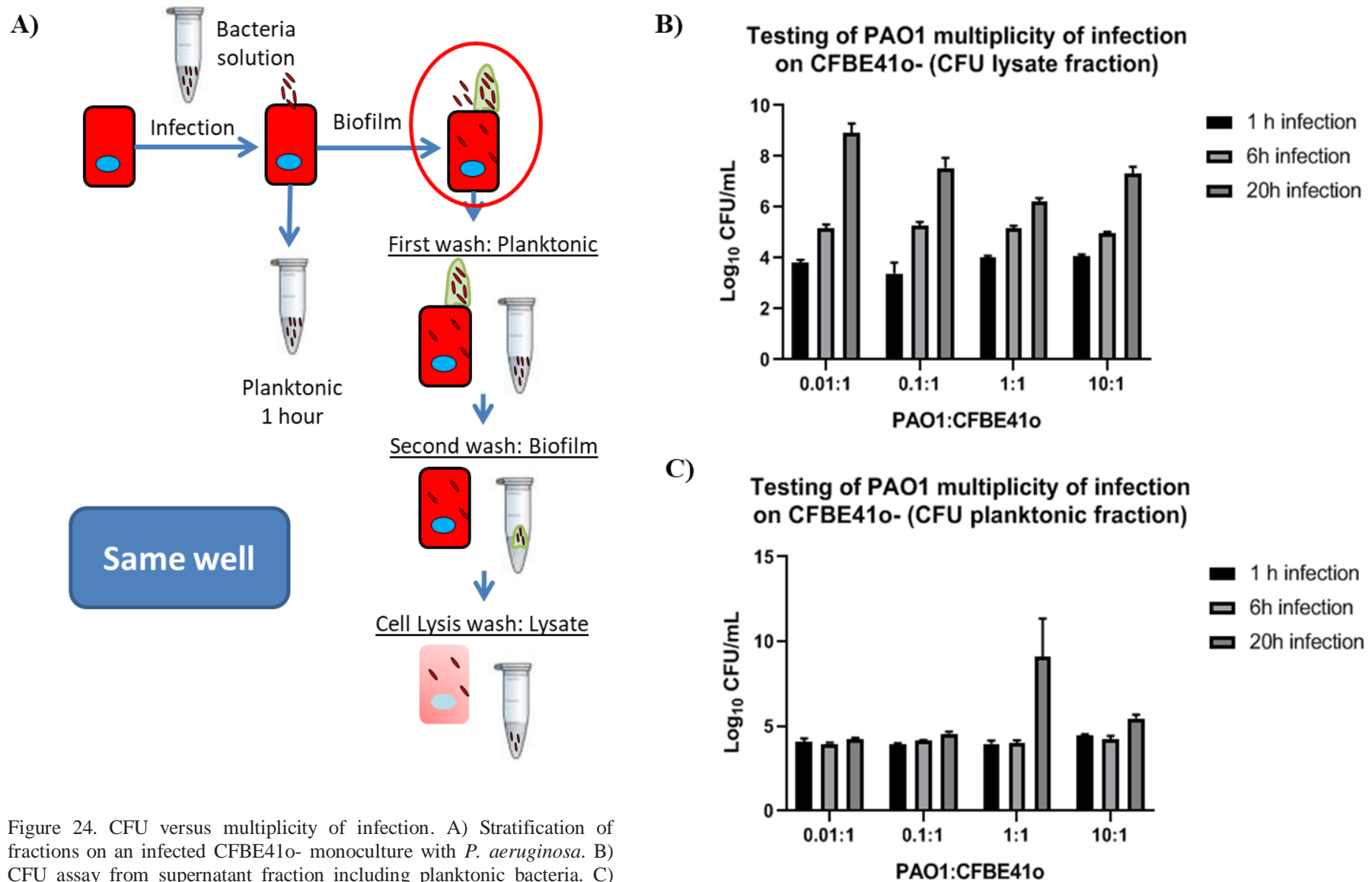
Figure 24. CFU versus multiplicity of infection. A) Stratification of fractions on an infected CFBE41o- monoculture with *P. aeruginosa*. B) CFU assay from supernatant fraction including planktonic bacteria. C) CFU assay of lysate fraction, including adhered/internalized bacteria. N = 2 experiments.

Figure 24B shows that along 1, 6, or 20h of infection, there is no significant difference in CFU growth in between the mentioned fractions. We cannot explain the reason behind the lack of variation, but the adaption of bacteria in contact with eukaryotic cells has been looked into, and even cytotoxicity is not altered by the increase of *P. aeruginosa*'s MOI[132].

An essential step of optimization then includes the reasoning of the ratio around the defined multiplicity of infection. Moreover, although we tried 4 variations of the MOI, including 10, 1, 0.1, and 0.01 of PAO1 to 1 of CFBE41o- cells, there were no apparent differences in cell morphology or bacterial proliferation, as demonstrated on figure 25.

We adopted MOI 1:1 as this showed a more stable epithelial layer (fig. 25 shows micrographs of more intact and few suspension cells) at time point 6 hours post-infection. Furthermore, this timepoint is one of our main interests since it allows experimentation of the model on the same day. However, in the future, we must pursue a more detailed characterization and cell-bacteria interaction, as other information here may lead to cues towards the rate of bacteria multiplication and how this leads to biofilm.
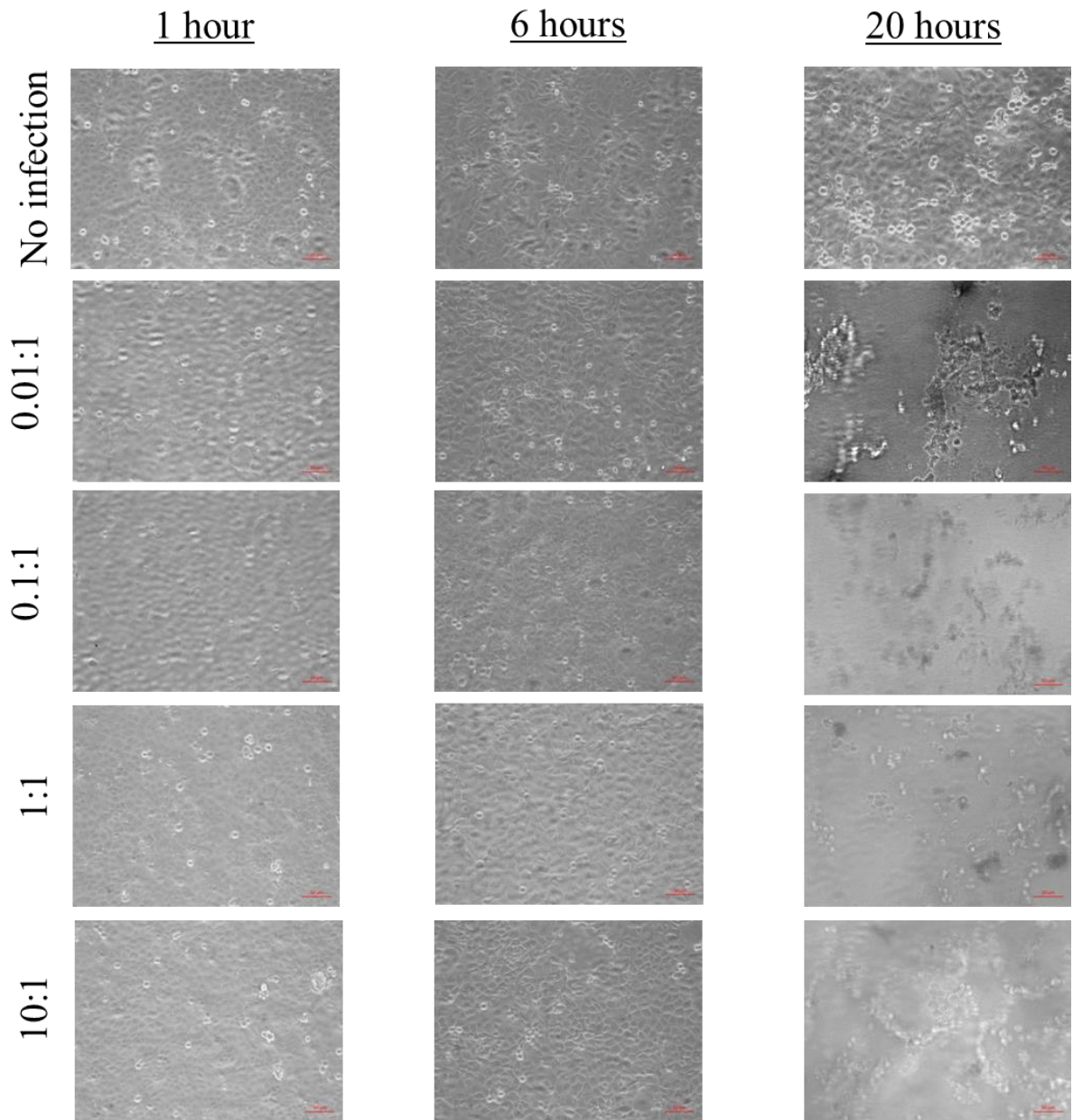
Figure 25. Light microscopy insights into epithelial cell morphology on transwell and variation of the multiplicity of infection of *P. aeruginosa*. Scale bar 10 µm.

3.2.1.7. Using fluorescent dyes to uncover *P. aeruginosa* biofilm formation on top of human cells
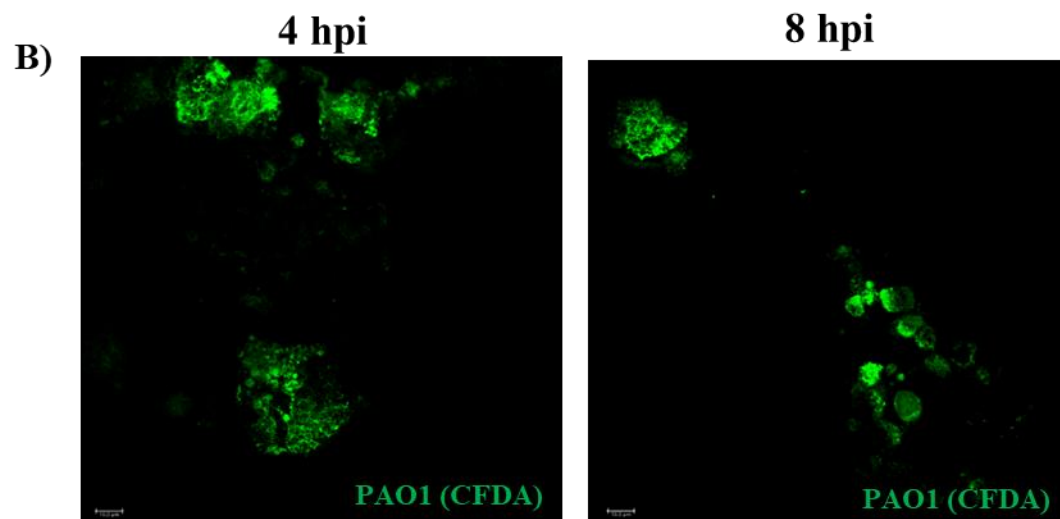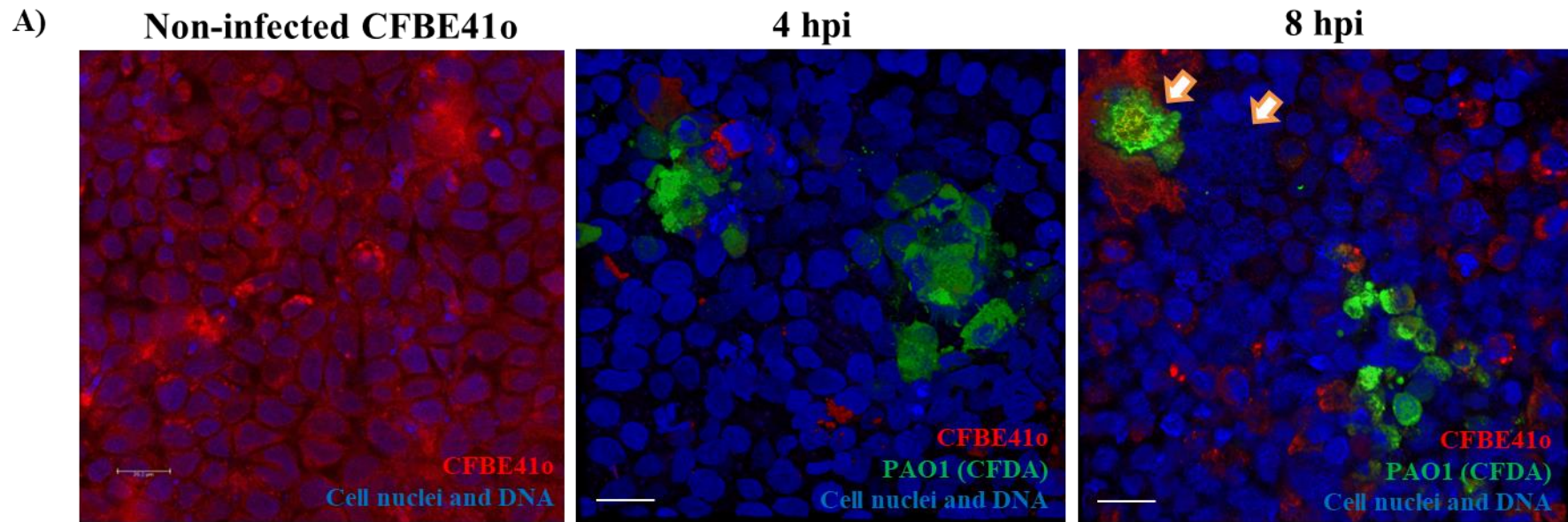
Using light microscopy provides a crude and qualitative visualization of infection and epithelial response, so the use of fluorescence in confocal laser scanning microscopy adds here the advantage of access to different parts of the epithelial layer thickness, plus the possibility to combine images to create a three-dimensional visualization model.

A pre-staining protocol can be used with CellTracer® viability dyes, focusing on the use of molecules that are only converted inside the cytoplasm of living cells by amino esterases. Besides, 4′,6-diamidino-2-phenylindole (DAPI) is a second dye that will help in the identification of cell nuclei and extracellular DNA.

Not only the epithelial layer can be pre-stained, but also *P. aeruginosa*. Using this combination, we aimed to observe areas of dense bacterial proliferation. With that, in figure 26A, CFBE41o- cells without infection are shown to be viable on the transwell; that is not the case after 4 and 8 hours of infection. Despite the use of the pre-staining method, bacteria have a high division rate, which does not attain the dye after many cycles. Even so, the visualization of infected wells shows bacteria aggregation surrounding dead cells that still maintain intact nuclei (although the nuclei membrane is more fragile-looking after 8 hpi). At 8 hpi, some of the aggregates present ramifications resembling a polymeric mesh and is surrounding by cell debris or extracellular DNA.

This architecture further observed in figure 26B where only the fluorescence from bacteria is shown; in some, the bacteria signal is visualized inside the dying cells. DNA and F-actin are known to provide triggers onto the genetic expression of bacteria to transition from planktonic to biofilm[133]. Furthermore, those polymers can even provide the architecture, swarming of *P. aeruginosa* and the efficient flow during and inside the formation of biofilm.

When F-actin staining is added to the samples (fig. 26C), we observed the needed use of this polymer on uninfected cells to provide membrane stability. On infected cells, F-actin co-localizes and surrounds bacteria aggregates and in the future, we hope to understand how this molecule could be engineering towards antibiofilm therapy. Also, when overlapped with transmitted light microscopy, we can understand that i) DAPI staining also marks bacteria nuclei and extracellular DNA where the biofilm matrix is present and ii) not all bacteria are properly retaining the CellTracer CFDA® viability dye, mainly because there is continuous multiplication.

A)

Non-infected CFBE41o   **4 hpi**   **8 hpi**

CFBE41o
Cell nuclei and DNA

CFBE41o
PAO1 (CFDA)
Cell nuclei and DNA

CFBE41o
PAO1 (CFDA)
Cell nuclei and DNA

B)

4 hpi   **8 hpi**

PAO1 (CFDA)

PAO1 (CFDA)

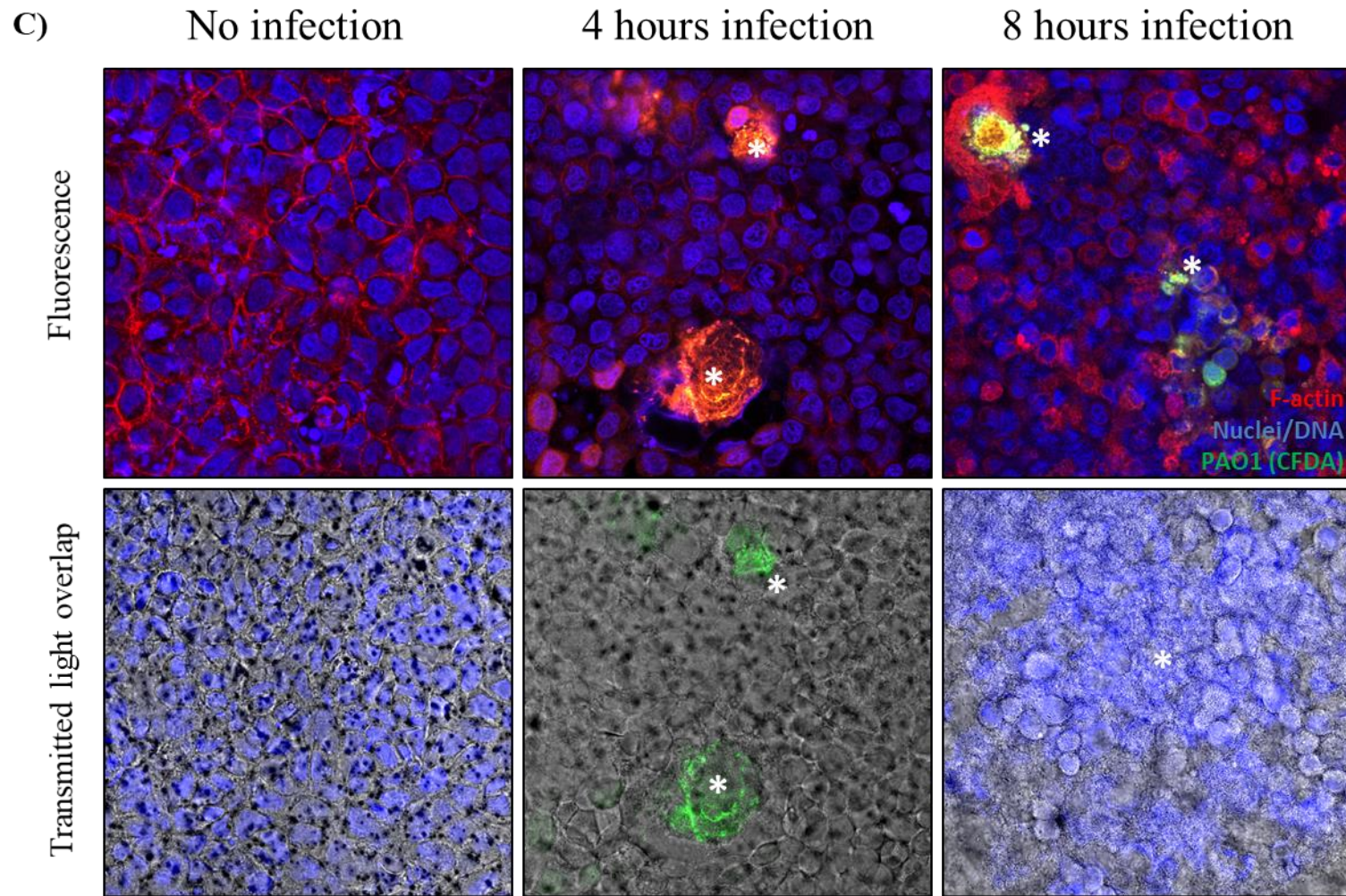Figure 26. Fluorescent micrographs of uninfected and infected CFBE41o- epithelial layer and *P. aeruginosa* MOI 1:20. A) Evolution of infection using pre-stained viability dyes. B) Selected bacteria signal to show early biofilm architecture. C) Use of F-actin and overlapping with transmitted light microscopy to show support of the biofilm architecture by cell debris and autolytic polymers. N= 2 independent experiments.

3.2.2. Co-culture infection

To bring the co-culture model on a diseased state of Cystic Fibrosis, the inclusion of bacteria is performed with the use of *P. aeruginosa* (PAO1-GFP).

As explained above, the infection was executed and six hours after infection, co-culture and monocultures controls were fixed and membranes were mounted for CLSM. Figure 27A shows bacterial aggregates resembling early biofilm are found on top of the epithelial layer while this layer has apparent missing cell spots. Those aggregates are considered as early biofilm due to its morphology and co-localization of the surroundings by DAPI-DNA staining, a characteristic of extracellular DNA used on the biofilm matrix[134]. Interestingly, macrophages can be found both at the basolateral and apical side and that will be approached in next sections.

When infection takes place for 24 hours, the co-culture is destabilized in which there are no epithelial layer and only a small number of macrophages (fig. 27). Nonetheless, mushroom-shaped aggregates now take over, together with a layer of planktonic bacteria.

A)
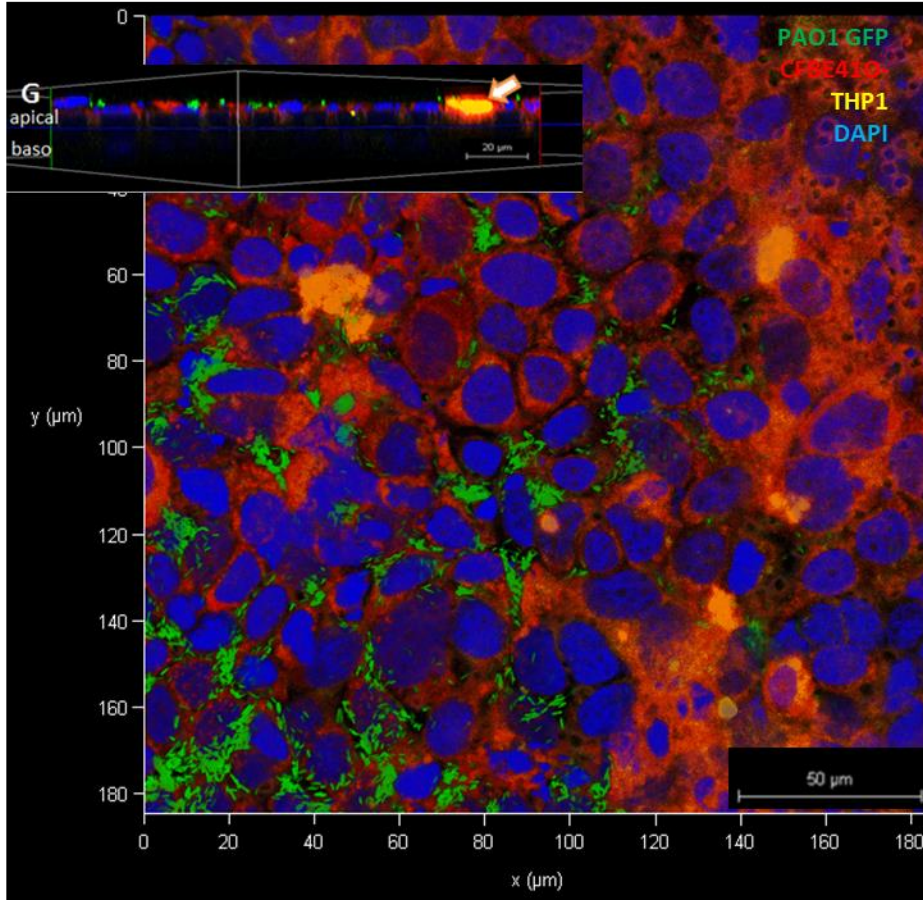
Apical view
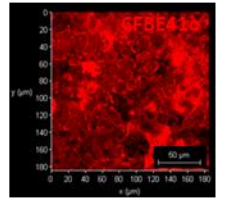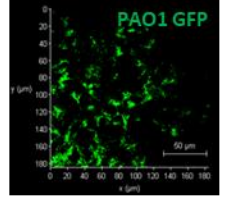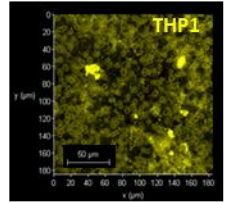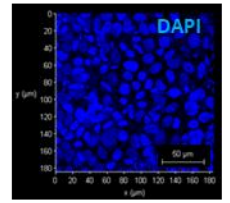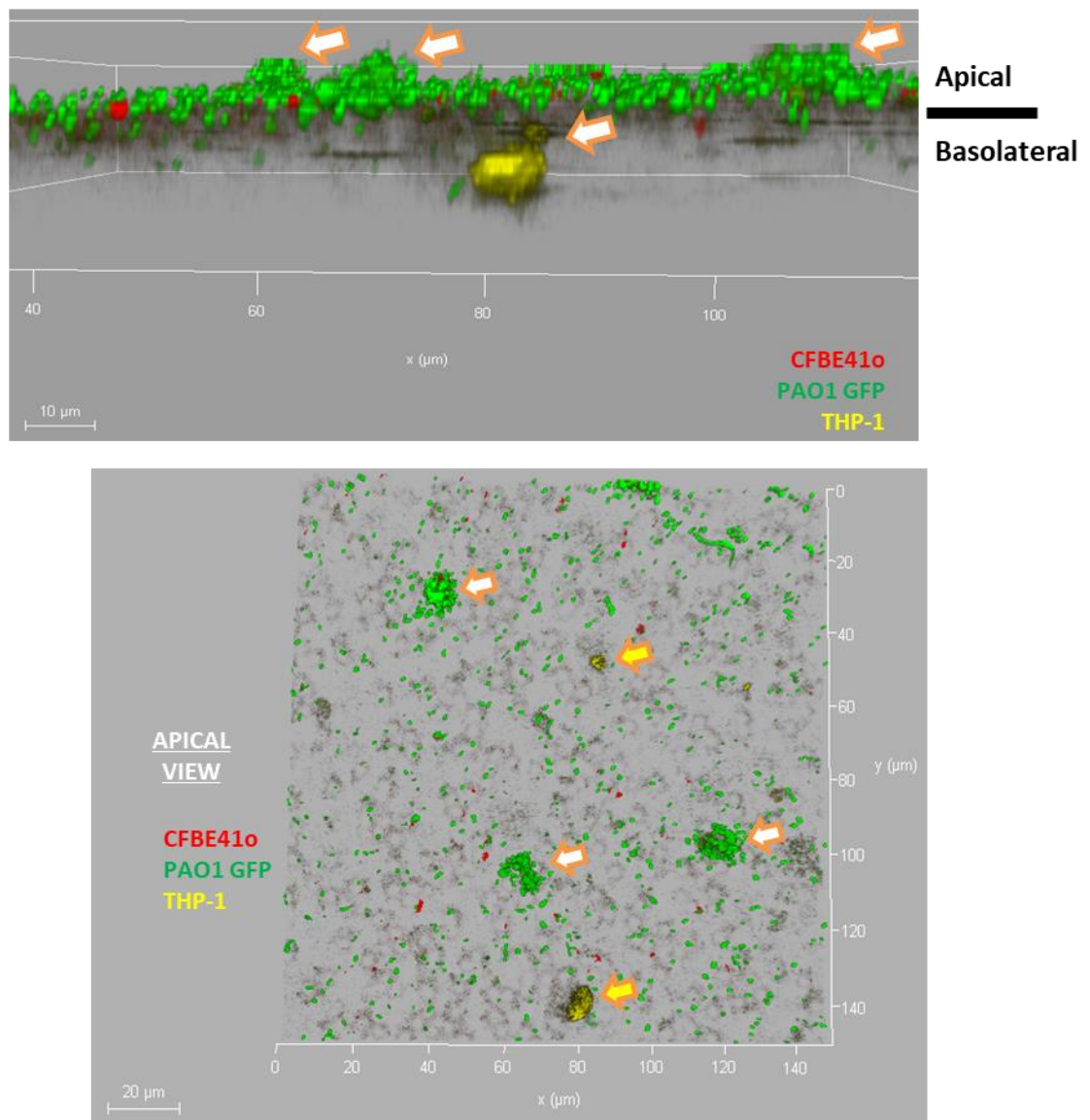
Figure 27. Confocal micrographs of co-culture establishment. A) Apical views per channel and cross-section of co-culture after 6 hours post-infection with macrophage transmigration (arrow). B) Apical view and cross-section of co-culture after 24 hours post-infection: the presence of resistant macrophages and formation of mushroom-like biofilm (arrows) — N= 2 independent experiments.

3.2.3. Macrophage transmigration and bacteria uptake through the transwell membrane and epithelial layer

To evaluate the combination of THP1-macrophages to the bottom side of a transwell membrane, we seeded 200,000 cells in 200µl of cell medium, and then we examined the recovery of macrophages onto the transwell after 1 hour of incubation. For each condition, the wells were followed for 1, 3, 6 and 18 hours after the macrophage seeding/incubation. We then fixed and mounted the membranes and used CLSM to image macrophages on the basolateral side.

We then investigated the kinetics of this migration on conditions of monoculture versus macrophages in co-culture with CF epithelial cells. Those observations were followed along time using CLSM of fixed samples at 1, 3, and 6 hours post-infection, as shown in figure 28. Cross-sections or orthogonal views were placed where the transwell membrane is in the middle as a separation of the apical and basolateral compartment. For the co-culture, the transwell area is filled with DAPI-stained CFBE41o-, while for monocultures of only THP-1 it is blank. At 1 hour, macrophages (red) are observed below the transwell membrane, while at 3 hours (and continuously at 6 hours), macrophages can be found in migration down-up towards the denser load of bacteria or infected CF epithelial layer. Notably, the co-culture reveals that is a biological barrier that does not allow bacteria to easily cross the membrane, but that selectively will enable macrophages to transmigrate to the air interface.

To further follow the role of this transmigration, we continued using CLSM to assess bacteria uptake by macrophages, as shown in Figure 29. For the macrophages monoculture, we used the orthogonal view from the z-stack-created 3D model; this allowed visualization inside the cells. For co-cultures, we used cross-sections after identifying the extension of the macrophage along the co-culture, either on basolateral side or apical side, depending on the time point assessed. Aligned with macrophage transmigration, bacteria uptake was also

occurring only after 3 hours post-infection and maintained at 6 hours. However, at 1h of macrophage monoculture when the macrophages are still at the basolateral side, bacteria can already be seen crossing the membrane to reach the cells, indicating that the macrophages do not immediately react and start migration even after bacteria has established at the air interface. While on the co-culture, there is the epithelial layer that can act as barrier and it communicates with macrophages to start migration; this barrier might prevent the detection of bacteria, as observed in fig. 29, 1hour.

Transmigration is one of the first actions derived from inflammatory signals[135], but we expect the modeling with this co-culture would also stimulate the inflammation scenario. On figure 30, we observe the kinetics (1, 3, 6, and 20 hours post-infection) of IL-8, IL-6, IL-1β, and TNF-α on mono and co-cultures. While *P. aeruginosa* is clearly a significant stimulus for inflammation, the time point of 6 hours is the best point to analyze future possibilities of anti-inflammatory therapy in the presence of the two cell types here considered. Plus, IL-8 and IL-1β are released as consequent of the co-culture establishment, while TNF-α is not and depends more exclusively on stimulation of macrophages.

Nuclei and cell layer of CFBE41o
THP1
P. aeruginosa

Figure 28. Kinetics of macrophage transmigration on mono and co-cultures. N= 2 images per sample of 3 independent experiments.

Monoculture THP1 + PAO1

Co-culture CFBE41o + THP1 + PAO1

1hpi

apical

basolateral

apical

basolateral

3hpi

apical

basolateral

apical

basolateral

6hpi

apical

basolateral

apical

Nuclei and cell layer of CFBE41o
THP1
P. aeruginosa
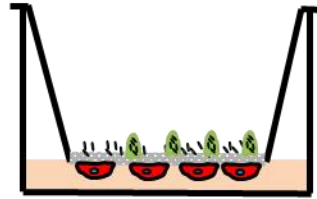
Monoculture THP1 + PAO1
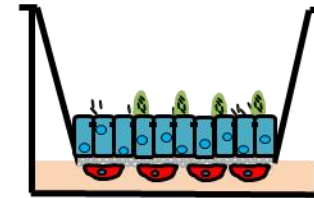
Co-culture CFBE41o + THP1 + PAO1
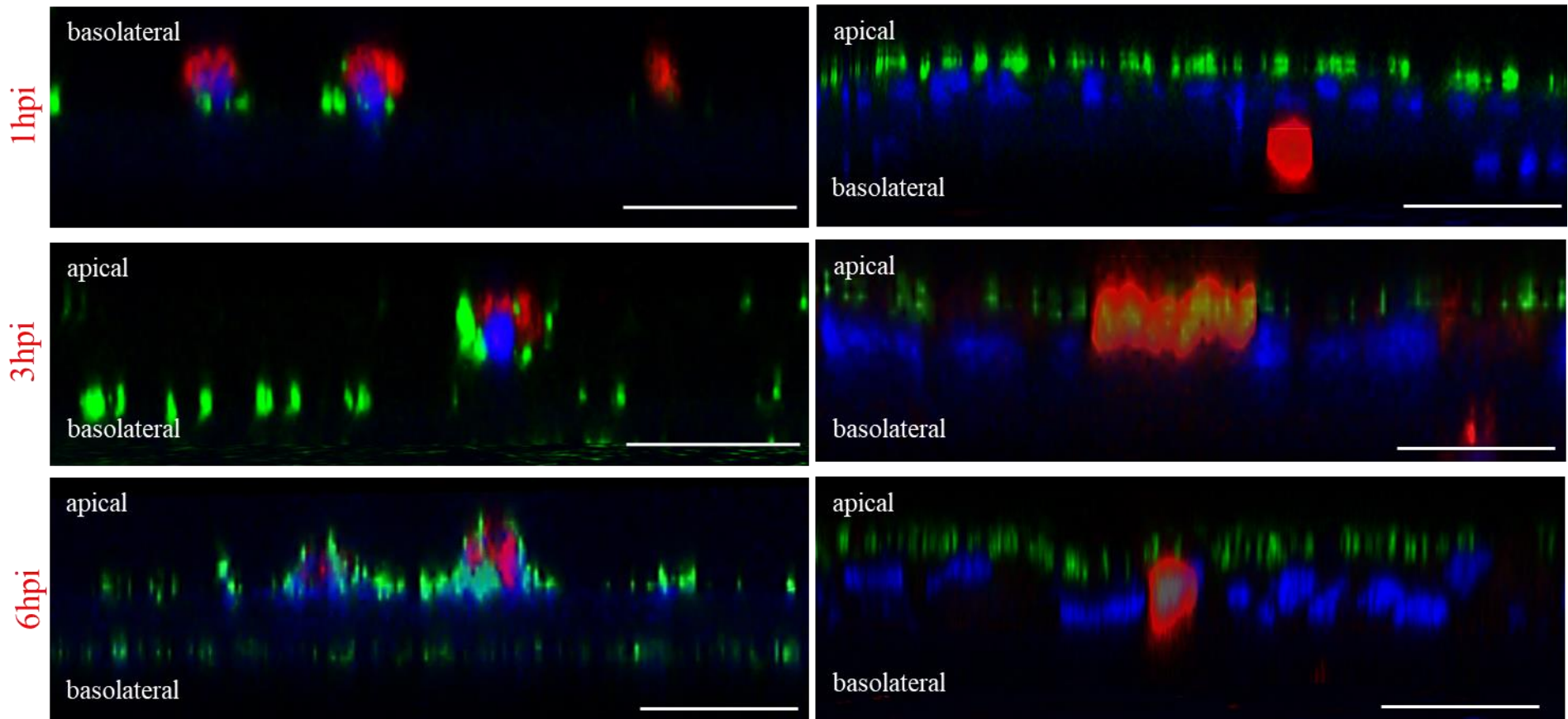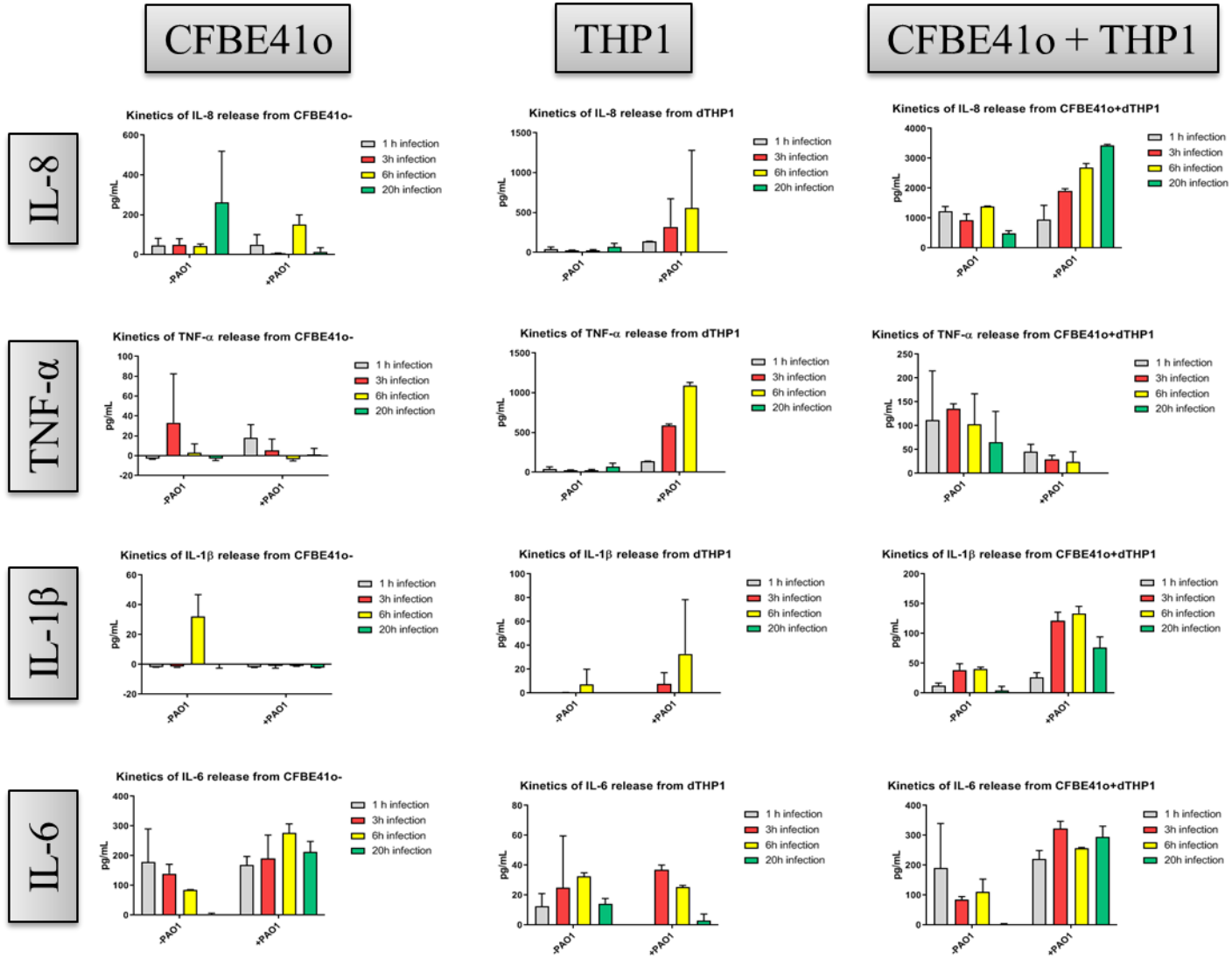
Figure 30. Supernatant results of cytokine release. A) Kinetics of uninfected and infected mono and co-culture releasing IL-8, IL-1β, TNF-α and IL-6. N= 2 independent experiments.

3.2.4. The pattern of ZO-1 tight junction in CFBE41o- mono or co-culture is expectedly disrupted with *P. aeruginosa* infection

Zona occludens is one of the main tight junctions relevant for any epithelial layer, also for the lung. The barrier formed by CFBE41o- cultivation is increased before and after co-culture establishment as observed in fig. 31. However, as expected, bacteria co-cultivation disrupts this barrier already after 6 hours of infection. This information can be quantified by measuring TEER, as will be shown in section 3.2.2.2. Particular regard must be taken towards the localization of ZO-1. At the confocal, one must look across the z-axis on the cell model to find the ZO-1, but, at the same time, not to confuse with the transwell signal. Plus, specific areas on the basolateral side must be observed to check if the presence of macrophages could influence the correspondent ZO-1 presence.
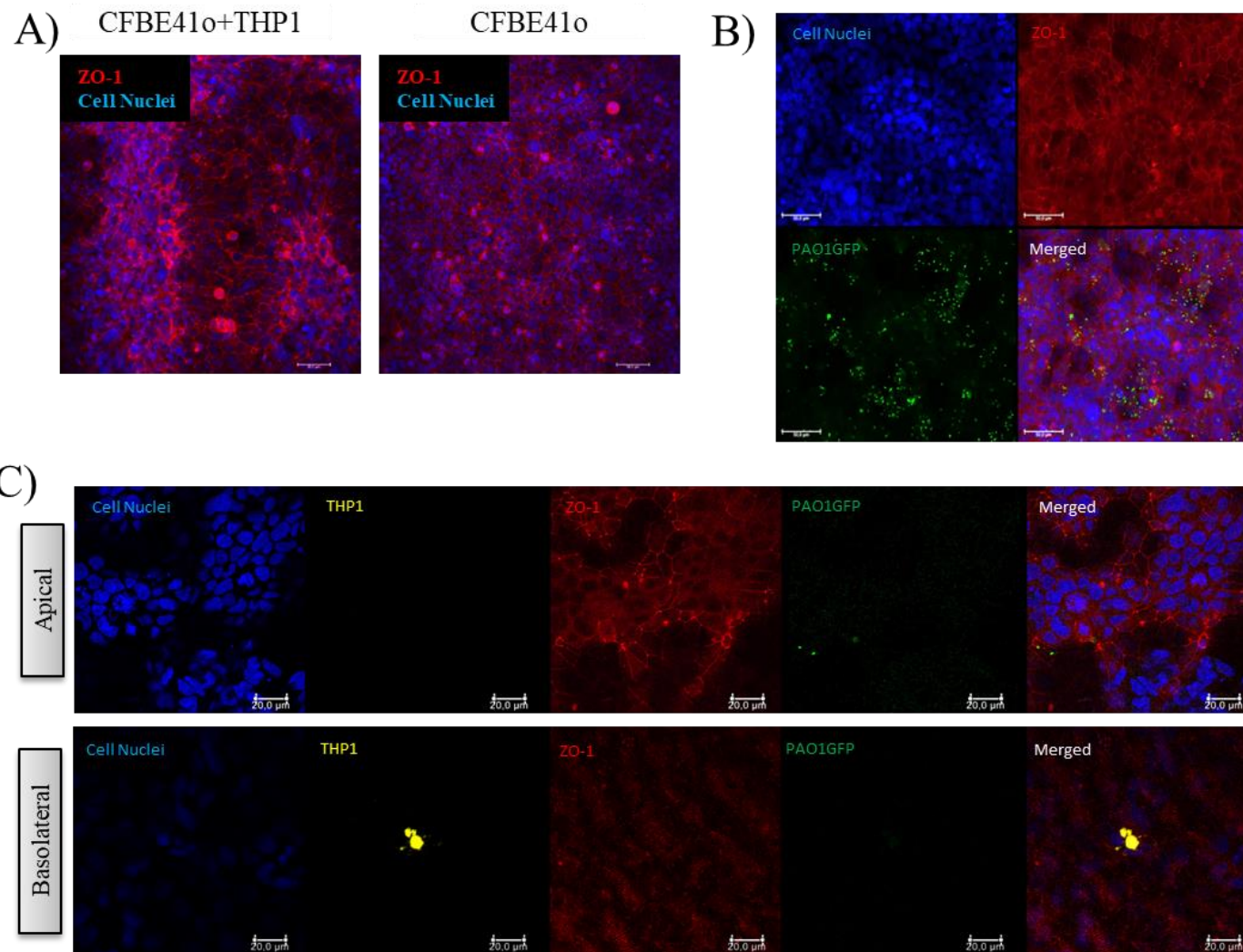
Figure 31. Investigation of ZO-1 tight junctions on the establishment of co-culture. A) ZO-1 on uninfected mono and co-culture of CFBE41o-cells. B) ZO-1 on CFBE41o-monoculture after 6 hours of infection. C) ZO-1 on CFBE41o-+ THP1 co-culture after 6 hours of infection. N= 2 images per sample of `2 independent experiments.

3.2.5. Treatment of infected co-culture

3.2.5.1. Biocompatibility and antibacterial effect of Tobramycin on CFBE41o- cells and *P. aeruginosa* PAO1-GFP

The most prescribed aminoglycoside antibiotic in CF disease is tobramycin. We chose a range of 0.1 to 1000 µg/mL of tobramycin. The analysis was towards the possibilities of dose increase versus antibacterial effect at 50 and 90% of the MIC against *P. aeruginosa*.

The high concentration of tobramycin had no cytotoxic effects on CFBE41o- cells after 24 hours of incubation (fig. 32A and B). Analyzing the kinetics of a tobramycin range of concentrations, 1 to 4 µg/mL of tobramycin allows bacterial proliferation on the first 1 to 8 hours of incubation (fig. 32C), but focusing on 24 hours of incubation 50% of bacterial growth was contained using 6 µg/mL of tobramycin, which, then, was the adopted concentration for further assays.
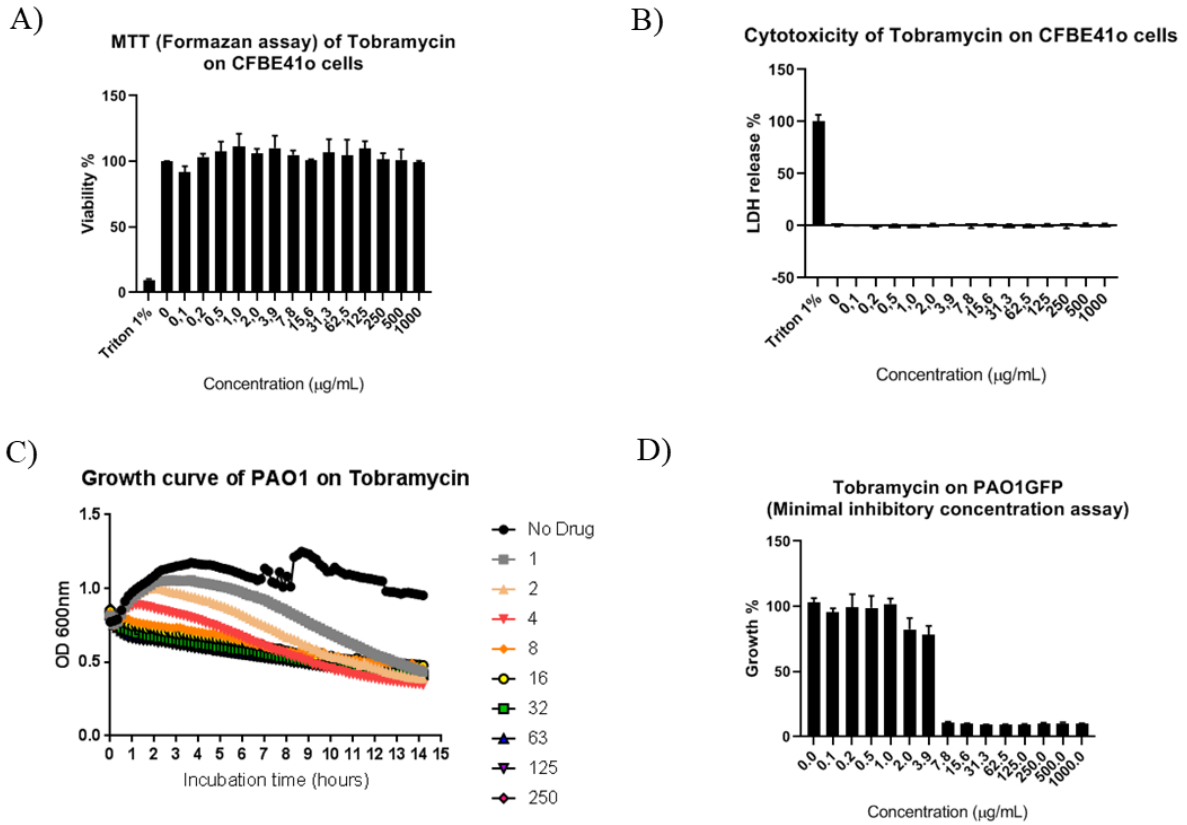
Figure 32. The activity of tobramycin on *P. aeruginosa* PAO1-GFP and biocompatibility on CFBE41o- cells. A) MTT assay for the viability of CFBE41o- cells within a range of 0.1 – 1000 µg/mL (24h). B) LDH release for cytotoxicity of CFBE41o- cells within a range of 0.1 – 1000 µg/mL (24h). C) Kinetics of antibacterial activity of tobramycin (1-250 µg/mL) on PAO1. D) Antibacterial activity of tobramycin after 24h of interaction with PAO1. N= 2 independent experiments.

3.2.5.2. Cytotoxicity and TEER values on the infected co-culture

Markedly, the induction of cytotoxicity is lower than expected for the bacterial challenge on the release of lactate dehydrogenase (fig. 33A), and in none of the time points analyzed, the LDH levels were above 40%.

In 1h, there is about 20% LDH release for CFBE monoculture and co-culture with infection. However, in 6h, non-infected CF monoculture and on the co-culture there is a release of LDH. This result is also seen in another report in which PMA is used as activation agents for THP-1 macrophages in co-cultures[136].

While at 20 hours post-infection, the observed cell death in other methods is not correlated to the alterations in LDH release, unless for non-infected co-culture. Here the literature reveals that variables as pH, media with sodium pyruvate, or production of certain acids might cause problems on the detection of LDH[137]. We recommend to this issue to be further investigated, however we focused on the timepoint of 6 hours to combine results with other important varaibles peaking at this time.

Nonetheless, co-culture conditions at 6 hpi show 20% of LDH for infected samples and a complete statistically significant decrease after tobramycin treatment, which is not observed for epithelia monoculture conditions.

The epithelial barrier integrity was checked via TEER, in co-cultures and monocultures (Figure 33B). After 6 and 20 hours, no difference was observed between the TEER of CFBE41o- in uninfected monoculture or co-culture. The infection, however, disrupted the barrier, as observed by the drop in the TEER. Nevertheless, once the cultures were treated with Tobramycin, the epithelial barrier integrity was restored, as observed by higher TEER values.

However, at our main timepoint of 6 hours, only on co-culture samples, we observed barrier recovery on infected tobramycin-treated cells (6hpi) and that this recovery is as high as it was for the uninfected cells. These results should be further analyzed on the regulation of tight junctions versus cells or the stability of other components of the co-culture.
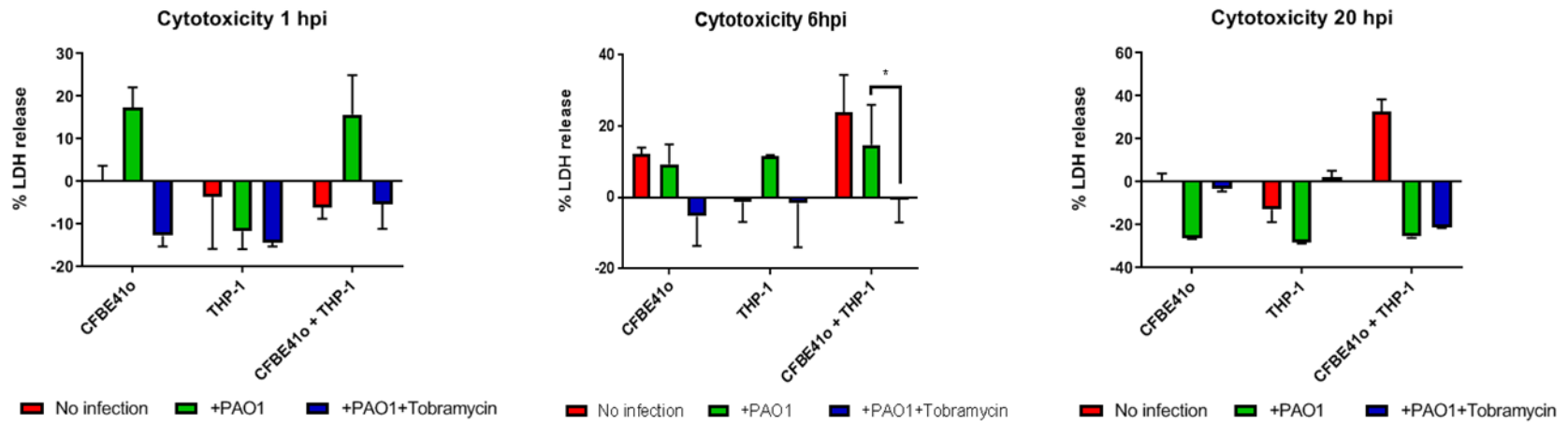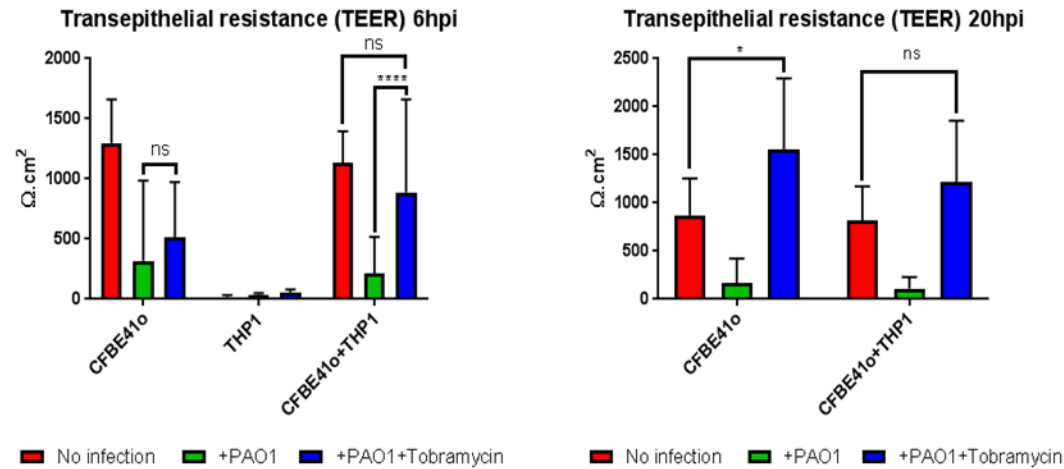
Figure 33. Biocompatibility of co-culture, infection and tobramycin treatment. A) Kinetics of LDH release assay on mono and co-cultures, treated and untreated. B) TEER measurements at 6 and 20 hpi on mono and co-cultures. N= 3 independent experiments.

3.2.5.3. Co-culture decreases CFU while tobramycin masks biofilm formation

Our previous results showed that macrophages migrated from basolateral to the apical side of the transwell, crossing the epithelial layer and uptaking *P. aeruginosa* (Fig 29). Confocal microscopy shows that bacteria aggregates are still formed even with the presence of macrophages on top of the CF epithelia (Fig 34).

Figures 35 A and B shows differential growth of adhered/internalized bacteria at 6 hpi grown in presence versus absence of human cells, but no difference in between the cell types used as substrate. Importantly, in tobramycin-treated samples for 6h, no bacteria colony was observed, although we have seen bacteria by the confocal microscopy (fig. 34). However, at the 20 hpi time point, treated samples now present cultivable *P. aeruginosa* on agar plates (Figure 35 D and E) (probably because there is no more pressure of host cells as observed on earlier confocal micrographs).

To further evaluate the results of tobramycin, we re-analyzed CFU 6 hpi (adherent/internalized bacteria). "Tobramycin killing" is then defined as:

Tob killing (log_{10}) = log infected not treated – log infected Tobramycin treated

Figure 35C shows the results comparing tobramycin killing 6hpi when PAO1 is alone and when PAO1 is on the co-culture. An approximate 1 log is the statistical difference between these groups. However, the same does not occur when the analysis is at 20 hpi.

Although the presence of human cells influences tobramycin to have an enhanced efficacy[138], our results showed bacteria with cells forces a decreased antibiotic efficacy. Further studies are required to check if the presence of cells influences on bacterial rate of growth or if the spatial availability is a variable on growth, and consequently CFU impact after treatment.
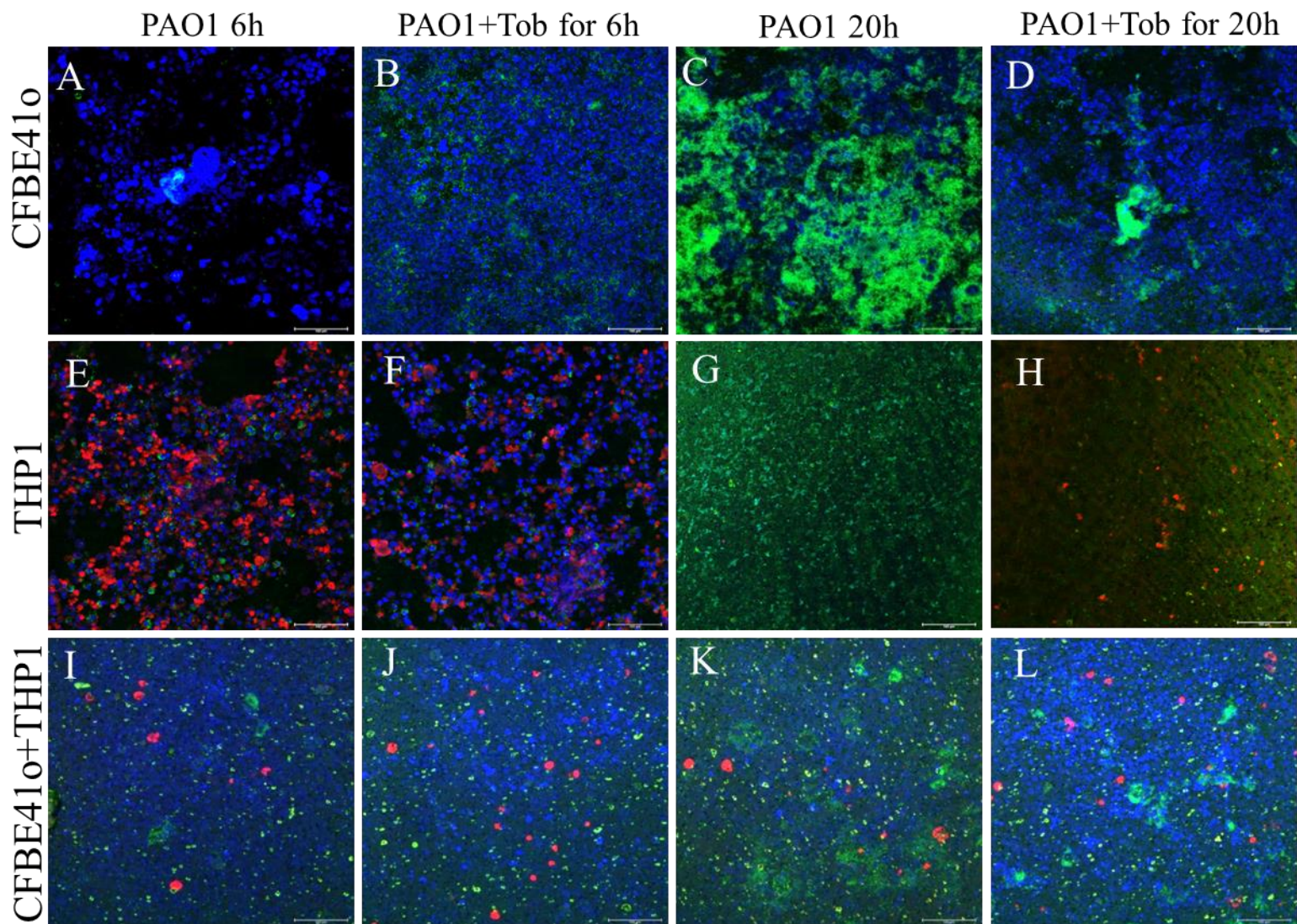
Figure 34. Confocal micrographs of mono and co-cultures with and without treatment with tobramycin 6μg/mL. From the acquisition of zeta stacks from the apical side only of the samples, DNA is stained by DAPI (blue), macrophages (red) and *P. aeruginosa* (green). N= 2 images per sample of 3 independent experiments. Scale bar 100μm
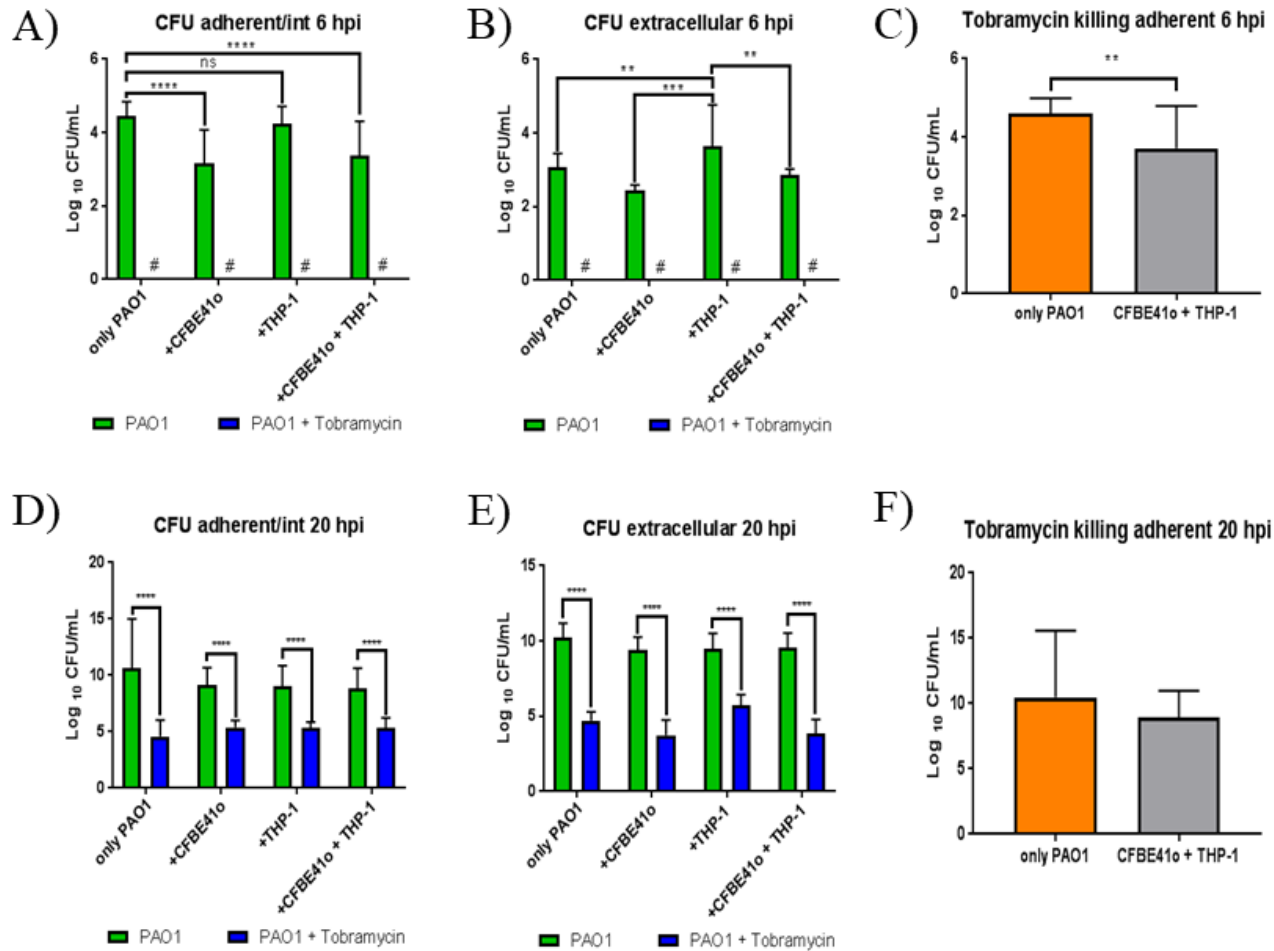
Figure 35. Bacteria proliferation on mono and co-culture at 6 and 20 hours post-infection. A) Colony-forming units (CFU) of adherent/internalized bacteria after 6 with tobramycin 6µg/mL treatment. B) CFU of extracellular bacteria after 6 with tobramycin 6µg/mL treatment. C) Tobramycin killing effects compared on bacteria alone versus bacteria on top of co-culture at 6h of infection. D) CFU of adherent/internalized bacteria after 20 with tobramycin 6µg/mL treatment. E) CFU of extracellular bacteria after 20 with tobramycin 6µg/mL treatment. F) Tobramycin killing effects compared on bacteria alone versus bacteria on top of co-culture at 20h of infection. N= 3 independent experiments.

3.2.5.4. Co-culture conditions increase immunological response without alterations from tobramycin treatment

To further evaluate the inflammatory response in our co-culture model, we checked the inflammatory response by looking at a panel of inflammatory cytokines (Figure 36). These are characterized as the following:

1. Pro-inflammatory signaling:

IL-6, IL-11, IL-1α, IL-18, IL-8, TNF-α, IL-1β and IFN-γ

2. Anti-inflammatory signaling:

IL-12p40, IL-23, IL-27, IL-10

3. Adaptive immunity:

IL-15, GM-CSF, IL-21, TSLP

From those 16 cytokines tested, we detected 6 cytokines that showed a higher release in the co-culture (IL-1α, IL-8, IL-12p40, IL-18, IL-23, TNF-α) and other 10 that did not show significative release (GM-CSF, IFN-γ, IL-1β, IL-6, IL-10, IL-11, IL-15, IL-21, IL-27, TSLP). Indeed these last 10 cytokines were previously released by the uninfected co-culture, which could account for their low secretion level after the infection.

Notably, treatment with tobramycin as the established conditions did not reduce the inflammation. Evaluating IL-8, IL-6, and IL-1β (fig. 30) revealed cooperation of epithelia and macrophages when in co-culture condition, providing an inflammation scenario reflecting the clinical correlation of *P. aeruginosa* in the cystic fibrosis lung environment [58,139].

Despite the seen moderate inhibition activity in the literature[140], the use of tobramycin (blue bars) has shown no cytokines decrease, except for IL-6 on the monoculture of macrophages versus the co-culture.
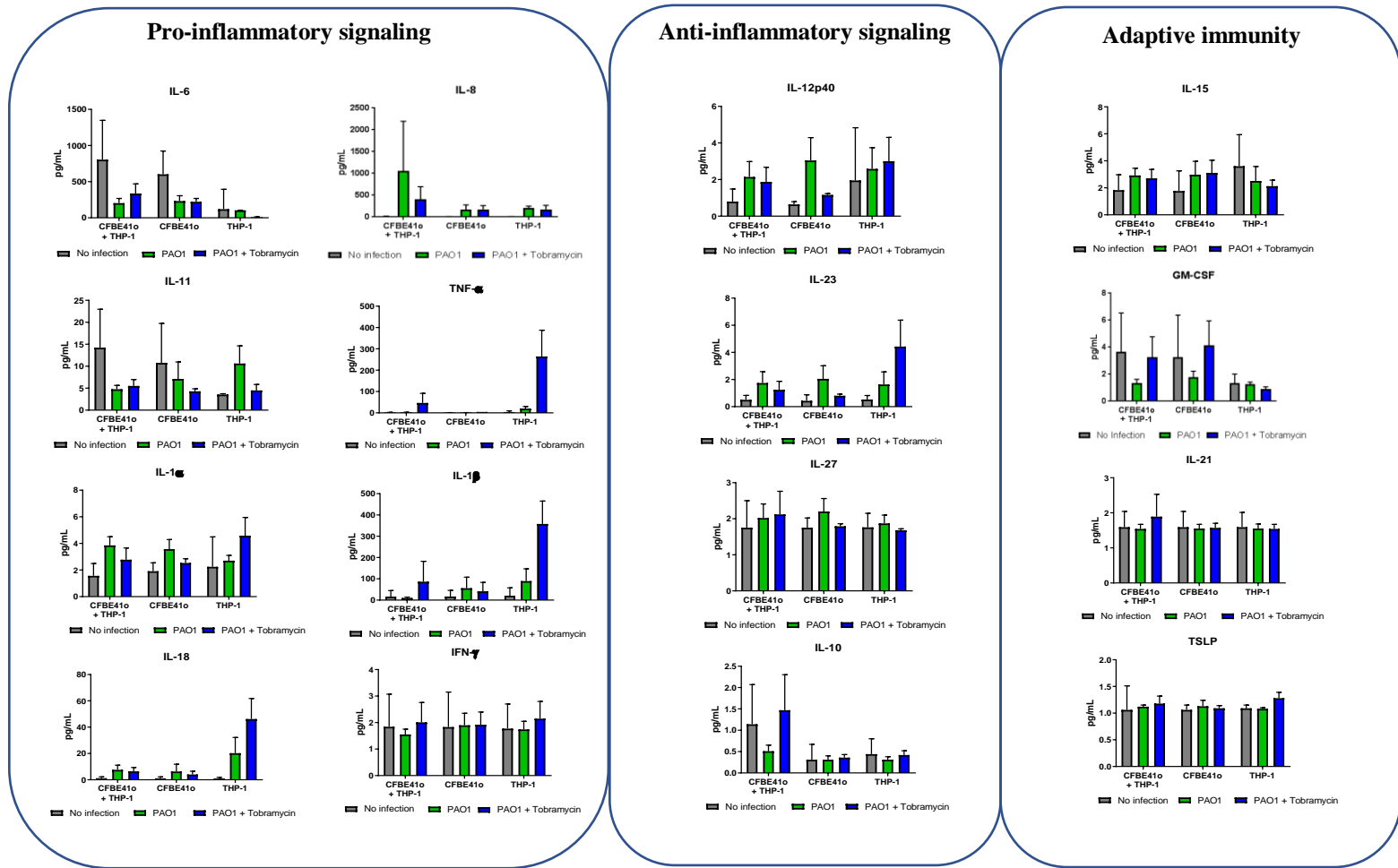
Figure 36. Supernatant results of cytokine release. Cytokine panel via flow cytometry of GM-CSF, IFN-γ, IL-1α, IL-1β, IL-6, IL-8, IL-10, IL-11, IL-12p40, IL-15, IL-18, IL-21, IL-23, IL-27, TNF-α and TLSP. N= 3 independent experiments.

3.2.5.5. Virulence factors can also be detected during co-culture conditions

Pyocyanin and pyoverdine are quorum-sensing molecules from the Pseudomonas quinolone signal (PQS) system[141]. Usually, these molecules are detected in *P. aeruginosa* biofilm growing on plastic substrate[142,143]. We then asked whether these molecules could also be detected in our co-culture model, which would be necessary for drug testing aiming to inhibit biofilm communication.

By using our system, with cells seeded on transwell, we could not detect pyocyanin or pyoverdine. Therefore we adapted our co-culture model to the 24-well microplates, keeping the same cell density. These changes allowed us to measure those quorum-sensing molecules.

As seen in Figure 37, pyocyanin and pyoverdine can also be quantified when human cells are present, but not on time points as early as 6 hours post-infection (Figure 37A). Although the levels do not change in between the different types of cells versus bacteria alone, tobramycin reduces pyocyanin and pyoverdine levels that could prevent biofilm formation because of bacteria-killing (Figure 37B, C). We used a synthetic PqsR inhibitor, HIPS1121, and this novel compound is able to exclusively regulate pyocyanin without direct bacteria killing[144].
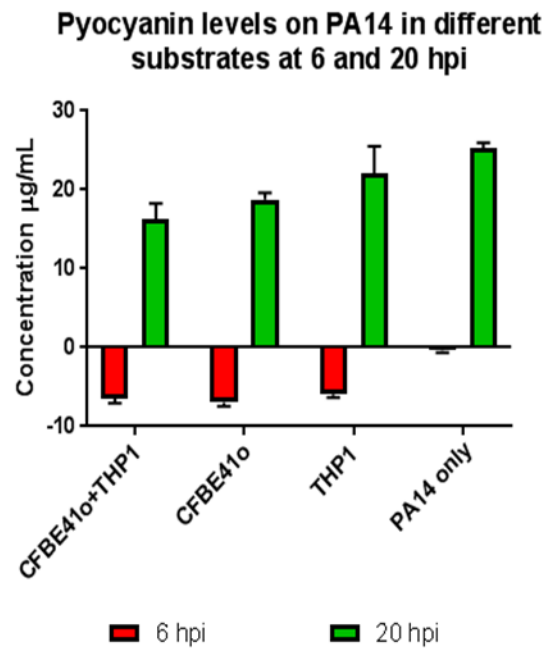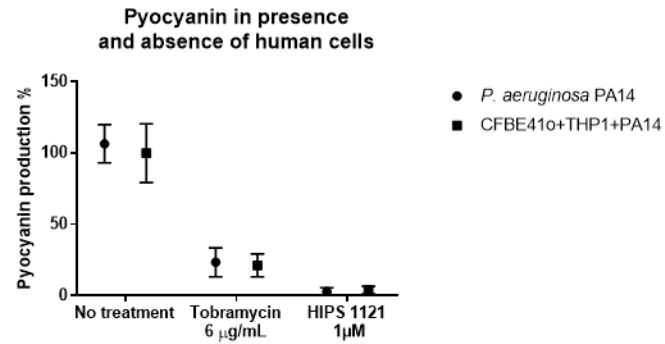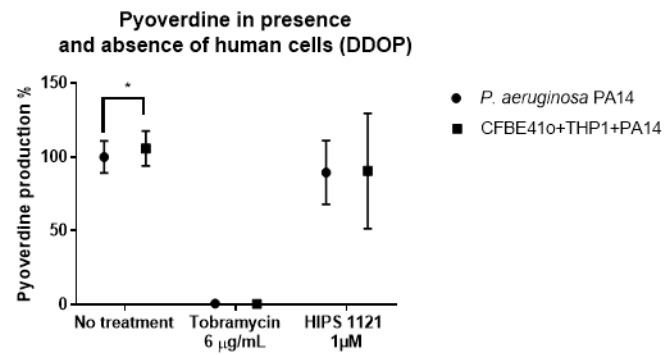
Figure 37. Measurement of virulence factors on mono and co-cultures transferring from the transwell to the flat plate model. A) Kinetics of the detection of pyocyanin on mono and co-cultures. B).Pyocyanin results of PA-14 infected co-cultures treated with tobramycin (6µg/mL) and pathoblocker HIPS1121 (1µM). C) Pyoverdine results of PA-14 infected co-cultures treated with tobramycin and pathoblocker HIPS1121. N= 3 independent experiments.

3.3. Discussion

In this investigation, we used the interaction of *P. aeruginosa* bacteria against abiotic and selective biotic substrates that could mimic the CF bronchial airways. On establishing a model of CF bronchial epithelia, macrophages, and *P. aeruginosa* we reveal alterations on host response and bacteria adaptation on top of human cells. On mimicking the bronchial area, we used a model of macrophage adherence based on the need for immune cells to migrate from the bloodstream towards the air interface to reach the bacteria infection.

The immune system is present during the evolution of bacterial growth, and the bronchial region of the lung is in contact with bacteria via the air interface during breathing. In the proceedings of acute infection, the epithelial layer senses danger signals of the bacteria and starts the recruitment of the immune cells[22]. For the specific case of the upper airways, this recruitment requires the transmigration of immune cells from the bloodstream, passing through several cell layers until reaching the air interface where the infection is taking place[145]. The proposed model involves a human Cystic Fibrosis bronchial epithelial cells, human macrophages, and *P. aeruginosa*. With this set, it is possible to evaluate i) the formation of a confluent lung epithelial layer, 2) the macrophage transmigration mimicked from basolateral to apical side of the Transwell® membrane, and 3) development of planktonic *P. aeruginosa* into an early biofilm.

Approaching drug testing, most reports include the use of animals and, even though the cost is high, *in vivo* research is still a majority. That said, by using animals, we fail to characterize details and steps during therapy response or other processes more related to cell behavior, including chronicity of infections. We opted for Cystic Fibrosis Bronchial Epithelial (CFBE41o-) cell line as a diseased model for the airways. This cell line is known to maintain an essential mutation associated with CF, the ΔF508. Moreover, more

characteristics are associated with CFBE41o-, as chloride transport impairment with high transepithelial resistance of an epithelial barrier formation [146].

The infection of CFBE41o- using *P. aeruginosa* has been described, mainly using a flow-cell chamber model with supplementation with arginine on the cell media composition to improve epithelial cell survival and support biofilm formation [147]. There, it was already observed that bacteria grown on top of cells were 25 times more resistant than bacteria alone and that the mutation from the CF cells increases the release of iron, consequently helping biofilm formation. Besides infection, the addition of immune cells has been used on bronchial cells. Ding *et al*. [104] used mouse Lewis lung carcinoma cells on Transwell® in combination with macrophages on the basolateral side and infected with *Staphylococcus aureus*, another critical pathogen of chronic infection in CF patients. Their method granted the observation of different macrophage movements (including Transwell®-cell transmigration) and even bacterial phagocytosis.

Our studies build a new model using only human cells grown at the air-liquid interface, in a Transwell® model that can be scaled-up for more than one well, if compared to a flow-chamber. The inclusion of THP-1 differentiated macrophages is an advantage for using a human immortalized cell line, instead of depending on the reproducibility and obtainment of primary cells from donors. By adding these macrophages on the basolateral side of a Transwell® insert, we could observe these macrophages not only create protrusions to reach the apical side, but also to follow transmigration.

With our results, we obtained a model that includes epithelia, macrophages, and bacteria, as seen in Figure 1, and three main accomplishments: i) observation of early biofilm formation after 6 hours, ii) macrophage transmigration, and iii)maintenance of epithelial cell survival. The next steps include using confocal microscopy to understand the development of

these 3 variables when into the co-culture. Importantly, our studies on macrophage transmigration show that the epithelia for a transwell model represents a natural barrier for bacteria (fig. 24), but instead a selectively permeable barrier to the diffusion of inflammatory mediators and its consequent stimulation of macrophage transmigration.

Notably, comparing treated samples and the rest of bacteria growth (tobramycin killing) on the only PAO1 versus PAO1 on co-culture, bacteria on top of cells react less to tobramycin treatment (Fig. 4C). Although the presence of human cells influences tobramycin on an enhanced efficacy[138], our results showed that using tobramycin as treatment responds differently when comparing bacteria alone versus bacteria in the presence of cells.

Marquis-Moreau *et al.*[147] observed resistant bacteria onto human cell growth; however, their model approaches treatment aimed for biofilm eradication, which means there was biofilm growth for 6h and then following tobramycin treatment. On our data, we show results on treatment performed at 1 hour after the bacterial adherence, focusing on the treatment of acute infection and possibly influencing further experiments on re-infection.

An adhered/internalized fraction, after human cell lysis and the removal of planktonic bacteria, is the most important on what has remained with or without treatment. Actually, the evaluation of different fractions will give you different answers accordingly: when you look at the bacteria that are adhered/internalized you are considering the population that remains attached to the bronchial tissue, as it is *in vivo*. In this case, the killing (20 hpi), after tobramycin treatment, is 10x times higher on bacteria alone than bacteria on top of cells.

The conclusion from this data must come with the thought that usually drug testing is performed on bacteria alone, hence the MIC, MBIC (biofilm inhibition), or MBEC (biofilm eradication) assay. When using just bacteria on abiotic surfaces, there is more killing, a finding that does not occur on bacteria grown on top of human cells, on the mimicking of

what happens *in vivo*. An overestimation of drug/antibiotic efficacy then occurs on the simplification of drug testing, either for planktonic bacteria, but even worse in the case of biofilm bacteria.

Pyocyanin and pyoverdine are quorum sensing-dependent PA-exclusive secondary metabolite regulated by the *Pseudomonas* quinolone signal quorum-sensing system (PQS-QS)[82,148]. In a recent report, only pyoverdine and not pyocyanin were recovered from the growth conditions applied to the co-cultivation of bacteria and human cells[118].

With our conditions, not only these phenazines were recovered on wells with bacteria alone, but also both pyoverdine and pyocyanin were recovered on bacteria that used the human cells as substrate. For us, the recovery of these compounds was only possible at 20 hpi, but not at 6 hpi (fig. 37A), which might be associated with the MOI variation.

In a similar fashion to Orazi and O'Toole[118], we also found there was a small difference of pyoverdine release when comparing bacteria on plastic versus on top of cells (fig. 37C). And, the same trend is observed for untreated samples on the version of pyocyanin (fig. 37B).

Although plastic versus cell did not show differences, this is a positive outcome for drug screening, in which at least for those compounds the interaction cell-bacteria may not be disturbed by differential cultivation.

The testing of tobramycin and HIPS1121, quorum-sensing inhibitor, shows the usefulness of the method and possibility of future combination of indicators that analyze bacteria and cells at the same time. The use of tobramycin has decreased levels of pyocyanin and pyoverdine. However, the reduction in pyocyanin was 75%, which means there will still

be a remaining level of pyocyanin to influence biofilm formation. If that would be enough to promote biofilm growth and other bacterial modifications should be further investigated.

HIPS1121 is a pathoblocker in a concept that biofilm control not always needs to be understood through the reduction of bacterial proliferation but on the decrease of virulence factors. This compound was confirmed to completely extinguish the release of pyocyanin since it influences directly on the PQS system, but not on the production of pyoverdine.

With differential bacteria growth, also host response can be altered. Observing figure 6, sixteen cytokines have been analyzed after infection, but even after tobramycin treatment. At first glance, we see success on the co-culture to provide the mimicking scenario resembling CF disease, especially for cytokines involved with pro-inflammation and neutrophil recruitment, linked with type-I interferon response. The immediate advantage observed is the maintenance of the levels during co-culture conditions within the majority of the detected cytokines, translating the inflammation scenario, but now with the combined cell types.

In fact, John *et al*[149] demonstrated with immunochemical histology assays that CF bronchial epithelial cells can show significantly reduced expression of TLR-4. This would directly regulate the release of IL-8 and impair local innate immunity, especially under the stimulation with *P. aeruginosa*. This sparkled that CFTR mutations from CF might be responsible for a state of hyper inflammation seen in patients. Although some work[150] has been done to clarify this, there is a limited understanding of the cytokine network during CF. The cytokines analyzed are limited central regulator cytokines like IL-8 and TNF-α, which can present in numerous secondary messenger cytokines affecting different aspects of innate and adaptative immunity.

We were expecting i) PA to be a potent stimulus for cytokine release and ii) the reduction on bacteria growth upon tobramycin treatment would rescue the inflammation. Because of CF alterations on the airways, this remodeling induces bronchiectasis and neutrophilic recruitment, which are very early characteristics of CF; plus, this is observed in a controversial state of absence of infection related to a combination of necrosis, hypoxia, and activation of the inflammasome via IL-1α[151]. On that note, Fig. 6 grey bars show cytokine release without infection during the set-up of the co-culture, which can be associated with the formation of the epithelial layer and aging, plus the transition/activation of THP1 monocytes to macrophages.

Although we did not measure cytokines versus multiplicity of PA infection, the observed bacteria growth, release of virulence factors and early biofilm would serve as a stimulus for a hyper inflammation state. Indeed, the fact that CFTR is a pattern recognition receptor for microbial sensing and the combination with the mutations related CF what impairs a strong inflammatory response[53]. This duality is demonstrated when 6 (IL-1α, IL-8, IL-12p40, IL-18, IL-23, TNF-α) out the 14 detected cytokines could be increased with *P. aeruginosa* challenge.

This network has been producing new hopes for therapy, as anti-TNF antibodies could potentially reduce inflammation and tissue damage[152]; although in practice, there is more concern on its medicine safety and the limiting inflammation to disarm immunity from opportunistic infections[153]. The opportunity can now be directed from other cytokines as future targets.

IL-1β is dependent on monocytes, in our case, from the interaction of CF epithelia and macrophages. Results of Figure 6 shows there is cooperation when CF epithelia and macrophages are combined into the co-culture. Furthermore, this cooperation can be

explained precisely because CF epithelia do not produce IL-1β, but it expresses IL-1 type I receptor (IL-1RI), IL-1 receptor accessory protein (IL-1RAcP), and IL-1 receptor antagonist (IL-1Ra) [154].

Bonfield *et al.*[154] describe alterations in CF human lungs. They measure the cytokines IL-10 (anti-inflammatory) and the pro-inflammatory IL-8 and IL-6, showing that CF patients do not release IL-10 and have higher levels of IL-8 and IL-6.

For that, we continue the exploitation of our co-culture model by measuring the pro-inflammatory cytokine IL-6 that activates the adaptive immunity through the maturation of T and B-lymphocytes[155], so the connection between the innate and adaptive immunity gains contributions from both the CF epithelia and macrophages; nonetheless, the co-culture maintains same levels of release. In general, the key messages by analyzing IL-8, IL-1β and IL-6 are the contributions of both cell types (in co-culture) for different cytokines.

Despite lower levels of TNF-α and IL-1β (central macrophage-releasing cytokines), the co-culture still secrete secondary cytokines from the TLR-4 domain, like IL-8 and IL-6.GM-CSF deficiency can impair the function of alveolar macrophages in a knock-out mice model of infection[156], while the neutralization of IL-27 in septic mice significantly improved survival and clearance of bacteria from the lungs of septic mice infected with *P aeruginosa*[157]. Both of those functions to be critical points of the development of sepsis.

As the second line of defense, adaptive immunity promotes the clonal expansion of lymphocytes and IL-6 is present to differentiate and mediate survival of T cells, as CD4$^+$ as long-lived memory T cells[158]. Still, in type 2 immunity, a similar role has been associated with TSLP as an alarmin derived from tissue damage; this cytokine is only known to play a role in helminth infection and asthma[159], but its involvement in pro-fibrosis should also be investigated for the pathological scenario of CF. As cascades of cytokines are altered during

diseases, other mechanisms to salvage immune cells can be achieved, for instance, as IL-15 therapy was found to increase Bcl2, an antiapoptotic protein, and to avoid death of crucial cells and NK and CD8^{+} T cells during sepsis[160].

While most cytokines were not affected by tobramycin treatment, we evident the trend of control of cytokines as IL-8 that would prevent neutrophil recruitment and the maintenance of IL-10 on the promotion of inflammation inhibition. In fact, the use of cytokines as therapy, at least in our model, can be further investigated as IL-11 has been shown to increase survival rate of a sepsis model, with the advantages of controlling inflammation via the production of TIMP-1[161], plus the known IL-10 which via inhibition of MHC class II and several other cytokines is considered the main anti-inflammatory cytokine[162]. However, even IL-10 as a master regulator of infection can be misused since early neutrophil and macrophage recruitment are instrumental developments to clear bacteria from the lungs[163].

The response to tobramycin is crucial to establish a CF model, especially on tobramycin being effective on inhibiting *P. aeruginosa* and even on biofilm mode of growth [164,165]. Our result shows no significant alteration of cytokine levels with treatment, what corroborates the incentive of adjuvant drugs on the control of inflammation, but supports a comprehensive investigation of antibiotic efficacy on adapted bacteria to correlated lung environments.

We must consider that the concentration used here is in the MIC range; despite that, it was not possible to eliminate all bacteria as observed by confocal microscopy. This could justify the non-antiinflammatory characteristic of tobramycin as a consequence of remaining bacteria to subsequently continue the induction of inflammation.

It is then recommended to analyze differential bacteria growth versus host response, based on the comparison towards increased efficacy of antibiotics on bacteria grown on plastic than on 3D cultures [138] and on the inefficacy of this class of drugs on precisely controlling the associated inflammation[166].

Some limitations can be pointed out related to the use of CLSM on the identification of bacteria uptake, as this does not show an individualized bacterium that could ease the quantification, and we recommend a follow-up study with techniques as flow cytometer and super-resolution microscopy. Limitations of this co-culture are related to the options we make when designing the complexity of the system. Ongoing improvement of the system would include the cultivation of biofilm on top of human cells for a period in which there is a mature biofilm with completely formed extracellular matrix and persister bacteria. A further addition would be to include mucus to investigate the effect of its changed rheology under the conditions of Cystic Fibrosis.

In conclusion, we provided a new platform for the analysis of bacterial growth (including *P. aeruginosa*) to create an environment that is particular to the bronchial airways with the incentive of macrophages transmigration. This creates a model that shows an epithelial integer layer as a permeably selective barrier, and it contributes to the understanding of how a close-related model can provide differential insights on antibiotic efficacy while responding to bacteria in synchrony with the host lung.

Chapter 2: Future applications for the co-culture: HL-60 as neutrophil-like cell and its use as potential nanoparticle hitch-hiking

1. Introduction

On CF, excessive inflammation is characterized by the infiltration of airways with neutrophils that fail to prevent extreme infection from the predominant microbes as *P. aeruginosa*[167]. This failure could be related to the defects on CFTR protein as well as the effects seen on the epithelia, mostly because the control of apoptosis on CF neutrophils is altered.[168] Nonetheless, one of the main issues with early neutrophil is the excess of oxidative stress; a strategy that is supposed to help kill bacteria but turns to injury the lung.[169]

Non-apoptotic neutrophils bring a negative correlation to lung function, and it promotes decline during CF disease[170]. However the prevention of neutrophil to die and release its contents might be inevitable.

The release of neutrophil content is known as respiratory burst, which in CF the impairment of this process will influence the degree of bacterial phagocytosis[171]. What occurs is that the frustrated phagocytosis and increased apoptosis of neutrophils overwhelm the lung with increased ROS and proteases. The effects of this increase are observed when pattern recognition receptors and opsonophagocytic receptors are cleaved, impairing the proper function of neutrophils[172].

If bacteria is uptaken by neutrophils, there is the formation of azurophilic granules containing antimicrobial molecules. If there is no phagocytosis, the neutrophil starts its programmed death. The release of its content counts with the last strategy for bacterial trapping: neutrophil extracellular traps (NETs)[173]. Some of the strategy and neutrophil reactions can be seen in figure 38.

Neutrophils are migratory cells that, after chemical signal move towards the bacterial targets (chemotaxis) and this is one of the bases of the innate immune system, for instance, in

wound healing.[168] For pursuing bacteria, neutrophils seek different gradients of formylated peptide as N-Formylmethionyl-leucyl-phenylalanine (fMLP) and these molecules together with LPS will stimulate e TLR4 and the IKKβ-IκBα signaling pathways to induce inflammation.[174]

In vitro, primary neutrophils are not easy-to-cultivate cells, and their lifetime after blood extraction is from 6 to 8 hours.[175] So, immortalized cell lines are the stable option for the modeling disease and cell interaction. HL-60 cells are human caucasian promyelocytic leukemia cell line and several reports have accomplished to use this cell as model for neutrophils[176–178].

Chu *et al*[179] reported that bovine serum albumin nanoparticles could be fed to neutrophils to hitchhike the activated cells and cross the endothelial barrier from the bloodstream towards the tissue. By loading those nanoparticles with an NF-κB inhibitor or with cefoperazone acid to hitchhike on neutrophils, those loaded-activated cells were used as treatment on *in vivo* of LPS inflammation and *P. aeruginosa* infection, providing anti-inflammatory and antiinfective activity.

This section aims to exploring the choices of differentiation agents of HL-60 in between all-trans retinoic acid (ATRA), calcitriol od dimethylsulphoxide (DMSO). When defined the agent, we characterized the differentiated HL-60 towards neutrophil functions and markers.

These cells were used to initially confirm the uptake of BSA nanoparticles and in the future, could be used to screen the kinetics and material of nanoparticle towards drug delivery. Moreover, neutrophils could be integrated into the 3D co-culture model[87] previously described to assess tissue destruction upon *P. aeruginosa* infection.
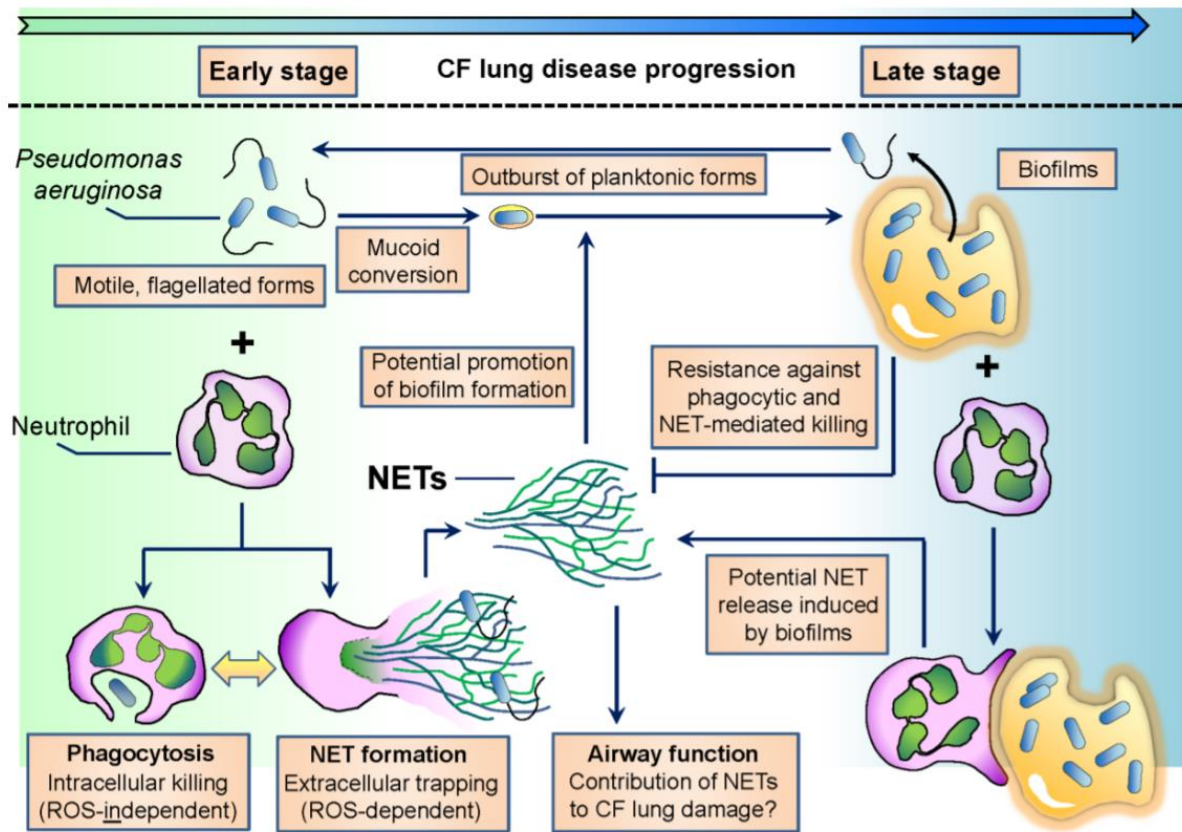
Figure 38. Interactions between polymorphonuclear neutrophil (PMNs) and *Pseudomonas aeruginosa* in CF airways. Reproduced from [173]

2. Material and methods

2.1. HL-60 cultivation and differentiation agents

Promyeloblast cell line HL-60 (ATCC® CCL-240™) derived from a 36-year-old Caucasian female with acute promyelocytic leukemia was grown from passage 16-40 in RPMI medium with 20% FCS. The cells were split g every 2-3 days and seeded at 10^6 cells/mL in a T75 cell culture flask. For differentiation, HL-60 (100,000 cells/ml) was seeded on a T75 per flask. Different differentiation agents were dissolved in RPMI medium and incubated in the HL-60 cells: 1μM all-trans retinoic acid (ATRA, ≥98% (HPLC), powder, Sigma, Germany), 1μM calcitriol (1,25-dihydroxyvitamin D3, Biomol, Germany), 1,25% DMSO (HPLC graded, Sigma, Germany) or as negative control of differentiation with 0.1% ethanol.

Cells were either differentiated on flask or microplates for 4 to 9 days in the RPMI medium. If using 12-well microplates (Greiner, Germany), we previously coated coverslips of 12mm with poly-L-lysine (0.1 mg/mL) for 1 hour and after cleaned by 5 washes of dH_2O, ultra-pure water, absolute ethanol, and 70% ethanol. Then place the coated coverslips inside the microplates and left for drying for 2 hours under the sterile flow bench. Differentiated cells on microplates or coverslips were stimulated with PMA 100nM for 30 minutes before characterization assays.

2.2. Nitroblue tetrazolium (NBT) assay of differentiated HL-60

In order to determine the intracellular level of the superoxide anion (O_2^-) for phagocytic cells, we used the NBT assay. This test is important for neutrophil characterization since intracellular oxidative stress is one of the specific weapons against engulfed microbes.

A method from Hirako *et al*[180] was adapted and PMA-stimulated HL-60 in 12-well microplates were incubated with 200µL of 2mg/mL of Nitroblue tetrazolium chloride (Sigma, Germany) then incubate at 37°C for 30 minutes. After labeling, each sample was focused on the search for intracellular blue-black formazan deposits and images were taken with the light microscope. Cells were incubated with 100% DMSO for 15 minutes and absorbance was measured at 550nm.

2.3. HL-60 nuclei morphology by DAPI staining

Nuclei staining was performed after fixation of PMA-stimulated HL-60 in coverslips using 3% of paraformaldehyde in PBS for 1 hour at room temperature (RT). Then sfluorescent cells were observed at the CLSM and 50 cells were counted for the percentage of altered nuclei morphology towards bi or tri-lobation.

2.4. Oxidation of 2',7'-dichlorofluorescein-diacetate (DCFH-DA) on differentiated HL-60

A second method to measure intracellular oxidative stress is via the detection of intracellular H_2O_2. Although an indirect measurement of H_2O_2, DCFH carboxylate anion retains the DCFDH-DA probe, and after oxidation, a fluorescent DCF is formed.

The method from Rastogi *et al*[181] was adapted, and PMA-stimulated HL-60 in 12-well microplates were incubated with 100µM of DCF-DA (Biomol, Germany) for 30 minutes at 37°C. Hydrogen peroxide 1mM was used as a positive control, and fluorescence was measured at excitation 465 and emission 535nm.

2.5. Flow cytometric for the detection of CD11b and BSA particle uptake

Using CD11b as a marker for activated neutrophils[182], we measured this surface marker on PMA-stimulated HL-60. Briefly, cells were trypsinized from cell culture T75

flasks as mentioned and centrifuged (220 G for 5 minutes), then resuspended in FACS buffer (PBS + 2% FCS) and transferred to glass tube for flow cytometry.

Cell suspension was incubated with 10µg/mL of purified human IgG (Sigma, Germany) for 15 minutes at room temperature, centrifuged and then stained with 2.5µg/mL of FITC/CD11b (FITC anti-mouse/human CD11b Antibody, Biolegend, USA) for 30 minutes at 4°C. Cells were centrifuged, resuspended in FACS buffer and used for flow cytometry. This was performed using a BD LSRFortessaTM (BD Biosciences, Heidelberg, Germany) using BD FACSDiva™ Software v8.0.1. Forward (FSC) and side scatter (SSC) were defined for live cells, using a non-stained control. From "living cell" populations (determined by cell granularity and size, green fluorescence data (excitation 488 nm, filter: 530/30) were collected on a minimum of 10,000 events (cells) per sample.

2.6. Detection of neutrophil extracellular traps among the differentiated HL-60

Differentiated and PMA-stimulated HL-60 were grown on 12-well microplates and poly-L-lysine coverslips. Then 5 µM Sytox Green (SYTOX™ Green Nucleic Acid Stain - 5mM Solution in DMSO) was used as a marker of extracellular DNA, which is the main component of the released neutrophil extracellular traps (NETs). Those traps are a response to microbes and a final attempt from the neutrophils to, at the same time, trap pathogens and release antimicrobial peptides as elastase and cathepsinB[183]. Cells were PFA-fixed, DAPI-stained, and mounted on microscope slides for confocal microscopy. On the confocal, NETs can be observed as an explosion of extracellular DNA associated with cell nuclei.

2.7. Production of bovine serum albumin (BSA) liposomes: characterization by dynamic light scattering and scanning electron microscopy

Particles were prepared according to Yu et al[184] with modifications. Bovine serum albumin (Sigma, Germany) was diluted in PBS and a 20mg/ml solution was prepared on

Erlenmeyer. Ethanol (an equivalent to 3.5 the BSA solution volume) was added at slow rate. For cross-linking, 0.2 % glutaraldehyde was added and the suspension was incubated on a magnetic stirrer (180 rpm/minute) for 18hours. After, particles were stained with rhodamine-labeled Ricinus communis Agglutinin I (2mg/ml for 2 hours, Vector Laboratories, Inc., Burlingame, CA, USA) and its physicochemical characteristics were measured with dynamic light scattering for size, polydispersity index, and zeta potential[185]. Or albumin concentration after particle production was measured using the bicinchoninic acid assay (Roche, Germany).

The morphological appearance of all nanoparticles was visualized using two different microscopical methods, including conventional Scanning Electron Microscopy (SEM, EVO HD15, Zeiss, Germany). For SEM visualization, liposomes were diluted in Milli-Q water and 2µL of the particle suspension was placed on the SEM copper grid. This grid has been previously coated with a carbon disc layered on top with pieces of alcohol-treated silica wafer. The drops of liposome suspension were dried and the gold-sputtered before visualization.

For nanoparticle uptake, cells were grown, differentiated and PMA-stimulated on poly-L-lysine coverslips. After that 10, 50 or 135 µg/mL of BSA nanoparticles were delivered to coverslip-adhered cells as suspensions on HL-60 cell medium for 2 or 24 hours and incubated at 37C, 5% CO_2.. Nanoparticle suspension was removed, twice PBS-washed then coverslips were stained for anti-CD11b-FITC (Biolegend) and fixed with 3% PFA (30 min) for confocal microscopy. For flow cytometry, suspended cells were incubated in test tubes with nanoparticles in FACS buffer (PBS + 1% FBS), after timepoints tubes were centrifuged (2580 g) for 4 min and resuspended with staining solution in FACS buffer for 1 hour in the dark. Another round of centrifugation was performed to removed staining, then cells were re-suspended on FACS buffer, maintained in ice for subsequent analysis on flow cytometer (BD Biosciences) and analyzed using the FlowJo software.

2.8. Confocal microscopy

Cells were imaged using confocal laser scanning microscopy (CLSM, Leica TCS SP 8; Leica, Mannheim, Germany). Analysis of obtained images was performed using LAS X software (Leica Application Suite X; Leica, Mannheim, Germany).

3. Results

3.1. Initial characterization of HL-60 on differentiation agents towards the functional capacity as neutrophil-like cells

After 4, 5, 6 and 7 days of incubation with differentiation agents, HL-60 cells were quantified and its viability was assessed. Because we used a CASY automatic counter (Roche Diagnostics International, USA), this equipment uses the application of electrical current against individual cells in a microfluidic system. This technology then considers viable cells as electrical insulators, so dead cells no longer present as an electrical barrier. This can be measured and together with a threshold for cell debris, cell size and viability can be obtained.[186]

We incubated HL-60 with all differentiation agents for 4-7 days and checked the cell viability and cell number (Figure 39A, B). The treatment with all agents did not induce cell toxicity or stop cell proliferation, except for DMSO (Figure 39B). It is known that the treatment with 1.2% DMSO for 72 hours has down-regulated the suppression of apoptosis-related to the expression of *Bcl-2* gene[187], which might explain the decrease in cell proliferation observed in our results. Even so cell proliferation has been reduced, there was growth when compared to cell seeding of 10^5 cells/flask.
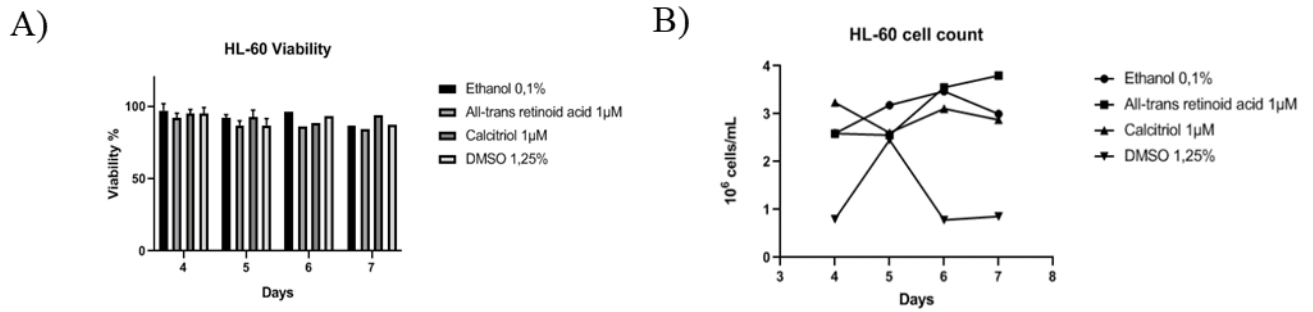
Figure 39. Initial characterization of HL-60 on differentiation agents towards the functional capacity as neutrophil-like cells. A) Cell viability via size/granularity for 4, 5, 6 and 7 days of stimulation. B) Cell growth number via automatic counter for 4, 5, 6 and 7 days of stimulation. Ethanol samples as non-stimulated controls. N=2 experiments.

If the cells are growing while differentiating, we used the first assay to assess the functionality of these neutrophil-like cells. Nitroblue tetrazolium (NBT) provides an insight into the activation of cells towards the use of NADH oxidase to reduce NBT into formazan crystals.[188] On figure 38C, light micrographs of differentiated PMA-stimulated HL-60 show the presence cell filled with formazan purple-black crystals. Compared to non-stimulated HL-60, the cells that activated its NADH oxidase were ^{DMSO}HL-60 after 6 days of exposure.
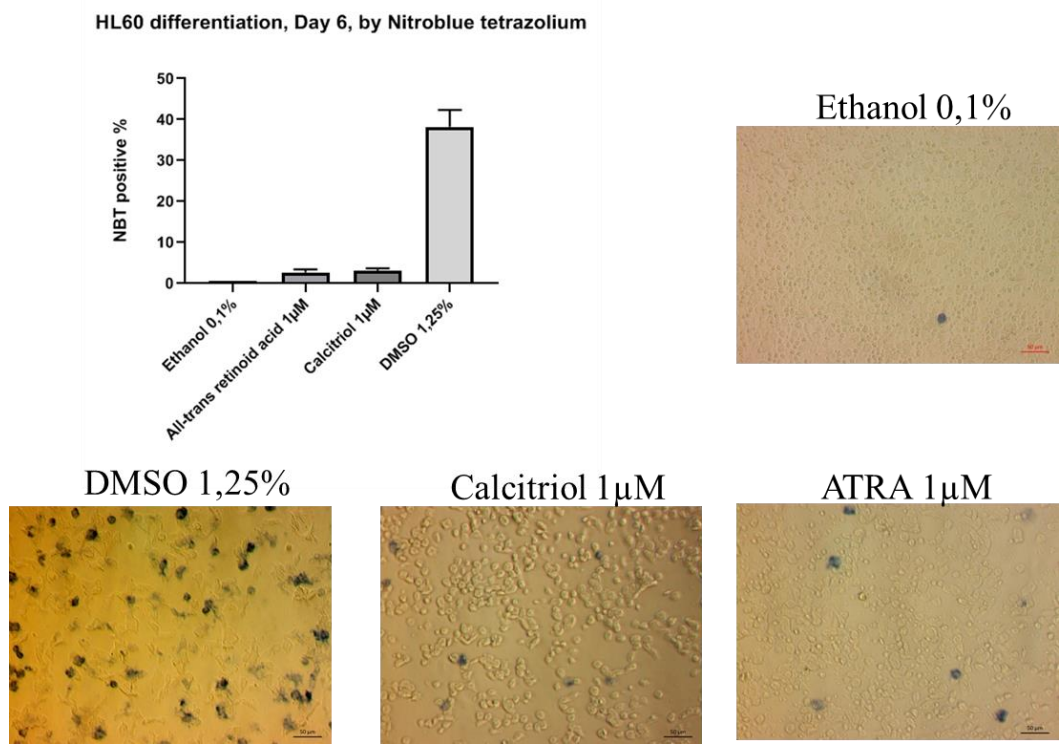

Figure 40. Quantification of positive cells for the nitroblue tetrazolium assay: differentiated HL-60 and the correspondent light micrographs. N= 3 wells per condition on 2 experiments.

Neutrophils can have 3 to 5 lobes as nuclei and this segmentation has been known to facilitate i) intranuclear chromatin organization and ii) dynamic shaping of the nuclei when negotiating to pass through narrow capillaries, transmigrating across the vessel wall and passage through tight tissue spaces[189]. Promyelocytic cells as HL-60 have spherical nuclei and the process of lobation can then indicate the commitment towards neutrophil differentiation.

For a straightforward assessment of nuclei morphology, HL-60 was observed after DAPI staining and, on figure 38D, nuclei are distinguished in all agents tests, however quantification the ratio of altered nuclei, it is DMSO that provides altered nuclei in more than 80% of the cells.
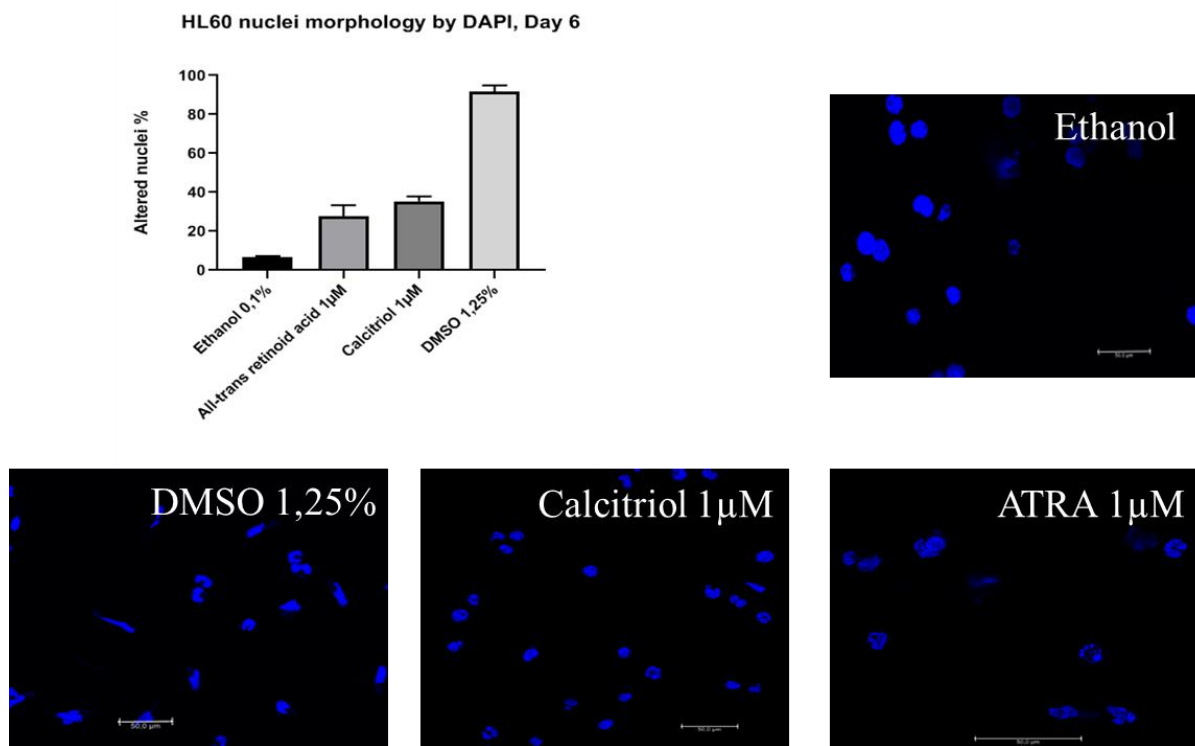

Figure 41. Quantification of nuclei lobation of differentiated HL-60 via DAPI assay on fluorescence micrographs. N= 2 wells per condition on 2 experiments.

Phagocytic cells as the immune cells have the opportunity to detect pathogens by engulfing it. That started a cascade of chemical signaling to define which actions to take. Intracellularly, phagocytic cells start a process called respiratory burst in which one of the main points is that NAPDH oxidase product reactive oxygen species (ROS). The entire coordination of immune responses can then depend on those ROS, but ROS molecules can also destroy microbe's compounds. But an essential role of ROS is to start the regulation of pattern recognition receptors, autophagy, NETs or T-cell activation; all those are indirectly responsible for eliminating microbes.[190]

By using the DCFH-DA assay, we indirectly measure levels of hydrogen peroxide to start the oxidation of this probe. We then checked the production of ROS in our differentiated-stimulated-HL-60 (fig. 42). The production of ROS was only observed with calcitriol, a secondary metabolite of vitamin D has approximately double of activity when compared to the positive control, 1mM hydrogen peroxide.
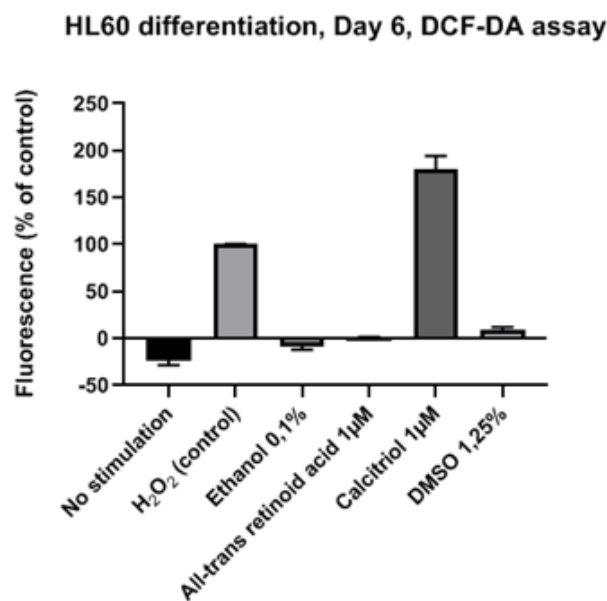

Figure 42. Quantification of oxidation of 2',7'-dichlorofluorescin-diacetate (DCF-DA) on differentiated HL-60. N= 2 wells per condition on 2 experiments.

To explore the differentiation towards neutrophils-like cells, HL-60 cells previously stimulated with different agents were labeled with CD11b. A summary is seen in figure 43 on which FSC and SSC are defined to find population 1 (P1) as size and granularity to represent possible live cells. While the second population (P2) focuses on the fluorescence at 488nm, representing the positive cells with the FITC/CD11b marker. This entire figure results from measurements on Day 3 of HL-60 differentiation.

Figure 43A shows the start of gating via finding the measurements of background (ethanol control as agent), or so, from the unstained "live" cells. Figure 43B shows ethanol-HL-60 cells that were still stained cells, but those cells are not neutrophil-differentiated. From those controls, we could use HL-60 differentiated cells.

Figure 43C and D compared ^{DMSO}HL-60 cells; however, here the main focus goes to the P2 gating. For that, fig. 43D at P2 shows the fluorescent population for 488nm excitation and this will then correspond to 63.5 % of the ^{DMSO}HL-60 cells.

Figure 43E shows a table that focuses on Day 6 after HL-60 differentiation. This day is important because it correlates that the differentiation of HL-60 can be accomplished for the other characterization variables as well. Here we continued the gating strategies to find the population of live cells, then find CD11b on live-differentiated HL-60. ^{DMSO}HL-60 at day 6 shows low "live-cells" number (~31%), but from that, 87.4 % of cells are expressing CD11b.

On that note, figure 43D shows results after 3 days of incubation of HL-60 with DMSO in which there is 89.2% of live cells (P1), from that 63.5 % are expressing CD11b. This could allow the use of ^{DMSO}Hl-60 on earlier incubation towards functional assays regarding neutrophil migration, but it needed to further studied for the other variables.
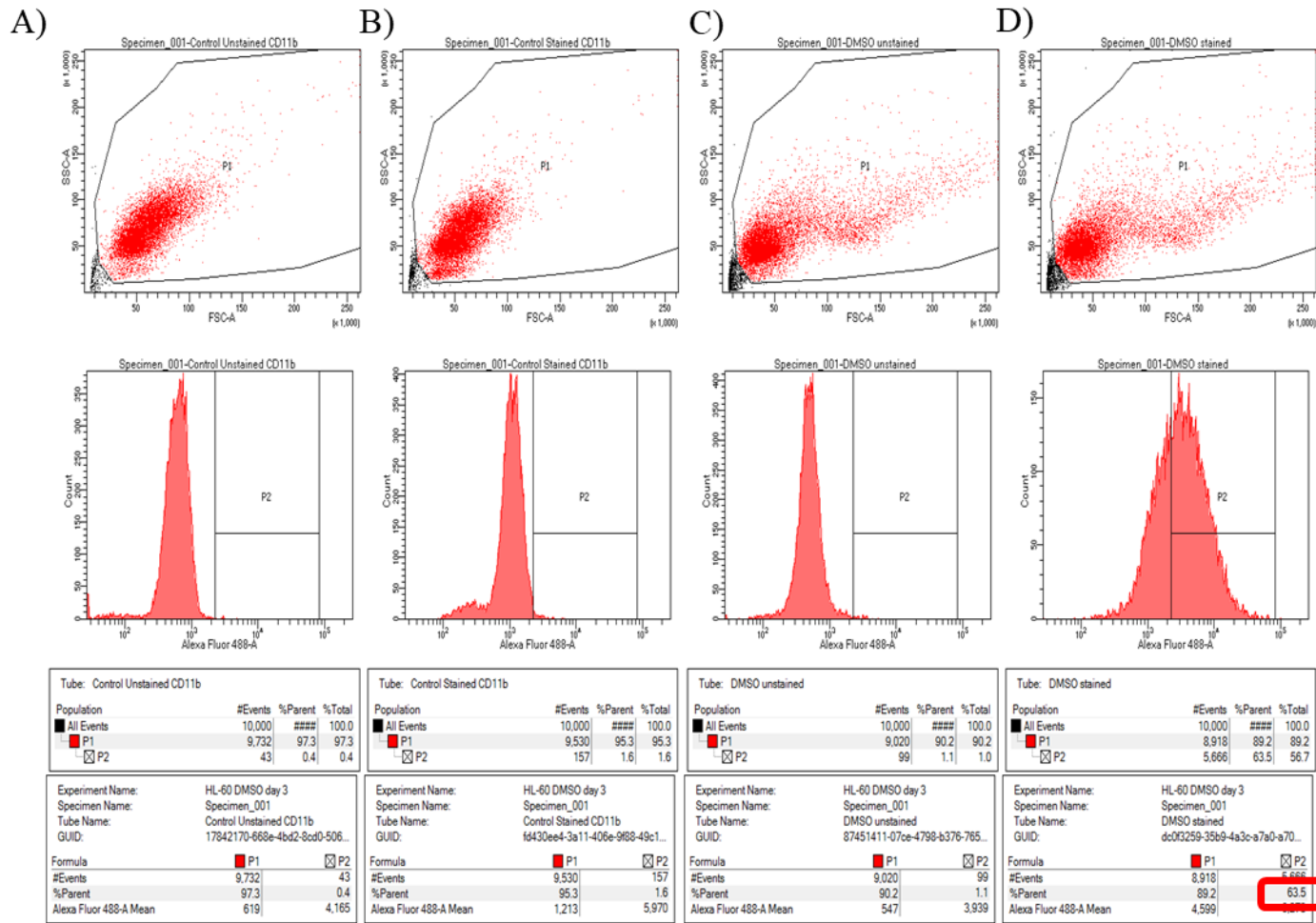
Figure 43. Detail of detection and gating of flow cytometric detection of CD11b. A) Non-stained ethanol exposed HL-60 (Day 3). B) Stained ethanol exposed HL-60 (Day 3). C) Non-stained DMSO exposed HL-60 (Day 3). D) CD11b-stained DMSO exposed HL-60 (Day 3). E) Summary of CD11b staining and "live" cells with the differentiation agents on day 6 of incubation. N= 3 samples per condition on 1 experiment.

Previously, neutrophils were already known to i) phagocytize microbes do its elimination into vacuoles or ii) proceed with the release of neutrophilic granules containing antimicrobial peptides. But it was uncovered that neutrophils can die via the release of all its nuclear content towards the outside of the cell and this release was made into the throw of a polymeric mesh containing extracellular DNA (decondensed chromatic) and antimicrobial proteins.[191]

Even so, DAPI is a DNA binding dye, Sytox Green has been considered the best option for NETosis assay[192]. With this assays, we investigated if NETs have been produced on the differentiated-stimulated HL-60. On figure 44, the qualitative observation of NETs is present for the 3 differentiation agents, although either more present or stronger in DMSO or calcitriol differentiated HL-60.
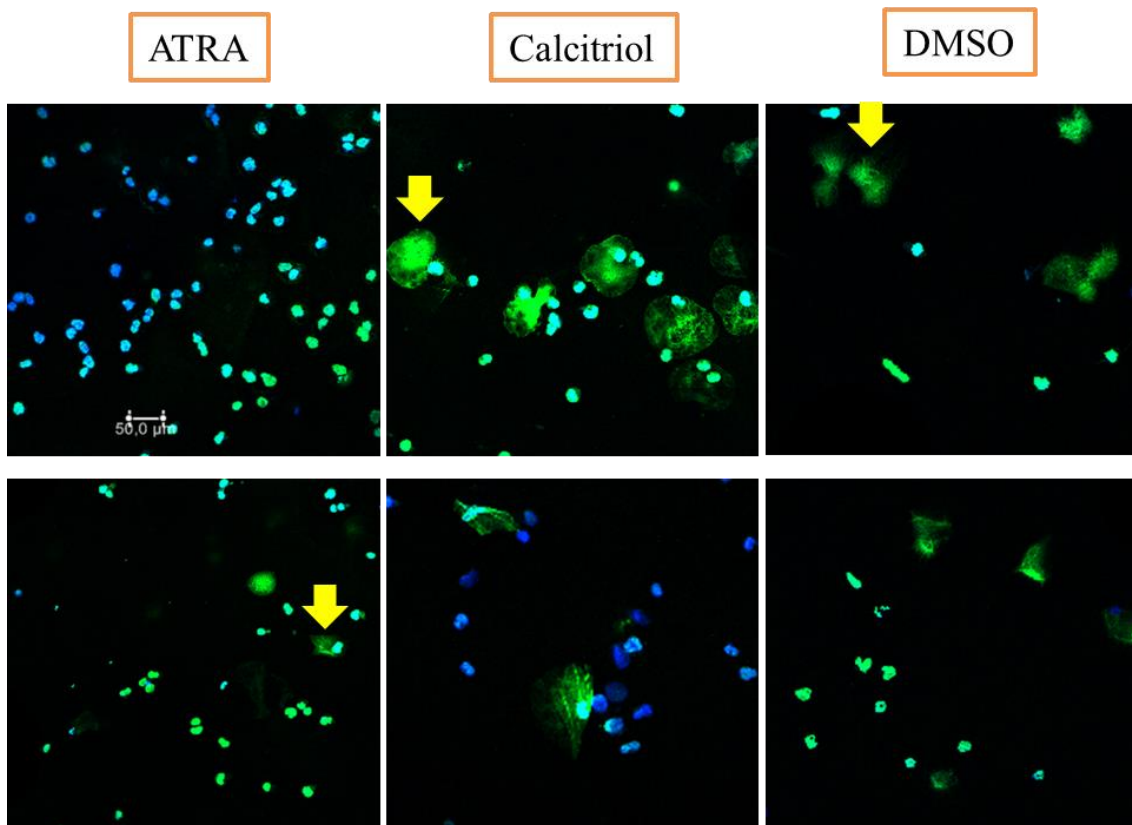

Figure 44. Fluorescent micrographs of SYTOX® Green on the detection of neutrophil extracellular traps, among the differentiated HL-60 at day 6 of incubation. N =2 samples per condition in 2 independent experiments.

Even though the exact confirmation of NETs is questionable on HL-60 differentiated cells, other reports have positively described on its findings[193]. Besides, NETs have been described in essential diseases, while for cystic fibrosis, it may influence the perpetuation of excessive inflammation and lung injury[194].

The yellow arrows on fig. 44 point out the presence of cells with traps coming out of their nuclear content, representing NETs, while other cells (as the ones from [ATRA]HL-60 cells) are positively stained for DAPI and Sytox Green, meaning, these represent cells which could potentially present NETs, but contained ones, not yet released. We did not proceed with NETs quantification, but importantly we confirmed the presence of these structures in [Calcitriol]HL-60 and [DMSO]HL60 cells.

3.2. Neutrophil hitchhiking by Bovine serum albumin (BSA) particles

We reproduced the BSA particles[179] with slight modification towards the cross-linking of albumin with glutaraldehyde. Normally BSA particles tend to form aggregates but glutaraldehyde helped on the maintenance of particle morphology. On fig. 45, the morphology and physicochemical characteristics of BSA particles are demonstrated from the DLS results (particles of around 126 nm) and spherical polydisperse particles on the scanning electron micrographs.

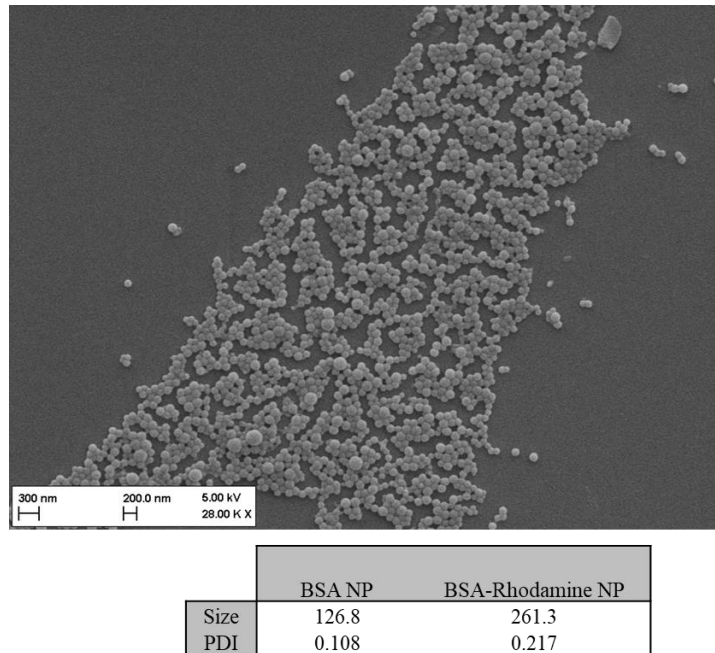|	BSA NP	BSA-Rhodamine NP
Size	126.8	261.3
PDI	0.108	0.217

Figure 45. Scanning electron micrographs of BSA liposomes and characterization by size and polydispersity index. N =1 independent experiment.

After particle production and checking of its stability, we measured the content of albumin into the particles via the BCA assay. That allowed us to define the concentration of the particle suspension based on the BSA content in µg/mL.

This uptake study was only performed on [DMSO]HL-60 differentiated cells and we used two concentrations of particle suspension in order to initially characterized if particle density would alter the particle uptake.

BSA particles were previously stained with rhodamine and then incubated with DMSO-differentiated cells. Those cells were previously differentiated and stained for CD11b as a phagocytic cell surface marker.

[CD11b/DMSO+]HL-60 cells with 10 or 135 µg/mL BSA particles for 2 hours in HL-60 cell media. On fig. 46, we observe the results of particle uptake after 2 hours of incubation in which for both concentrations.
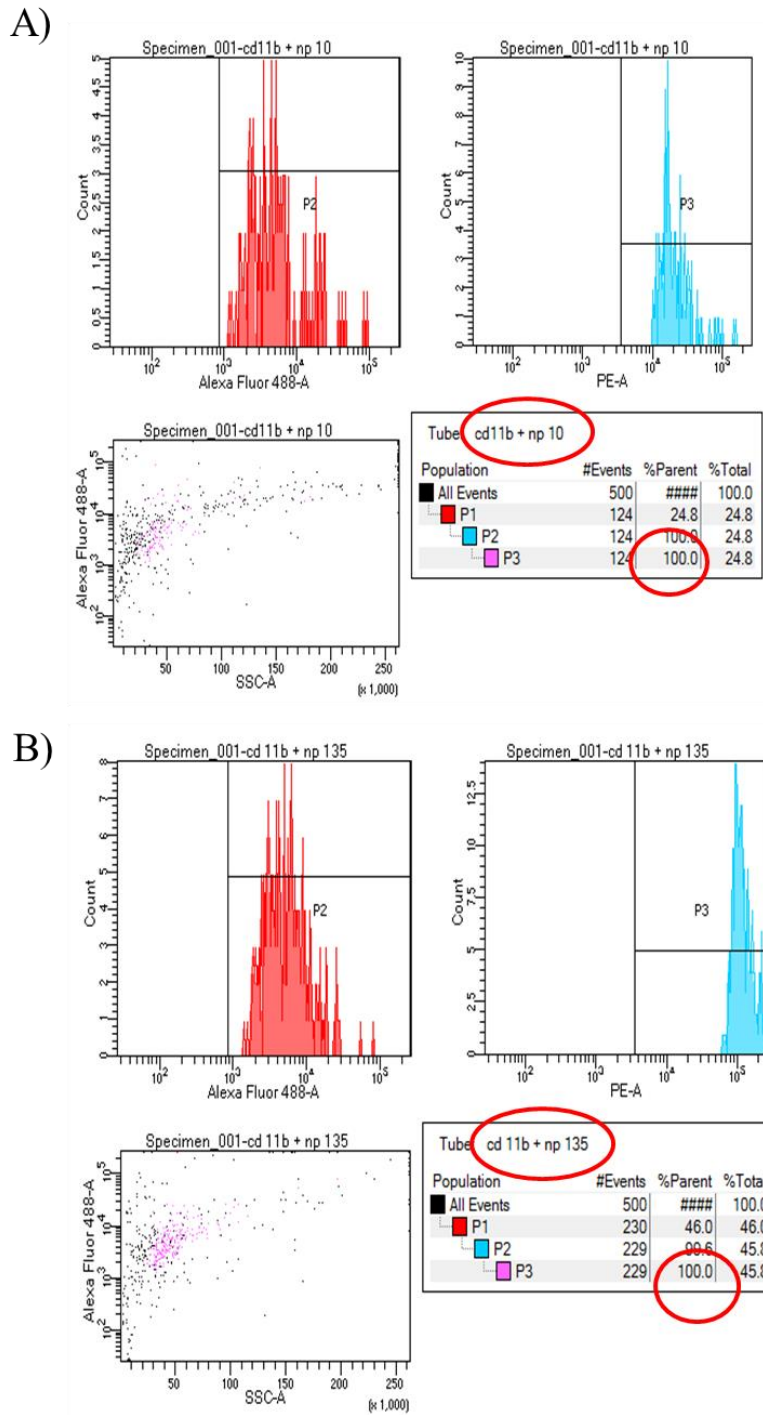
Figure 46. Neutrophil hitchhiking by Bovine serum albumin (BSA) liposomes. After using diameter and granularity to define P1, from those cells, we gated for FITC/CD11b fluorescence (P2), and from this population we looked for a population that is also stained by rhodamine (membrane-bound or intracellular). Application of 10 (A) and 135 (B) µg/mL of BSA liposomes was checked on this uptake study on DMSO-differentiated $^{CD11b+}$HL-60 cells. N =1 independent experiment.

After gating for "live" cells, CD11b positive cells, we defined a population positively stained for rhodamine (P3) and in figure 46A for 10 µg/mL and 46B for 135 µg/mL of BSA particles. The table shows that 100% of the particles were uptaken or associated with the cells.

To check the results from flow cytometry, we used CLSM to observe BSA particles interacting with the HL-60. We could not find BSA particles using a lower concentration of 10 µg/mL. With the confocal, we observed the membrane staining for CD11b/FITC (fig.47A), while BSA nanoparticles can be seen associated with the $^{CD11b/DMSO+}$HL-60 cells but not defined if uptaken intracellularly.

A) HL60 + DMSO 1,25%, Day 6

B) $^{CD11+}$DMSO-HL60 + 135 µg/mL 2h

C) Cross section from sample above

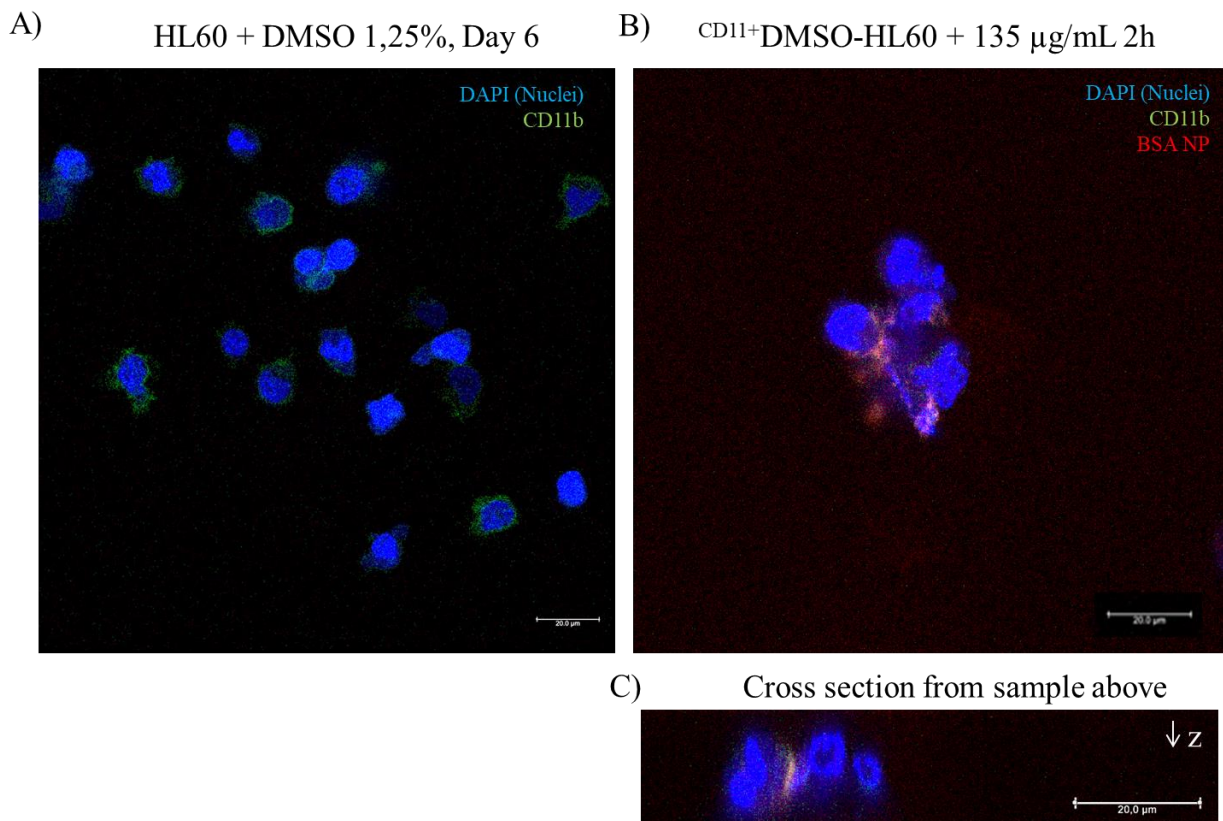Figure 47. Neutrophil hitchhiking by Bovine serum albumin (BSA) liposomes. A) Confocal micrographs of the investigation of DMSO-differentiated $_{CD11b+}$HL-60 cells. B) BSA nanoparticle uptake by DMSO-differentiated $^{CD11b+}$HL-60 cells after 2 hours of administration. C) Cross-section of DMSO-differentiated $^{CD11b+}$HL-60 cells uptaking BSA nanoparticles after 2 hours. N =1 independent experiment.

4. Discussion

One of the main features of neutrophils is that these are mature cells with lobated nuclei, instead of ovoid ones. This transition is also observed in regular granulopoiesis, and the nuclei of cells, including HL-60, have already been analyzed after exposure, for instance, of retinoid acid[195].

Exposure to all-trans retinoic acid (ATRA) provokes arrest on cell cycle and myeloid differentiation, while other agents, as calcitriol can provide a monocytic differentiation[196]. For chemicals as ATRA, HL-60 has already defined mechanisms as a specific retinoic acid receptor (RAR) or regulation via microRNAs[197]. Our testing of agents of differentiation clarified the role of DMSO but demonstrated the issues with viability.

In the activation of neutrophils, the production of intracellular reactive oxygen species (ROS) (located in the phagosome) is one of the main strategies to kill bacteria, and ROS alters H_2O_2 to be the source of myeloperoxidase to generate other ROS, including hypochlorous acid to fight against bacterial growth[198]. So the fusion of granules forming the phagosome and production is ROS is one of the markers for a neutrophil model.

Our results show two assays for oxidative stress. For the NBT assay, 40% of the cells differentiated with DMSO presented formazan granules that can only be formed by intact oxidative cell machinery of a mature phagocytic cell. Another indication of the neutrophil commitment of the HL-60 is via the oxidation of DCDH probe.

Our results show that exposure of HL-60 cells to calcitriol show oxidation of 175% when compared to the positive control of H_2O_2. For DMSO exposed cells, the release was only 15%, which questions the functionality of this cell line for this specific function. But, at the same time, it asks us the importance of this oxidation for microbe elimination and towards a balanced control against lung injury.

If neutrophils reach the target (bacteria) to promote phagocytosis and killing, its machinery towards migration needs activation.

This migration takes place when β_2-integrins are activated via Mac-1 that is dependent on the surface markers CD11/CD18[199]. HL-60 activated by retinoic acid or DMSO can use Mac-1 and extracellular regulated kinases (ERK1/2) across the lung epithelium, as demonstrated in Calu-3 epithelia[200]. The role of epithelia is not passive towards the approach from neutrophil migration as on the intestinal epithelia there are specific fucosylated proteoglycans that bind CD11/CD18[201].

Our results show it is possible to find CD11b on differentiated HL-60, but mostly on DMSO-exposed cells and not on cell exposed with the other differentiation agents. This starts to confirm that HL-60 could be used as neutrophil-like cells when DMSO is the leading agent.

The last functional assay is a dramatic format of cell death called NETosis, as neutrophils can decide to extrude a meshwork of DNA/chromatin fibers that are decorated with antimicrobial proteins as elastase, cathepsin G and myeloperoxidase; these are the neutrophil extracellular traps (NETs). The extrusion of these fibers produces a trap mechanism to immobilize and kill pathogens.[202]

Although it has been described that HL-60 does not provide NET after differentiation with DMSO or ATRA against *S. aureus*[203]. Our results after PMA stimulation show an early indication of extracellular DNA resembling decondensed chromatin as mesh structures resembling NETs.

If further confirmed (compared to primary neutrophils) that our HL-60 differentiated cells present NETS, it can in the future elucidate two things: i) how NETs can be formed and

what its composition in primary to cell lines of neutrophils and ii) how the NETosis can be useful to release encapsulated strategies inside the neutrophils, as nanoparticle formulations.

Using the 3 agents for differentiation of HL-60, we contemplate that HL-60 does not comprise all neutrophil functionality with one specific differentiated cell. However, it can have NAPDH machinery to be activated, expresse phagocytic cell surface marker, show neutrophil-like nuclei lobation. All these characteristics after exposure to DMSO.

Even though cell viability decrease with DMSO expose, we can adapt this towards that fact that specific mechanisms of death of HL-60 neutrophils can be useful for

i)   The release drugs or regulated expression of antimicrobial proteins on NETs and

ii)   the launch of cytoplasmatic content can release particles if these formulations are stable inside the cells.

Chu *et al*[179] has shown that BSA particles can be stable inside primary neutrophils and hitchhike within these cells using their migratory potential to reach inflamed or infected sites, crossing biological barriers to overcome the tissue.

On DMSO-differentiated [CD11b+]HL-60, our preliminary results demonstrated cell uptake; compaction around the cell nuclei and degree of BSA release, plus aggregation, must be assessed in future experiments. Further investigation should be performed on primary neutrophils, with specific controls of non-differentiation and with another possible particle that can be stable inside the cell.

5. Conclusion

HL-60 was used here as a cell model of neutrophils in which its potential to replace their functionality could be the option to overcome the short life-span of primary neutrophils.

Chemical signals can be purified and used as strategies to promote differentiation and further activation of cell models. For neutrophil-like cells, we used DMSO, ATRA, and calcitriol. These agents promote differentiation in different degrees[176,178,196].

Although no agent can differentiate HL-60 to have the full characteristics of neutrophils, some new functions can be mimicked. The use of DMSO can promote activation of enzymes to produce ROS; it can alter chromatin composition reflected on the nuclei shape, it expresses surface markers as CD11b contributing to cell migration, and it can promote the specific cell death in combination with strategies for bacteria-trapping, or so, the NETs.

Focusing not on the neutrophil functions, but on its potential to release content upon NETosis, the use of BSA particles can facilitate a hitchhike for these particles to use the migration and chemical signaling of neutrophils. Our BSA particles were uptaken by DMSO-differentiated HL-60, and now this cell can be used as a model to investigate the mechanisms of particle uptake, the stability of different materials inside neutrophils, and the possibilities of release within extrusion of NETs.

Chapter 3: Coupling quaternary ammonium surfactants to the surface of liposomes to inhibit bacterial adherence

1. Introduction

The search for new bactericidal molecules has shaken the scientific world on a wave of research focusing on how bacteria protein synthesis or respiration chain can be inhibited. However, a related investigation is following the potential of molecules or even other bacteria to outcompete adhesion onto the human surfaces.[204]

Reports on inhibition of bacteria communication[205] or specifically adherent proteins, as lectins3, have proposed us the opportunity of using nanotechnology and interface chemistry to create active surfaces. Responsive surfaces can be developed to inhibit determined bacteria, but also to aim for a broader range of bacteria inhibition, depending on the interactions with the outer bacteria membrane[206].

With the fact these surfaces can displace and kill bacteria, we observed the predominance of quaternary ammonium surfactants (QAS) as primary modifiers. The cationic surfactants are primarily employed as antibacterial ingredients in ophthalmic preparations[207], mouthwashes[208], drug delivery food manufacturing[209]. One example of QAS is cetylpyridinium chloride. This compound has antimicrobial activity but in combination with cytotoxicity, known as a skin irritant and restricted human application.[210]

Successful reports on avoiding bacterial adherence on surfaces have been achieved using polymeric coatings with alkylated polyethyleneimine or chitosan derivatives[211]. A commonly seen strategy is to use cationic charge together with a long hydrophobic chain as a leading group of the coating solution. This had worked for surfaces[212]; however, it could be applicable for the fight against bacterial adherence, biofilm formation, and resistance.

When microorganisms gather in communities and attach on abiotic and living surfaces, it is called biofilms. From those communities, the related infections, for instance, in the USA, account for the $94 billion/year on healthcare costs and around 500,000 deaths/per

year[213]. An immediate need for new molecules against biofilm specific conditions has launched the potential of nanotechnology. Mainly for its modulation of size, high surface-to-volume and possibility of engineering towards strong affinity to bacteria[214]. Besides the feasibility of antibiotic encapsulation into nanoparticles, we can also explore for treating bacterial infection with nanomaterials with inherent antimicrobial characteristics[215].

QAS has self-assembly property and soyaethyl morpholinium ethosulfate (SME) nanoparticles have recently been proved to eradicate *S. aureus* and MRSA while penetrating bacteria and inducing oxidative stress. Nonetheless, the use of SME-whole micelles mediates 50% cytotoxicity with only 10 µg/mL[210].

Instead of using QAS on surfaces or as free compounds, we want to functionalize the surface of nanoparticles (liposomes) to deliver anti-adherence formulation compatible with human epithelia, while the search for new antibacterial cationic surfactants can resolve the drawbacks of the currently used surfactants.

The (11-Mercaptoundecyl)-N,N,N-trimethylammonium bromide (MTAB) is a quaternary ammonium surfactant that has been used on surface functionalizations of gold particles[216], and its derivate Cetrimonium bromide (CTAB) onto gold nanorods is already known for antibacterial properties[217], a difference that is related just to number of aliphatic chains. Choi *et al.*[218] used MTAB to create surfaces with gold particles that can tune in its antibacterial activity via electrical stimulations, so its influence on bacteria is being studied with positive feedback.

Our focus is that the integration of MTAB onto liposomes will be easy to produce, transfer the properties of QAS as anti-adherence activity and in a less cytotoxic fashion; providing the opportunity to use future drugs encapsulation that comprises a combination therapy for the remaining non-adherent bacteria.

2. Material and methods

2.1. Preparation of Liposome

Liposomes were prepared by extrusion procedure using polycarbonate filters (100 nm pore size diameter) and were composed of sphingomyelin (Avanti Polar Lipids Inc. Alabaster, AL, USA) and cholesterol (Sigma-Aldrich (Milano, Italy). (1:1mol/mol), containing 2.5 mol% of 1,2-stearoyl-sn-glycero-3-phosphoethanolamine-N-[maleimide (-poly(ethylene glycol)-2000)](mal-PEG-PE; Avanti Polar Lipids Inc. Alabaster, AL, USA) for further surface functionalization with cationic amino group. Briefly, lipids were mixed in chloroform/methanol (2:1, vol/vol) and dried under a gentle stream of nitrogen followed by a vacuum pump for 30 minutes to remove traces of organic solvent. The resulting lipid film was rehydrated in phosphate-buffered saline (PBS, -Aldrich (Milano, Italy)), vortexed, and then extruded (LipexBiomembranes, Vancouver, BC) 10 times at 65°C through a stack of two polycarbonate filters (Millipore Corp., Bedford, MA; 100-nm pore size diameter) under 20 bar nitrogen pressure[219]. Phospholipid recovery after extrusion was determined by a phosphorous assay using the method of Stewart[220]. This formulation is quoted here as "LipoBlank".

2.2. Preparation of Liposomes functionalized with a cationic amino group (Lipo-MTAB)

(11-Mercaptoundecyl)-N,N, N-trimethylammonium bromide (MTAB) was added to the LipoBlank dispersion in PBS to give a final cationic amino-to-liposome molar ratio of 2:1 in the incubation mixture and incubated overnight at room temperature to form a thioether bond with mal-PEG-PE. Functionalized liposomes were separated from unbound cationic amino linker by dialysis against MilliQ water, using a dialysis membrane MWCO= 12-14 KDa (Medical International Ltd, London, UK) at 4°C for 2 days. This formulation is quoted here as "LipoMTAB."

2.3. Physico-chemical characterization of LipoMTAB Dynamic Light Scattering

Liposomes size and polydispersity index (PDI) were obtained using a ZetaPlus particle sizer (Brookhaven Instruments Corporation, Holtsville, NY, U.S.A.) at 25 °C in PBS. Size and PDI were obtained from the intensity autocorrelation function of the light scattered using a 652 nm laser beam at a fixed angle of 90°. The correlation function was analyzed through two cumulant expansion. Size and PDI measurements were performed in PBS for at least 1 month. ζ-potential analysis (Brookhaven Instruments Corporation, Holtsville, NY, U.S.A.) was performed under an electrical field of 29.7 V/cm. Standard deviations were calculated from at least three independent measurements.

2.4. Nuclear Magnetic Resonance (NMR)

All the NMR ^{1}H experiments were carried out on a Bruker Avance I 600 spectrometer, (Bruker Italia Srl, ^{1}H base frequency = 600 MHz) equipped with a superconducting *Ultrashield Plus* magnet of 14.1 Tesla, using a 5-mm BBI reverse broadband probe. Lipo-Blank (5 mg) and Lipo-MTAB (5 mg) were suspended in 700 µl of D_2O and introduced in 5mm NMR high-performance tubes for NMR analysis. ^{1}H spectra were acquired, for about an hour, at 30 °C, not spinning, with and without the presaturation of the residual H_2O signal (*zgpr* Bruker sequence), using following parameters: spectral width (sw) = 7200 Hz, acquisition time (at) = 2.28 s, number of data points in t2 (TD) = 32k, relaxation delay (d1) = 5 s and number of scans (ns) = 400.

2.5. Bacterial cultivation

Escherichia coli DH5α was used for the microbiological work. After overnight incubation (18h) of a single colony in Luria-Bertani broth (Sigma-Aldrich, Germany), the optical density at 600nm (OD_{600}) was measured (Spectrophotometer; MultiskanGo 1510, Germany).

The same medium was used for biofilm growth, together with PBS. Biofilm was grown by adding 2.10^7 bacterial cells inside a 12-well microplate (when needed bacteria was grown on uncoated glass coverslips 12mm). These plates were incubated at 37°C for 18 hours without shaking.

2.6. Monitoring of bacterial growth by Minimal inhibitory concentration (MIC) assay

Using 96-well plates, liposome suspension and free MTAB solution, after 2-fold serial dilutions, were incubated for 20 hours with *E. coli* DH5α (10^7 CFU/mL). Bacterial growth was monitored via OD_{600}, using a spectrophotometer. The percentage of inhibition was calculated comparing wells with LB medium only.

2.7. Bactericidal activity by Colony-forming units (CFU) assay

From the MIC assay, the supernatant of selective concentrations was serially diluted in PBS/Tween80 0.05%, drop-plated (3x 20µL drops per dilution) on LB-agar plates and incubated for 24 hours at 30°C to determine the CFU.

2.8. Antiadherence activity by drop diffusion on agar

Modified from Balouiri *et al.*[221], we prepared LB-agar plates and spreading 100 µL of 0.2 OD *E. coli* DH5α. The plates were then dried under the bench flow for 30 minutes. Using liposomes and free MTAB solutions, we placed 20 µL drops on the inoculated agar surface and let it dry under the bench flow for 30 minutes. Plates were then incubated at 37 °C for 24 h. The anti-adherence activity was expressed as the mean of the diameter of inhibition halos (mm) produced by the formulations.

2.9. *E. coli* DH5α biofilm on glass coverslips for SEM and membrane assay

Using 24-well plates, 250 µL of liposome suspension or free MTAB or controls (PBS and LB) were placed on top of sterilized glass coverslips of 12mm and 15 µL of *E. coli* DH5α suspension (10^7 CFU) was added to the wells. Plates were incubated at 37°C for 72 hours.

Wells were PBS-washed (500µL) and supernatant with non-adherent bacteria was collected (with care not to touch the coverslips), while adherent bacteria on coverslips were fixed with 500µL of 3% paraformaldehyde (PFA; Electron Microscopy, PA, USA) for 1 hour.

2.10. Membrane disruption assay by propidium iodide uptake

Modified from Cho *et al.*[222], from the biofilm assay, we collect its supernatant containing bacteria and then incubated 1µl of 1.5mM propidium iodide (Sigma, Germany) as an indicator of membrane disruption for 2 hours and centrifuged at 14000 RPM for 10 minutes, resuspending the pellets on PBS. Using black glass-bottom 96-well plates (Greiner BioOne, Germany), we added 100 µL supernatant containing stained bacteria per well and determine fluorescence through Fluorimeter (Excitation 400/Emission 460nm; TECAN Infinite M200Pro, Austria).

2.11. Evaluation of Liposomes biocompatibility via MTT and lactate dehydrogenase (LDH) assays on A549 cells

An adenocarcinoma human alveolar basal epithelial cells (A549 cells; No. ACC 107, DSMZ GmbH, Braunschweig, Germany) was grown in complete cell culture medium (RPMI 1640; PAA Laboratories GmbH, Pasching, Austria) with 10% FCS and used as model cell line to test human cell viability. Cells were passaged with trypsin–EDTA and seeded (20 000 cells per well in 200 µL) on 96-well plates (Greiner, Germany). Liposomes and free MTAB were diluted with cell medium (RPMI + 10% FCS) and incubated on the cells for 20 hours.

The supernatant of cells exposed and unexposed to liposomes was placed in a new 96-well plate and centrifuged (5000 RPM for 10 minutes), then 100 µL of supernatant was separated for LDH assay (Roche Cytotoxicity LDH kit, Germany). LDH kit mix was incubated with the supernatants for 5 minutes in the dark at room temperature, according to

manufacturer instructions. The absorbance was read by a Tecan microplate reader (Germany) at 492 nm.

Plates with cells were incubated with MTT [3-(4,5-Dimethylthiazol-2-yl)-2,5-diphenyltetrazolium bromide] stock solution (0.5 µg/mL)[223] and placed at 37°C for 4 hours. After removing the MTT solution, the formazan crystals were resuspended with DMSO (100%) for 30 minutes. The absorbance was measured with a spectrophotometer at a wavelength of 550 nm.

Both MTT and LDH were calculated in reference to negative (medium only, 0% cytotoxicity) and positive controls (1% Triton-X100, ICN, Eschwege, Germany, positive control, 100% of cytotoxicity).

2.12. Scanning Electron Microscopy (SEM) for liposome and bacteria morphology

From the biofilm assay, PFA-fixed coverslips dehydrated by an ethanol row with 300 µl of 30, 40, 50, 60, 70, 80, 90, 96 and 100% for 10 minutes each. Hexamethyldisilazane (HDMS; Sigma, Germany) 100% was incubated on wells for 20 minutes then coverslips were left to dry overnight under the fume hood. Coverslips were then placed on top of a carbon disc and gold-sputtered. Visualization of samples was performed via SEM (copper grid with applied liposomes were then placed onto a carbon disc and gold-sputtered).

3. Results

3.1. Production and characterization of LipoMTAB

LipoBlank and LipoMTAB were prepared as described above. Both liposomal formulations were characterized by DLS and ζ-potential devices. Lipo and LipoMTAB showed a size of 147.8 ± 1.6 nm and 160.8 ± 3.5 nm, respectively and were monodispersed (polydispersion index, PDI < 1) (fig. 48B). The liposomes size increased after functionalization with MTAB. Also, the ζ-potential value increase from -31.8 ± 5.8 (LipoBlank) to -20.6 ± 2.6 (LipoMTAB) suggesting the successful liposomes

functionalization. Both liposomal preparations maintained a constant size, PDI and ζ-potential values for at least 1 month, (Fig. 48B). Scanning electron micrographs (fig. 48C) showed that both nanoparticle formulations appeared as spherical vesicles and uniform, mostly for LipoMTAB that has an additional step of purification via dialysis.

From a comparison of NMR spectra of Lipo-Blank and Lipo-MTAB in figure 49A it is possible to discriminate the signals of $(CH_3)-N+-$ (d) at 3.1 ppm and the signals of CH_2-N- between 3.1 and 3.3 ppm (c), at 2.7 ppm the signal of CH_2-S- (a) and between 1.00 and 2.00 ppm the signals of aliphatic chain of the linker (b). Also, in the magnification of the spectra (figure 449D) in the range between 5.80-6.00 a single peak attributable to the maleimide signal is present just in the LipoBlank (*) and disappears in the Lipo-MTAB sample. Notable, as the difference between magnification of Spectra 3.b, is present a small peak at 5.96 (°) that could be related to the residual unreacted hydrolyzed maleimide.
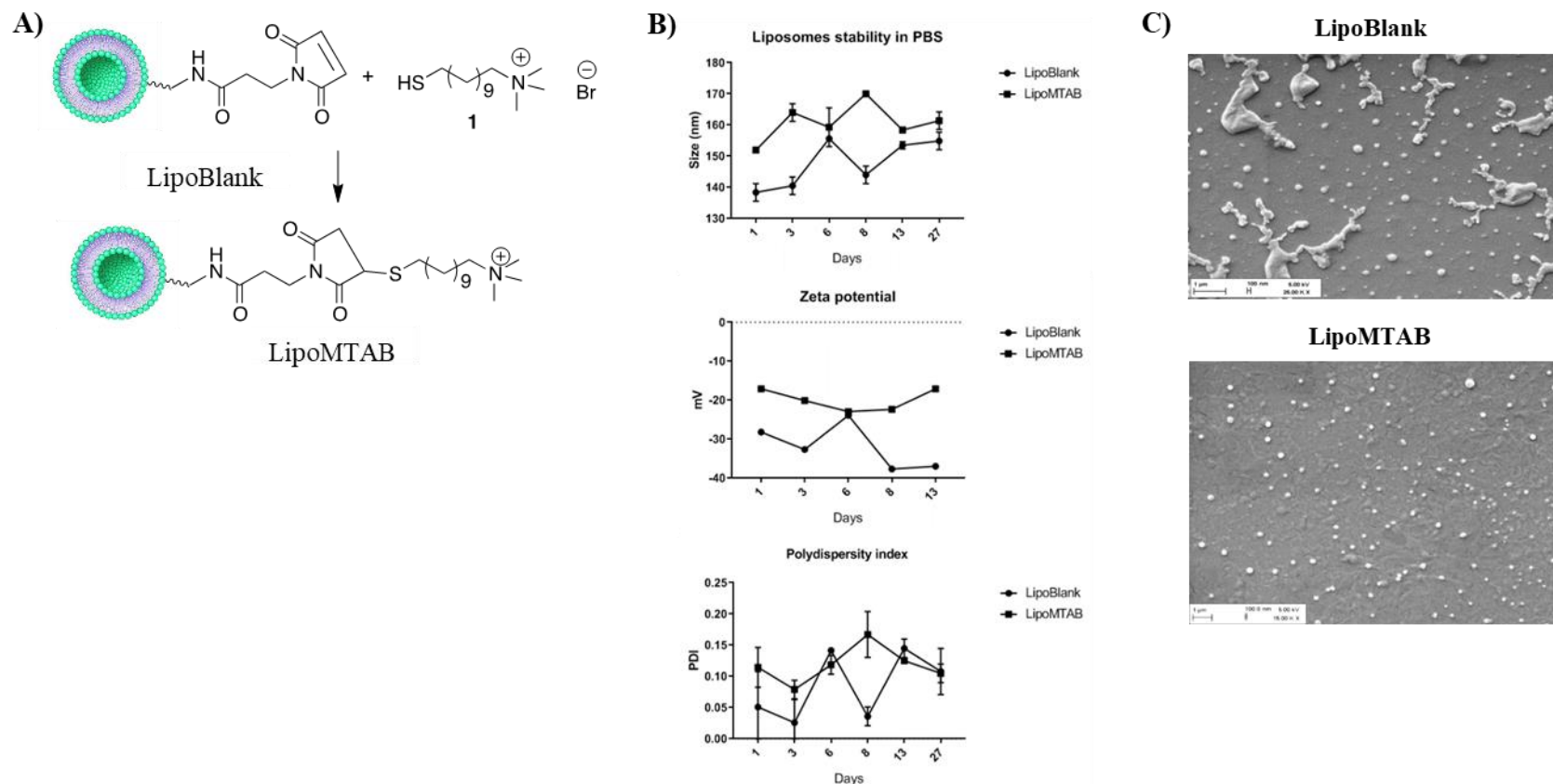
Figure 48. Physico-chemical and morphological characterization of liposomes. A) Scheme of liposome production via thiol-maleimide reaction: LipoBlank composed of sphingomyelin-cholesterol-DSPE-maleimide with (1) (11-mercaptoundecyl)-N,N,N-trimethylammonium bromide. B) Liposome size over time, measured by DLS. C) Stability via size, zeta potential values of liposomes over time assessed by DLS equipped with zeta-pals analyzer and polydispersity index (PDI) of liposomes, measured by DLS. All these data are referred to liposomes stored during storage in PBS at 4°C (n=3); C) Scanning electron micrographs of LipoBlank and LipoMTAB (n= 3 micrographs per sample of 3 experiments).
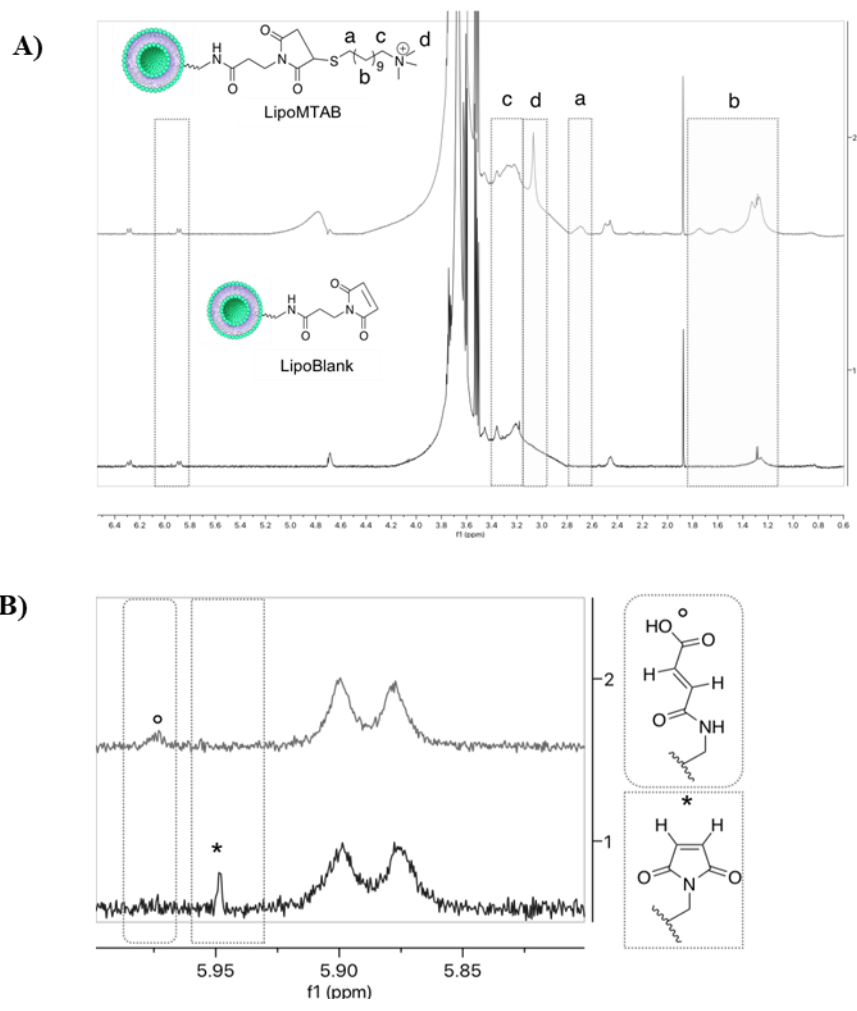
Figure 49. Surface characterization of liposomes via NMR. A) Spectra with H$_2$O presaturation; B) Magnification of spectra between 5.80 and 6.00 ppm – differences between Lipo-Blank with maleimide group(*) and Lipo-MTAB with partially unreacted hydrolyzed maleimide group(°)

3.2. LipoMTAB as a formulation against the adherence of *E. coli* DH5α

In figure 50A, a representative image relative to the formation of halos, or zones-of-inhibition, obtained after a 16h of incubation is reported. The results indicate that the LipoMTAB (1.8 and 3.6 µmol of lipids, corresponding to 33.8 and 67.5 µg/mL of attached MTAB), as the free MTAB (25-200 µg/mL), present well-defined boundaries on halos, independent on the presence of the liposomes *per se*. From the comparison of the results reported in fig. 50B, we can observe that LipoMTAB displayed an average halo-of-inhibition of 1 cm in diameter at a concentration that corresponds to 33.8 µg/mL of attached MTAB, while free MTAB gave halos with the same dimensions only when used at a concentration of 200 µg/mL (fig. 50C).

A)

| | 3.6 | 1.8 | 0.9 | (μmol) |

LipoMTAB

LipoBlank

| | 200 | 50 | 25 | 10 | (μg/ml) |

Free MTAB

No drug

B) Drop diffusion of LipoMTAB on *E. coli* DH5α

C) Drop diffusion of Free MTAB on *E. coli* DH5α
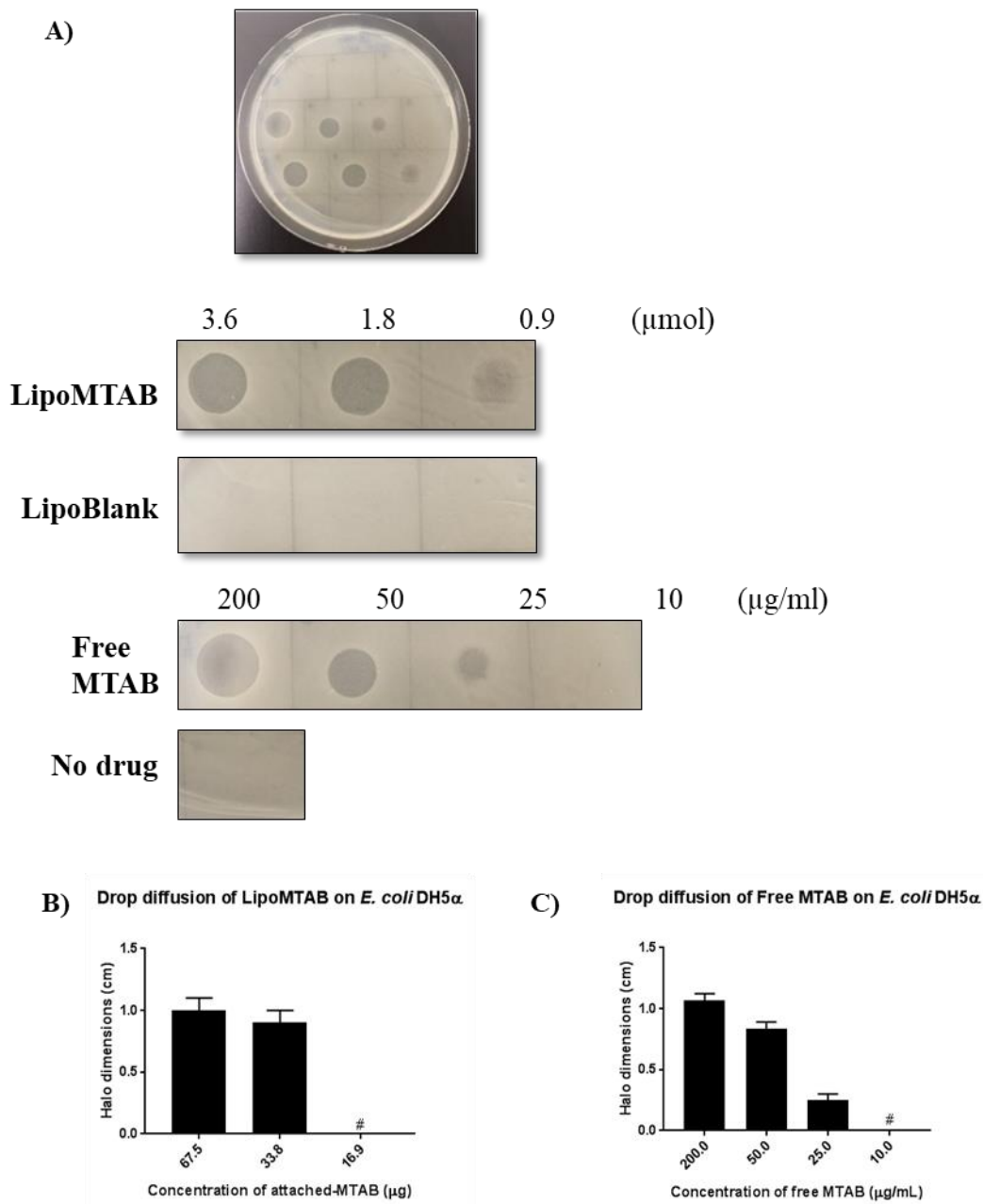
Figure 50. Liposome activity as bacterial anti-adherence formulation. A) Halo formation during the growth of *E. coli* DH5α on agar plates: Free and liposome-attached MTAB are the only samples where there is halo formation, showing attached MTAB has maintained its biological activity. Diameters of halos (3 halos per condition per experiment) during the drop diffusion assay of LipoMTAB (B) and free MTAB (C): the amount of MTAB and the halo formation is compared on free MTAB (50μg/mL) and on LipoMTAB (67.5 μg/mL of MTAB attached to liposome surface) (n=3).

3.3. Liposomal formulation did not inhibit bacterial growth or survival

The antibacterial activity of free MTAB (range of 4-1000 µg/mL) was evaluated on *E. coli*. Growth inhibition was observed with MTAB in a range of 4-1000 µg/mL (Figure 51A). However, no antibacterial effect could be seen with the formulations (LipoBlank or LipoMTAB, in a range of 0.1-67.5 µg/mL of attached-MTAB) (data not shown).

The focus on bactericidal activity was approached with the colony-forming unit assay. In this assay, we focused on the supernatant fraction of the samples, in which we determined whether bactericidal effects would derive from leachates, instead of a surface-based inhibition, where the liposomes would be deposited. The surface will be further discussed in the next section, focusing on electron microscopy imaging.

Fig. 51B shows *E.coli* survival, focusing on the liposomal particles and controls (positive Colistin and negative, PBS no drug). Compared to PBS control, only Colistin had bactericidal effects by 50% and free MTAB provided no counted colonies during the experiment (data not are shown). LipoBlank and LipoMTAB do not possess a bactericidal effect derived from leachates; however, as seen in Fig. 43B, there is also no inhibition of bacterial proliferation.
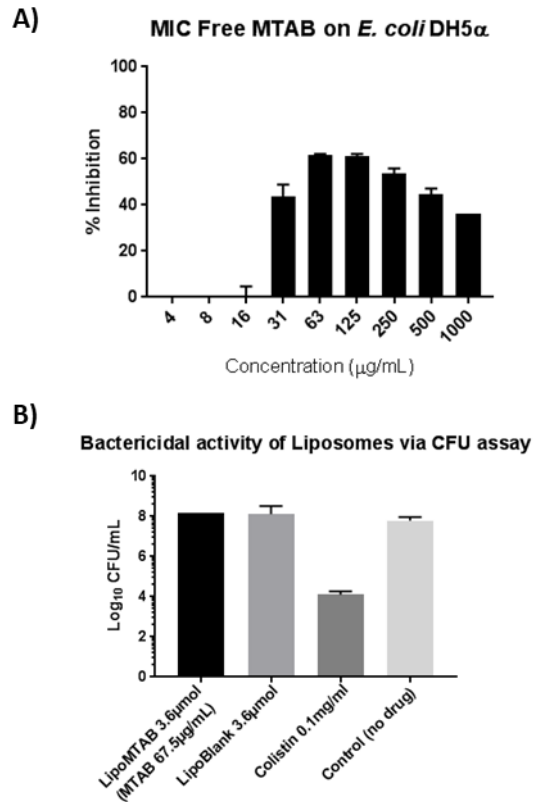
Figure 51. Influence of MTAB on E coli growth and survival. A) Minimal inhibitory concentration (MIC) follows changes in the turbidity of bacterial culture over 24h; only MTAB from 31-1000 µg/mL can provide inhibition (nor LipoBlank or LipoMTAB, at different concentrations, had inhibitory activity). B) Colony-forming units assay results from bacterial proliferation on agar; comparing Liposomes to no treatment and Colistin, as a positive control, there was no inhibition of bacteria survival of the liposomal formulations (n=3).

3.4. Liposomal formulation rescue cytotoxicity of MTAB onto lung epithelial cells

The advantages of bacteria inhibition of free MTAB is hampered by its cytotoxicity. Covalent coupling of MTAB on liposomal surfaces also aims to avoid its cytotoxic effect. To validate the effect of MTAB functionalized liposomes compared to free MTAB, LDH and MTT assays on A549 cells have been performed. The results in fig. 52 showed that when MTAB is attached to the surface of the liposome, there is a 25% reduction in LDH release, and there was a recover on cell viability to 100%.
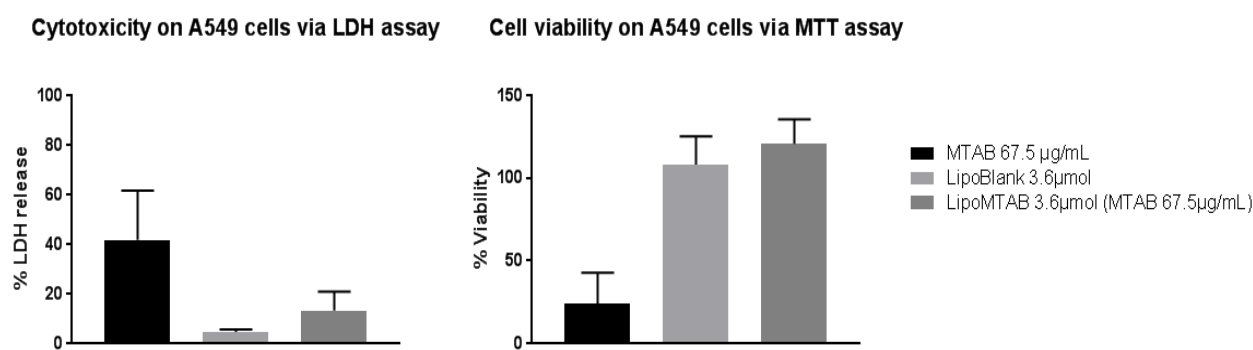
Figure 52. Viability of A549 lung epithelial cells on liposomal formulations and free MTAB. The detection of Lactate dehydrogenase (LDH) occurs during membrane burst with the release of cytoplasmatic content as a cytotoxic activity, while Tetrazolium MTT is converted to formazan detection only in live cells as a sign of cell metabolic activity. Free MTAB is cytotoxic; however, this can be rescued if MTAB is attached to the surface of liposomes (n=3).

3.5. LipoMTAB reduces bacteria coverage and destabilizes bacterial membrane, resembling Colistin

Our liposomal particle brings attached MTAB to a biocompatible formulation, focusing on the production of a surface to inhibit bacterial adherence. This surface needs further assessment, and SEM was our chosen method. Fig. 53A demonstrates area coverage of bacteria growth, and on a qualitative assessment, we observe lower coverage on samples treated with Colistin and LipoMTAB, while LipoBlank shows increased coverage when compared to the control without treatment.

A second evaluation was provided by selected images of individual bacteria exposed to different treatments. SEM allows observing morphological alterations bacteria at high resolution. Zoomed details of Fig. 53A provides the main example of modifications as membrane blebbing caused by exposure to high doses of Colistin (0.1 mg/mL; 4 times higher than the MIC[224]). Micrographs from the surface where *E. coli* was treated with LipoMTAB show indentations producing a rough surface on bacteria that possibly induce the release of cytoplasmatic content (pointed by the black arrow on Fig. 53A).

From the shown bacteria during SEM, we assessed membrane stability on the remaining *E. coli*, since CFU was not able to define culturable differences. Fig. 53B shows results on the use of propidium iodide as an indicator of membrane impairment[212,225]. Via membrane damage, propidium iodide enters the cells, and its fluorescence can be detected. LipoBlank samples do not show fluorescence, and, in comparison to the control, this indicates no membrane damage. Using 0.1mg/mL Colistin and control of bacteria damage, we found that the treatment with LipoMTAB provides membrane impairment of 74% when compared to Colistin.
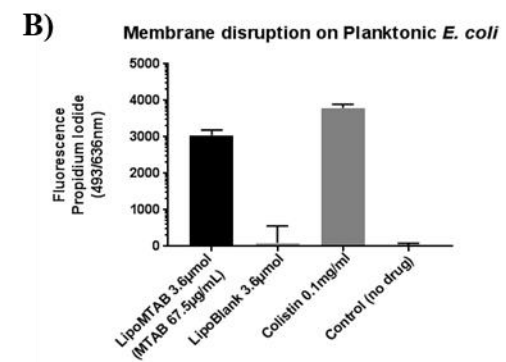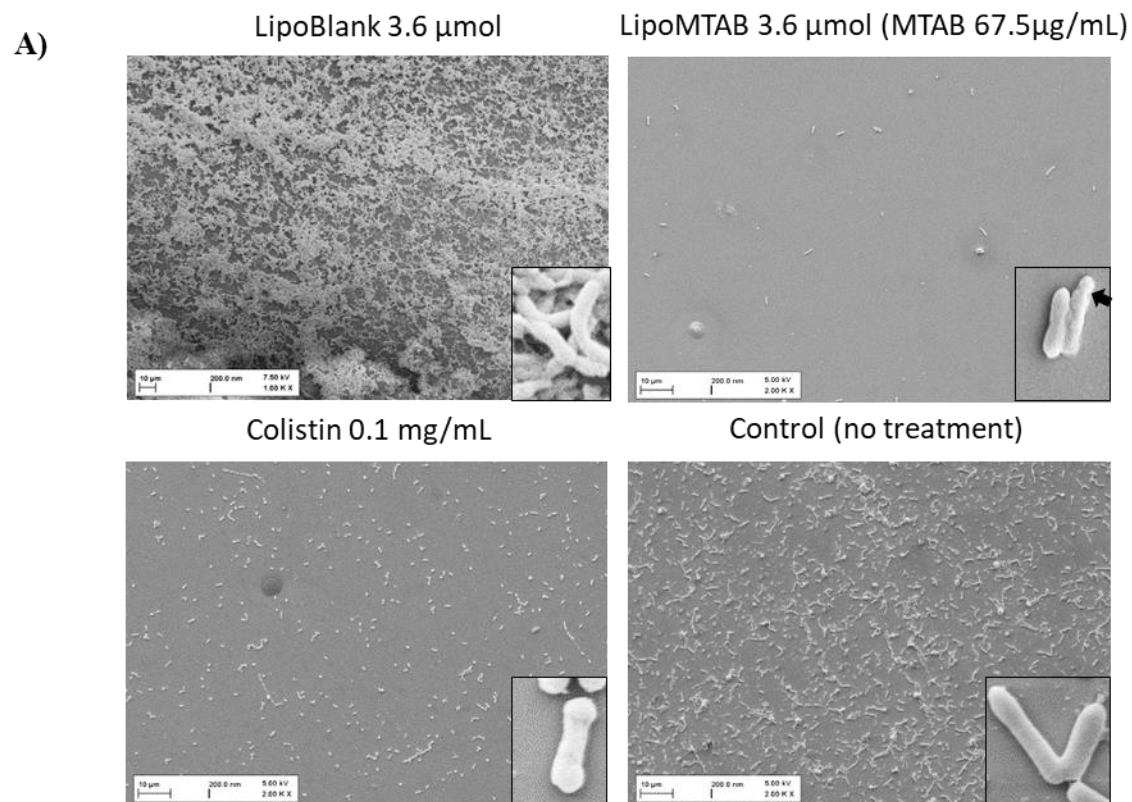
A)

LipoBlank 3.6 μmol   LipoMTAB 3.6 μmol (MTAB 67.5μg/mL)

Colistin 0.1 mg/mL   Control (no treatment)

B)

Membrane disruption on Planktonic *E. coli*

Figure 53. Liposome activity on E coli surface growth and bacterial membrane. A) Micrographs of liposomes, Colistin and control with selected views from bacteria membrane. (n=3 images per sample of 3 experiments). B) Fluorescence of propidium in membrane-impaired-only (n=3).

4. Discussion

The use of QAS as anti-adherence compounds have been extensively studied in the last years. One of the main obstacles in their application as anti-biofilm agents in the human sphere is due to the cytotoxicity they usually carry out. To overcome this issue, we exploited liposomes to obtain a biocompatible anti-adherence formulation of QAS. The (11-mercaptoundecyl)-N,N, N-trimethylammonium bromide (MTAB) was chosen as QAS for its molecular structure: while its reaction and final product are shown in Figure 1. Although it has commonly been assumed that the hydrophobic chain plays a pivotal role in the surfactant antimicrobial properties, it was also demonstrated that the head group is essential to perform the biological activity. In this context, the MTAB positive charged head group strongly enhances the interaction with the negatively charged bacterial membrane. Moreover, the counterion is also involved in exerting antimicrobial activity. It was proven that the bromide counterion is more effective when compared to the others[226].

It was proposed that a "phospholipid sponge effect" explains the results of specific adhesion from bacterial anionic phospholipids onto hydrophobic surfaces produced by quaternary ammonium groups[227]. On the development of microbe-killing polymers with QAS, it is shown that it can be achieved via non-releasing surfaces. More importantly, it is now being acknowledged that the use of surface-attached QAS develops a mechanism that can enlist negatively charged phospholipids from the bacterial cell wall and seize those within the matrix, in our case, of liposomes.[228]

Our hypothesis is that surface-bound MTAB onto liposomes can exploit the phospholipid sponge effect, in the account that MTAB is a QAS.

With the successful production of functionalized liposomes, we, therefore, assessed specific adherence of bacterial colonization. We decided to spread the planktonic *E. coli* on agar surfaces in a variation of the Kirby-Bauer disk diffusion susceptibility

test[229], using drops of treatment solution/suspension, instead of the known antibiotic disks. Although this kind of assay does not comprise bacterial killing, it still allows us, to mimic a field of action in which the influences on bacteria are dependent on surface interactions.

Thus, the surface covered by bacteria was challenged with free MTAB at different concentrations and liposomes with or without MTAB surface functionalization. As MTAB is known to inhibit adherence, we used this assay as the primary screening point, to achieve an anti-adherence formulation regarding the dose-dependency of the attached MTAB liposome.

The data from Fig. 42 suggests that the efficacy of MTAB is enhanced when the molecule is exposed on the nanoparticle surface rather than free in solution. These results are the first proof of the possibility to transfer the anti-adherence bacterial activity of MTAB onto a liposomal formulation by attaching the molecule on the nanoparticle surface avoiding encapsulation, a method that probably makes more effective its activity.

This shown anti-adherence activity must be further explored, and the first expected question is the release of MTAB, either from the breakdown of the liposomes or from a non-sufficient purification of the formulation after the MTAB functionalization. Despite no bactericidal effects of the liposomal formulations, this data from the drop diffusion on agar shows that the role of the formulations will focus on the surface of growth.

On that note, liposome fluidity influences how these particles interact with bacteria and, depending on the bacteria, also on its phospholipid composition, e.g., 91% of phosphatidylethanolamine on the outer membrane of *E. coli*[230]. Our formulations were analyzed on a 24 h of interaction with *E. coli,* and this time point, together with bacteria proliferation and consequent lower pH, is expected to promote liposome fusion to be delivered to the surface (in our case of the glass coverslips) or bacterial

membrane/biofilm surface. From imaging the washed surface of the sample by SEM, we concluded the remaining small number of bacteria could not differentiate the effects of free versus attached-MTAB via the CFU assay.

If its action on bacteria was shown, we checked the safety of the formulation. In an initial assessment, we saw that the advantage of using covalent linked Lipo-MTAB is the formation of stable thioether linkage along with the functionalization to the phospholipid layer. By coupling MTAB to the surface of liposomal carriers, we could reduce this compound toxicity while improving biological activity against bacteria.[231]

Micrographs from the surface where *E. coli* was treated with LipoMTAB show indentations producing a rough surface on bacteria that possibly induce the release of cytoplasmatic content

SEM micrographs showed indentations and more irregular surfaces on bacteria with an indication of the opening of membrane barrier. Using propidium iodide as an indicator of membrane impairment[212,225], we checked for membrane damage, as propidium iodide enters the cells, and its fluorescence can be detected.

The results of LipoMTAB providing membrane impairment of 74% - when compared to Colistin – point out our initial proof of mechanism of action.

5. Conclusion

QAS has provided the primary tool to develop surfaces that kill and inhibit bacterial adherence. This effect can now be used on the engineering of QAS into a well established, and FDA approved nanoparticle formulation that also allows encapsulation of drugs. We used liposomes on the usefulness of its fluidity to provide easy encapsulation of drugs, but also on fusion to the bacterial membrane. LipoMTAB is quickly produced via a thiol-maleimide Michael reaction using a commercial QAS (11-mercaptoundecyl)-N,N,N-trimethylammonium bromide. This formulation was characterized and shown to be homogenous and pharmaceutically stable.

Using *E. coli* DH5α, LipoMTAB showed similar results on the inhibition of bacterial adherence than its free counterpart, with the advantage of decreasing cytotoxicity of MTAB when covalently attached to our liposome. Despite no detectable effect on bacteria growth or survival, SEM showed improved antiadhesion properties on washed surfaces, as comparable as colistin, while remaining bacteria on LipoMTAB samples were demonstrated to present membrane damage as initial insight into the mechanism of action of this formulation. The presented study provides facile production of a new formulation that presents an influence on bacterial adherence, leading the path for combination therapy against bacterial infection and biofilm formation.

Chapter 4. General conclusions and future perspectives

The lung is one of the most critical routes concerning the entering of particles and pathogens in the human body and this brings advantages and disadvantages. The benefits consist of the possibility to deliver drugs directly on targets that are exposed to the air-interface of the lung. Furthermore, the inhalation of particles can be used to deliver drugs with solubility issues, target problems in different areas of the lung or specific cells and crosse specific biological barriers as the bacterial biofilm.

This dynamic counts with other challenges that alter the physiology and structure of the lung. The blockage of the airways is known as bronchiectasis, in which the leading causes are related to lung infection, alteration on lung fluid/mucus, or neonatal remodeling. Cystic fibrosis counts with all these alterations. As a genetic disease, it brings defects on the CFTR channel affecting mostly the lungs, pancreas and gastrointestinal tract.

For the lungs, CF remodels the airways, decreases the absorption of chloride that impairs the transport of water into the cells, alters mucus viscosity that contributes to the blocking of airways, facilitates the adherence of bacteria and thereby allowing the transition of bacteria from planktonic to biofilm, while inducing excessive inflammation, lung damage and alterations of the immune system.

Passing by these characteristics, the complexity of this disease was attempted to be modeled on small animals, and in mice, it can be observed the non-conformity of CFTR or EnaC mutations or even simple resolution of infection/inflammation. There are advantages from this and other *in vivo* models, but to provide focus on molecular mechanisms, the use of cells is recommended[232].

From direct lung cells to immortalized cell lines, the use of CF cells has started the field on the modeling of this disease. Cells as CFBE41o-, intrinsically presenting deletion of CFTR via the ΔF508 mutation, bring the potential to understanding epithelial alterations in

the presence of disease. When combining cells and pathogens, we increase the complexity of the system and get closer to the *in vivo* situation. Important cells command the immune reaction, while others create a biological barrier, and with those, the insight on pathogen adaptation and growth is further analyzed.

This thesis presents a combination of CF epithelia, macrophages, and *P. aeruginosa* in the view of providing a platform to test new antibacterial agents while allowing them to investigate host-pathogen interaction. From optimizing cell adaptation to bacterial growth, this first step allowed the understanding of how to perform the first co-culture of cells and bacteria. A second optimization was required to include the second cell type and then promote infection.

A co-culture of CFBE41o- epithelia, THP-1 macrophages, and *P. aeruginosa* provided the comprehension of cell death facing infection, but also the potential for stability among regulation of cell growth, epithelial barrier, and macrophages transmigration. Even though we would still require more information on cell interactions, the insights into alterations of cell morphology and viability will capture the need to understand how and why bacteria develop differently on top of cells versus when bacteria are alone.

Our model is stable for 24h without infection and 6 hours after the infection with *P. aeruginosa*, bringing an essential window for the investigation on biofilm initiation, cell behavior towards the regulation of cell surface markers, stimulation of migration and initiation/maintenance of inflammation. This was observed within 3 hours of infection in which macrophages cross the transwell membrane and the epithelial layer to reach bacteria. However, without treatment, this migration does not avoid the formation of *in vitro* mushroom-shaped biofilms.

If macrophages are transmigrating, we could observe the immediate (3hpi) uptaking of bacteria by those cells when on top of the epithelial layer. This brings opportunities to new

strategies to identify mechanisms of macrophage transmigration, of improvement of epithelia-macrophage interaction, and on clearing of infection.

Because these cell dynamics are occurring, we investigated how *P. aeruginosa* adapted its growth on top of the different cell types when compared to the abiotic environment as plastic microplates.

When growth could present differences, the efficacy of known drugs could be assessed to alter this infected environment. Tobramycin administration on the different conditions was able to control bacterial early growth, but not the formation of biofilm and potential pressure for increased expression of resistance genes. Importantly, this drug efficacy was shown to be statistically different when comparing bacteria-only surfaces versus bacteria on a cellular surface. One log of difference is found on infected double cell co-culture if compared to bacteria alone, and this could influence drug potential during the preclinical testing of discoveries.

Associated with infection, inflammation has its production via the release of cytokines, and on a panel analysis of uninfected, infected, and infected treated mono and co-cultures, we observe the proinflammatory potential of sterile interaction in between the cells and the stimulation via *P. aeruginosa* growth. This potential was associated with cytokines related to neutrophil recruitment, activation of the inflammasome via NF-κB and the regulation of foreign DNA-sensing in cells. Plus, new cytokines are now demonstrated to influence infection and tobramycin treatment, focusing on how models that combine key cells for disease progression can bring a platform for the control of inflammation.

This control will not mean the complete extinguishment of cytokine production. An important lesson here is that cytokines must be remembered as regulatory signals and its network is designed to increase inflammation to fight infection. Most cytokines are molecular effectors to initiate bacterial killing. Immunomodulation on anti-inflammation cytokines as

IL-10 or proinflammatory as IL-6 and IL-8 will connect the physiological and the excessive reaction of the immune system, but also bring the potential of discovery antibodies and particles as therapy.

If the host response was initially characterized, bacteria growth is beyond being a regular aggregation. Its formation of communities required communication and this is regulated by virulence factors as pyocyanin and pyoverdine. Those molecules regulate the Pseudomonas Quinolone System and are in demand for drug testing/delivery platforms[233]. For us, although variation on cell types did not influence the production of these factors, the regular release of bacteria that are re-adapting in a live and different substrate is an advantage to integrate results on a more complex model, providing simultaneous analysis of cells and bacteria.

This co-culture was successful in integrating macrophages as representative of immune cells. Other cells from the innate immunity will provide tools of inflammation control and even new technologies on drug delivery. Neutrophils are critical cells on the production of antimicrobial peptides and specific trapping for bacteria-killing. These short-lived cells are challenging to handle, and cell lines as the HL-60 have been considered an option. During this thesis, there was a characterization for the differentiation of HL-60 promyelocytes as neutrophil-like cells.

By using the early cell death of neutrophils, a new strategy is provided: the use of particle to hitchhike activated neutrophils towards the infected site. It was shown that BSA particles have this potential, and in combination with HL-60 as a cell model, there is the chance to analyze: what are the material (lipids, polymers, etc.) that regulate this uptake and what sort of surface chemistry influences this stability inside neutrophil-like cells? Can the migration of neutrophils be integrated into the presented co-culture to mimick the CF infected

environment and the need for specific delivery drugs and particles? Is the use of drug-loaded particles and NETs effective therapy against bacterial infections?

Once bacteria is installed, the formation of biofilm alters all possibilities of drug efficacy and few models present alternatives for testing. The use of particles to protect drug stability or targeting is everyday, including the potential to modify the surface of these particles. Understanding the use of quaternary ammonium salts as antimicrobial molecules bring this use to decorate particles, especially liposomes. With our Sphingomyelin-Cholesterol-DSPE liposomes decorated with MTAB, *E. coli* adherence can be inhibited with the potential to disrupt the bacterial membrane, rendering potential to avoid biofilm formation. There is a need to continue to investigate these particles towards its use on drug-loading and influence on the growth of other relevant bacteria.

Finally, the co-culture is now a platform where drug testing is now brought to the level of complexity that gathers markers from both cells and bacteria. Future experiments on the interaction of cells can provide insights into the increase of antimicrobial molecules on lining fluid or its transport to mucus. Mucus needs to be considered here as an additional barrier to understanding the regulation of viscosity, propensity for infection and particle clearance during the modeling of CF disease.

Different barriers are created upon the interaction between cells and bacteria. Not only drug transport is altered, but the application of nanoformulations for the lower airways should be investigated on cell uptake, stimulation of migration and cell morphology and its consequent effects from bacterial adaptation.

As the infected model is stable with all components until 6 hours post-infection, new efforts should be considered to prolong this time window, especially on the potential to develop mature biofilm and the possibility of drug administration in repeated doses.

Drug delivery as a field must look for the needed and complex environment that molecules or particles will interact with. It will be then closely-related to cell metabolism and physiology. Co-cultures like this provide the substrate, a living substrate that can be controlled, but that at first, it must be characterized.

V. List of Abbreviations

μg   micrograms

μL   microliters

μM   micromolar

3D   three-dimensional

ALI   air-liquid interface

ATCC American Type Culture Collection

ATRA all-trans retinoic acid

BBI   Broadband Decoupling Inverse

BETR baseline, exacerbation, treatment, recovering

BSA   bovine serum albumin

cAMP 3',5'-cyclic adenosine monophosphate

CD   cluster of differentiation

CF   Cystic Fibrosis

CFBE Cystic Fibrosis bronchial epithelia

CFDA 5-Carboxyfluorescein diacetate

CFTR cystic fibrosis transmembrane conductance regulator

CFU   colony-forming units

CLSM Confocal Laser Scanning Microscopy

cm   centimeters

COPD Chronic obstructive pulmonary disease

CTAB cetrimonium bromide

DAPI   4′,6-diamidino-2-phenylindole

DCFH-DA   2',7'-dichlorofluorescein-diacetate

DCs   dendritic cells

DLS   Dynamic Light Scattering

DMSO   dimethylsulfoxide

DSMZ *Deutsche Sammlung von Mikroorganismen und Zellkulturen*

DSPE-PEG(2000)   1,2-distearoyl-sn-glycero-3-phosphoethanolamine-N-[amino(polyethylene glycol)-2000]

EDTA Ethylenediaminetetraacetic acid

ELISA   Enzyme-linked immunosorbent assay

ENaC epithelial sodium channel

ERK   extracellular regulated kinases

ESKAPE   *Enterococcus*, *Staphylococcus aureus*, *Klebsiella* species, *Acinetobacter baumannii*, *Pseudomonas aeruginosa*, *Enterobacter*

EVOM epithelial volt ohmmeter

FDA   United States Food and Drug Administration

FITC fluorescein isothiocyanate

fMLP N-Formylmethionyl-leucyl-phenylalanine

FSC   forward scatter

GFP   green fluorescent protein

GM-CSF   Granulocyte-macrophage colony-stimulating factor

h   hours

HDMS Hexamethyldisilazane

HIPS Helmholtz-Institute for Pharmaceutical Research Saarland

HL   human leukocyte

hpi   hours post-infection

HPLC High-performance liquid chromatography

IFN   interferon

IL   interleukin

IL-1Ra IL-1 receptor antagonist

IL-1RAcP   IL-1 receptor accessory protein

IL-1RI IL-1 type I receptor

iPSC   inducible pluripotent stem cells

kDa   kilodaltons

LAS   Leica Application Suite

LB   Luria-Bertani

LDH   lactate dehydrogenase

LPS   lipopolysaccharide

M   molar

MBEC Minimum biofilm eradication concentration

MBIC Minimum biofilm inhibitory concentration

MEM   Minimum Essential Media

mg   milligrams

MHC   Major histocompatibility complex

MIC   Minimum inhibitory concentration

min   minutes

mL   milliliters

MMP   matrix metalloproteinases

MOI   multiplicity of infection

mRNA   messenger Ribonucleic acid

MRSA Methicillin-resistant *Staphylococcus aureus*

MTAB (11-mercaptoundecyl)-N,N,N-trimethylammonium bromide

MTS   3-(4,5-dimethylthiazol-2-yl)-5-(3-carboxymethoxyphenyl)-2-(4-sulfophenyl)-2H-
tetrazolium

MTT   3-(4,5-dimethylthiazol-2-yl)-2,5-diphenyltetrazolium bromide

MWCO   molecular weight cut-off

NADH   oxidized Nicotinamide adenine dinucleotide

NBT   Nitroblue tetrazolium

NEAA non-essential amino acids

NET   neutrophil extracellular traps

NF-κB nuclear factor kappa-light-chain-enhancer of activated B cells

NK   natural-killer

nM   nanomolar

NMR   Nuclear Magnetic Resonance

OD   optical density

OTUs operational taxonomic units

PAMPs   pathogen-associated molecular patterns

PAO   *Pseudomonas aeruginosa*

PBS   phosphate-buffered saline

PDI   polydispersity index

PET   Polyethylene terephthalate

PFA   paraformaldehyde

pg   picograms

pH   potential hydrogen

PMA   phorbol 12-myristate 13-acetate

PMN   polymorphonuclear neutrophil

PPGAS   protease peptone glucose ammonium salt

PQS   Pseudomonas quinolone signal

QAC   quaternary ammonium compounds

QAS   quaternary ammonium surfactants

RAR   retinoic acid receptor

ROS   reactive oxygen species

RPM   rotations per minute

RPMI Roswell Park Memorial Institute

RT   room temperature

SD   standard deviation

SEM   Scanning Electron Microscopy

SME   soyaethyl morpholinium ethosulfate

SSC   side scatter

TEER   transepithelial electrical resistance

TIMP   tissue inhibitors of metalloproteinases

TJ   tight junctions

TLR   Toll-like receptors

TNF   tumor necrosis factor

tob   tobramycin

TSLP   thymic stromal lymphopoietin

TTSS   type III secretion system

ZO-1   zona occludens-1

VI. List of Figures

VII. References

1. Bishop, A. E. & Polak, J. M. Pulmonary Epithelium. *Methods Enzymol.* **418**, 333–349 (2006).

2. Chang, M. M.-J., Shih, L. & Wu, R. Pulmonary Epithelium: Cell Types and Functions. *Pulm. Ep. Heal. Dis.* 1–26 (2008). doi:10.1002/9780470727010.ch1

3. Berube, K., Prytherch, Z., Job, C. & Hughes, T. Human primary bronchial lung cell constructs: The new respiratory models. *Toxicology* **278**, 311–318 (2010).

4. Hou, J., Scientist, S. & Epithelium, H. A. Airway Epithelial Cells Airway Epithelium and Its Region- Specific Stem And Progenitor Cells. 1–4 (2015).

5. Van Ree, R., Hummelshøj, L., Plantinga, M., Poulsen, L. K. & Swindle, E. Allergic sensitization: Host-immune factors. *Clin. Transl. Allergy* **4**, 1–9 (2014).

6. Tomashefski, J. F. & Dail, D. H. *Dail and Hammar ' s Pulmonary Pathology.* (Springer International Publishing, 2008). doi:10.1007/978-0-387 -68792-6

7. Fanning, A. S. & Anderson, J. M. Zonula Occludens-1 and -2 Are Cytosolic Scaffolds That Regulate the Assembly of Cellular Junctions. *Ann N Y Acad Sci* **1165**, 113–120 (2009).

8. Coyne, C. B., Gambling, T. M., Boucher, R. C., Carson, J. L. & Johnson, L. G. Role of claudin interactions in airway tight junctional permeability. *Am. J. Physiol. Cell. Mol. Physiol.* **285**, L1166–L1178 (2003).

9. Knight, D. A. & Holgate, S. T. The airway epithelium : Structural and functional properties in health and disease. *Respirology* **8**, 432–446 (2003).

10. Bauer, R. N., Diaz-Sanchez, D. & Jaspers, I. Effects of air pollutants on innate

immunity: The role of Toll-like receptors and nucleotide-binding oligomerization domain–like receptors. *J Allergy Clin Immunol* **129**, 14–26 (2012).

11. Fisher, J. T., Zhang, Y. & Engelhardt, J. F. Comparative biology of cystic fibrosis animal models. *Methods Mol. Biol.* **742**, 311–334 (2011).

12. Zosky, G. R. & Sly, P. D. Animal models of asthma. *Clin. Exp. Allergy* **37**, 973–988 (2007).

13. Miller, A. J. & Spence, J. R. In Vitro Models to Study Human Lung Development, Disease and Homeostasis. *Physiology* **32**, 246–260 (2017).

14. Ruggeri, B. A., Camp, F. & Miknyoczki, S. Animal models of disease: Pre-clinical animal models of cancer and their applications and utility in drug discovery. *Biochem. Pharmacol.* **87**, 150–161 (2014).

15. Metzger, R. J., Klein, O. D., Martin, G. R. & Krasnow, M. A. The branching programme of mouse lung development. *Nature* **453**, 745–50 (2008).

16. Perrin, S. Make mouse studies work. *Nature* **507**, 423–425 (2014).

17. Sakagami, M. In vivo, in vitro and ex vivo models to assess pulmonary absorption and disposition of inhaled therapeutics for systemic delivery. *Adv. Drug Deliv. Rev.* **58**, 1030–1060 (2006).

18. Hittinger, M. *et al.* Preclinical safety and efficacy models for pulmonary drug delivery of antimicrobials with focus on in vitro models. *Adv. Drug Deliv. Rev.* **85**, 44–56 (2014).

19. Pezzulo, A. A. *et al.* The air-liquid interface and use of primary cell cultures are important to recapitulate the transcriptional profile of in vivo airway epithelia. *Am. J.*

Physiol. Cell. Mol. Physiol. **300**, L25–L31 (2010).

20. Chen, Y. W. *et al.* A three-dimensional model of human lung development and disease from pluripotent stem cells. *Nat. Cell Biol.* **19**, 542–549 (2017).

21. Wong, A. P. *et al.* Directed differentiation of human pluripotent stem cells into mature airway epithelia expressing functional CFTR protein. *Nat. Biotechnol.* **30**, 876–882 (2012).

22. Hiemstra, P. S., McCray, P. B. & Bals, R. The innate immune function of airway epithelial cells in inflammatory lung disease. *Eur. Respir. J.* 1–13 (2015). doi:10.1183/09031936.00141514

23. Tan, Q., Choi, K. M., Sicard, D. & Tschumperlin, D. J. Human airway organoid engineering as a step toward lung regeneration and disease modeling. *Biomaterials* **113**, 118–132 (2017).

24. Huang, S., Wiszniewski, L. & Constant, S. The Use of In Vitro 3D Cell Models in Drug Development for Respiratory Diseases. *Drug Discov. Dev.* 169–190 (2007).

25. Hittinger, M. *et al.* Preclinical safety and efficacy models for pulmonary drug delivery of antimicrobials with focus on in vitro models. *Adv. Drug Deliv. Rev.* **85**, 44–56 (2015).

26. Blank, F. *et al.* Macrophages and dendritic cells express tight junction proteins and exchange particles in an in vitro model of the human airway wall. *Immunobiology* **216**, 86–95 (2011).

27. Hermanns, M. I., Unger, R. E., Kehe, K., Peters, K. & Kirkpatrick, C. J. Lung epithelial cell lines in coculture with human pulmonary microvascular endothelial

cells: development of an alveolo-capillary barrier in vitro. *Lab. Invest.* **84**, 736–752 (2004).

28. Chowdhury, F., Howat, W. J., Phillips, G. J. & Lackie, P. M. Interactions between endothelial cells and epithelial cells in a combined cell model of airway mucosa: Effects on tight junction permeability. *Exp. Lung Res.* **36**, 1–11 (2010).

29. Papritz, M. *et al.* Side-specific effects by cadmium exposure: Apical and basolateral treatment in a coculture model of the blood-air barrier. *Toxicol. Appl. Pharmacol.* **245**, 361–369 (2010).

30. Cutting, G. R. Cystic fibrosis genetics: from molecular understanding to clinical application. *Nat. Rev. Genet.* **16**, 45–56 (2015).

31. MacKenzie, T. *et al.* Longevity of patients with cystic fibrosis in 2000 to 2010 and beyond: Survival analysis of the Cystic Fibrosis Foundation Patient Registry. *Ann. Intern. Med.* **161**, 233–241 (2014).

32. Cystic Fibrosis Foundation. About Cystic Fibrosis | CF Foundation. (2016).

33. Zielenski, J. Cystic Fibrosis: Genotypic and Phenotypic Variations. *Annu. Rev. Genet.* **29**, 777–807 (1995).

34. Saint-Criq, V. & Gray, M. A. Role of CFTR in epithelial physiology. *Cell. Mol. Life Sci.* **74**, 93–115 (2017).

35. Hull, J. Cystic fibrosis transmembrane conductance regulator dysfunction and its treatment. *J. R. Soc. Med.* **105 Suppl**, S2-8 (2012).

36. Smith, J. J., Travis, S. M., Greenberg, E. P. & Welsh, M. J. Cystic fibrosis airway epithelia fail to kill bacteria because of abnormal airway surface fluid. *Cell* **85**, 229–

236 (1996).

37.   Stutts, M. J. *et al.* CFTR as a cAMP-dependent regulator of sodium channels. *Science (80-.).* **269**, 847–850 (1995).

38.   Matsui, H. *et al.* Evidence for periciliar liquid layer depletion not abnormal ion composition, in the pathogenesis of cystic fibrosis airway disease. *Cell* **95**, 1005–1015 (1999).

39.   Jiang, C., Finkbeiner, W. E., Widdicombe, J. H. & Miller, S. S. Fluid transport across cultures of human tracheal glands is altered in cystic fibrosis. *J. Physiol.* **501**, 637–647 (1997).

40.   Mogensen, T. H. Pathogen recognition and inflammatory signaling in innate immune defenses. *Clin. Microbiol. Rev.* **22**, 240–273 (2009).

41.   Patel, V. I. & Metcalf, J. P. Airway macrophage and dendritic cell subsets in the resting human lung. *Crit. Rev. Immunol.* **38**, 303–331 (2018).

42.   Hartl, D. *et al.* Innate Immunity of the Lung: From Basic Mechanisms to Translational Medicine. *J. Innate Immun.* **10**, 487–501 (2018).

43.   Duque, G. A. & Descoteaux, A. Macrophage cytokines: Involvement in immunity and infectious diseases. *Front. Immunol.* **5**, 1–12 (2014).

44.   Laval, J., Ralhan, A. & Hartl, D. Neutrophils in cystic fibrosis. *Biol. Chem.* **397**, 485–496 (2016).

45.   Koller, B. *et al.* Innate immune receptors on neutrophils and their role in chronic lung disease. *Eur. J. Clin. Invest.* **39**, 535–547 (2009).

46.   Kreda, S. M., Davis, C. W. & Rose, M. C. CFTR, Mucins, and Mucus Obstruction in

Cystic Fibrosis. *Cold Spring Harb Perspect Med.* **2**, (2012).

47. Hartl, D. *et al.* Innate immunity in cystic fibrosis lung disease. *J. Cyst. Fibros.* **11**, 363–382 (2012).

48. Ormerod, L. P., Thomson, R. A., Anderson, C. M. & Stableforth, D. E. Reversible airway obstruction in cystic fibrosis. *Thorax* **35**, 768–772 (1980).

49. Cole, A. M., Dewan, P. & Ganz, T. Innate antimicrobial activity of nasal secretions. *Infect. Immun.* **67**, 3267–3275 (1999).

50. Wagner, V. E. & Iglewski, B. H. P. aeruginosa Biofilms in CF Infection. *Clin. Rev. Allergy Immunol.* **35**, 124–134 (2008).

51. Janeway, C. A. Pillars article: approaching the asymptote? Evolution and revolution in immunology. Cold spring harb symp quant biol. 1989. 54: 1-13. *J. Immunol.* **191**, 4475–87 (2013).

52. Bodas, M. & Vij, N. The NFκB Signaling in Cystic Fibrosis Lung Disease: Pathophysiology and Therapeutic Potential. *Discov. Med.* **9**, 346–356 (2010).

53. Schroeder, T. H. *et al.* CFTR is a pattern recognition molecule that extracts Pseudomonas aeruginosa LPS from the outer membrane into epithelial cells and activates NF- B translocation. *Proc. Natl. Acad. Sci.* **99**, 6907–6912 (2002).

54. Levy, H. *et al.* IL1B polymorphisms modulate cystic fibrosis lung disease. *Pediatr. Pulmonol.* **44**, 580–593 (2009).

55. Ratner, D. & Mueller, C. Immune responses in cystic fibrosis: Are they intrinsically defective? *Am. J. Respir. Cell Mol. Biol.* **46**, 715–722 (2012).

56. Gao, L., Kim, K. J., Yankaskas, J. R. & Forman, H. J. Abnormal glutathione transport

in cystic fibrosis airway epithelia. *Am. J. Physiol. Cell. Mol. Physiol.* **277**, L113–L118 (2017).

57. Chen, J. *et al.* CFTR negatively regulates cyclooxygenase-2-PGE 2 positive feedback loop in inflammation. *J. Cell. Physiol.* **227**, 2759–2766 (2012).

58. Bhagirath, A. Y. *et al.* Cystic fibrosis lung environment and Pseudomonas aeruginosa infection. *BMC Pulm. Med.* **16**, 1–22 (2016).

59. Zhao, J. *et al.* Decade-long bacterial community dynamics in cystic fibrosis airways. *Proc. Natl. Acad. Sci.* **109**, 5809–5814 (2012).

60. Peterson, J. *et al.* The NIH Human Microbiome Project. *Genome Res.* **19**, 2317–2323 (2009).

61. Hiemstra, P. S., McCray, P. B. & Bals, R. The innate immune function of airway epithelial cells in inflammatory lung disease. *Eur. Respir. J.* **45**, 1150–1162 (2015).

62. Gollwitzer, E. S. *et al.* Lung microbiota promotes tolerance to allergens in neonates via PD-L1. *Nat. Med.* **20**, 642–647 (2014).

63. Sibley, C. D. *et al.* Culture enriched molecular profiling of the cystic fibrosis airway microbiome. *PLoS One* **6**, 25–27 (2011).

64. Pezzulo, A. A. *et al.* Abundant DNase I-Sensitive Bacterial DNA in Healthy Porcine Lungs and Its Implications for the Lung Microbiome. *Appl. Environ. Microbiol.* **79**, 5936–5941 (2013).

65. Lyczak, J. B., Cannon, C. L. & Pier, G. B. Establishment of Pseudomonas aeruginosa infection: Lessons from a versatile opportunist. *Microbes Infect.* **2**, 1051–1060 (2000).

66. Lyczak, J. B., Cannon, C. L. & Pier, G. B. Lung Infections Associated with Cystic

Fibrosis Lung Infections Associated with Cystic Fibrosis. *Clin. Microbiol. Rev.* **15**, 194–222 (2002).

67. Goodman, A. L. *et al.* A signaling network reciprocally regulates genes associated with acute infection and chronic persistence in Pseudomonas aeruginosa. *Dev. Cell* **7**, 745–754 (2004).

68. Moradali, M. F., Ghods, S. & Rehm, B. H. A. Pseudomonas aeruginosa Lifestyle: A Paradigm for Adaptation, Survival, and Persistence. *Front. Cell. Infect. Microbiol.* **7**, 39 (2017).

69. Jefferson, K. K. What drives bacteria to produce a biofilm? *FEMS Microbiol. Lett.* **236**, 163–173 (2004).

70. Ventre, I. *et al.* Multiple sensors control reciprocal expression of Pseudomonas aeruginosa regulatory RNA and virulence genes. *Proc. Natl. Acad. Sci.* **103**, 171–176 (2006).

71. Hauser, A. R., Jain, M., Bar-Meir, M. & McColley, S. A. Clinical significance of microbial infection and adaptation in cystic fibrosis. *Clin. Microbiol. Rev.* **24**, 29–70 (2011).

72. D'Argenio, D. A., Worth Calfee, M., Rainey, P. B. & Pesci, E. C. Autolysis and Autoaggregation in Pseudomonas aeruginosa Colony Morphology Mutants. *Microbiology* **184**, 6481–6489 (2002).

73. D'Argenio, D. A. *et al.* Growth phenotypes of Pseudomonas aeruginosa lasR mutants adapted to the airways of cystic fibrosis patients. *Mol. Microbiol.* **64**, 512–533 (2007).

74. Kirisits, M. J., Prost, L. & Parsek, M. R. Characterization of Colony Morphology

Variants Isolated from Pseudomonas aeruginosa Biofilms. *Am. Soc. Microbiol.* **71**, 4809–4821 (2005).

75. Cigana, C. *et al.* Pseudomonas aeruginosa exploits lipid a and muropeptides modification as a strategy to lower innate immunity during cystic fibrosis lung infection. *PLoS One* **4**, (2009).

76. Yang, L., Chen, L., Shen, L., Surette, M. & Duan, K. Inactivation of MuxABC-OpmB Transporter System in Pseudomonas aeruginosa Leads to Increased Ampicillin and Carbenicillin Resistance and Decreased Virulence. *J. Microbiol.* **49**, 107–114 (2011).

77. Martha, B. *et al.* In-vivo impact of the MexXY efflux system on aminoglycoside efficacy in an experimental model of Pseudomonas aeruginosa pneumonia treated with tobramycin. *Clin. Microbiol. Infect.* **12**, 426–432 (2006).

78. Rowe, S. M. *et al.* Progress in cystic fibrosis and the CF Therapeutics Development Network. *Thorax* **67**, 882–90 (2012).

79. Genilloud, O. Actinomycetes: Still a source of novel antibiotics. *Nat. Prod. Rep.* **34**, 1203–1232 (2017).

80. Baumann, S. *et al.* Cystobactamids: Myxobacterial topoisomerase inhibitors exhibiting potent antibacterial activity. *Angew. Chemie - Int. Ed.* **53**, 14605–14609 (2014).

81. Boucher, H. W. *et al.* Bad Bugs, No Drugs: No ESKAPE! An Update from the Infectious Diseases Society of America. *Clin. Infect. Dis.* **48**, 1–12 (2009).

82. Thomann, A., De Mello Martins, A. G. G., Brengel, C., Empting, M. & Hartmann, R. W. Application of Dual Inhibition Concept within Looped Autoregulatory Systems toward Antivirulence Agents against Pseudomonas aeruginosa Infections. *ACS Chem.*

Biol. **11**, 1279–1286 (2016).

83.	d'Angelo, I. *et al.* Improving the efficacy of inhaled drugs in cystic fibrosis: Challenges and emerging drug delivery strategies. *Adv. Drug Deliv. Rev.* **75**, 92–111 (2014).

84.	Limoli, D. H. *et al.* Pseudomonas aeruginosa Alginate Overproduction Promotes Coexistence with Staphylococcus aureus in a Model of Cystic Fibrosis Respiratory Infection. *MBio* **8**, 1–18 (2017).

85.	Yu, Q. *et al.* In vitro evaluation of tobramycin and aztreonam versus Pseudomonas aeruginosa biofilms on cystic fibrosis-derived human airway epithelial cells. *J. Antimicrob. Chemother.* **67**, 2673–2681 (2012).

86.	Stanton, B. A., Coutermarsh, B., Barnaby, R. & Hogan, D. Pseudomonas aeruginosa reduces VX-809 stimulated F508del-CFTR chloride secretion by airway epithelial cells. *PLoS One* **10**, 1–13 (2015).

87.	Flitter, B. A. *et al. Pseudomonas aeruginosa* sabotages the generation of host proresolving lipid mediators. *Proc. Natl. Acad. Sci.* **114**, 136–141 (2017).

88.	Semaniakou, A., Croll, R. P. & Chappe, V. Animal models in the pathophysiology of cystic fibrosis. *Front. Pharmacol.* **9**, 1–16 (2019).

89.	Hoffmann, N. *et al.* Novel mouse model of chronic Pseudomonas aeruginosa lung infection mimicking cystic fibrosis. *Infect. Immun.* **73**, 2504–2514 (2005).

90.	Meyerholz, D. K. *et al.* Loss of cystic fibrosis transmembrane conductance regulator function produces abnormalities in tracheal development in neonatal pigs and young children. *Am. J. Respir. Crit. Care Med.* **182**, 1251–1261 (2010).

91. Wine, J. J. The development of lung disease in cystic fibrosis pigs. *Sci. Transl. Med.* **2**, (2010).

92. Bonfield, T. In Vivo Models of Lung Disease. *Lung Dis. - Sel. State Art Rev.* (2012). doi:10.1103/PhysRevLett.109.037003

93. Wine, J. J. *et al.* Genomic DNA sequence of Rhesus (M. mulatta) cystic fibrosis (CFTR) gene. *Mamm. Genome* **9**, 301–305 (1998).

94. Williams, S. H. *et al.* Evaluation of gene targeting by homologous recombination in ovine somatic cells. *Mol. Reprod. Dev.* **66**, 115–125 (2003).

95. Sun, X. *et al.* Disease phenotype of a ferret CFTR -knockout model of cystic fibrosis. *J. Clin. Invest.* **120**, 3149–3160 (2010).

96. de Souza Carvalho, C., Daum, N. & Lehr, C. M. Carrier interactions with the biological barriers of the lung: Advanced in vitro models and challenges for pulmonary drug delivery. *Adv. Drug Deliv. Rev.* **75**, 129–140 (2014).

97. Rothen-Rutishauser, B. *et al.* A newly developed in vitro model of the human epithelial airway barrier to study the toxic potential of nanoparticles. *ALTEX Altern. zu Tierexperimenten* **25**, 191–196 (2008).

98. Kasper, J. Y., Hermanns, M. I., Unger, R. E. & Kirkpatrick, C. J. A responsive human triple-culture model of the air–blood barrier: incorporation of different macrophage phenotypes. *J. Tissue Eng. Regen. Med.* **11**, 1285–1297 (2017).

99. Takai, D., Nagase, T. & Shimizu, T. New therapeutic key for cystic fibrosis: a role for lipoxins. *Nat. Immunol.* **5**, 357–358 (2004).

100. Janssen, W. J., Stefanski, A. L., Bochner, B. S. & Evans, C. M. Control of lung

defence by mucins and macrophages: Ancient defence mechanisms with modern functions. *Eur. Respir. J.* **48**, 1201–1214 (2016).

101. Deng, Y., Herbert, J. A., Smith, C. M. & Smyth, R. L. An in vitro transepithelial migration assay to evaluate the role of neutrophils in Respiratory Syncytial Virus (RSV) induced epithelial damage. *Sci. Rep.* **8**, 1–12 (2018).

102. Dartmouth Medical School. Lab #4 Slides: Blood, Bone Marrow, Respiratory System, Integument & Mammary Gland. (2011).

103. Klein, S. G., Hennen, J., Serchi, T., Blömeke, B. & Gutleb, A. C. Potential of coculture in vitro models to study inflammatory and sensitizing effects of particles on the lung. *Toxicol. Vitr.* **25**, 1516–1534 (2011).

104. Ding, P., Wu, H., Fang, L., Wu, M. & Liu, R. Transmigration and phagocytosis of macrophages in an airway infection model using four-dimensional techniques. *Am. J. Respir. Cell Mol. Biol.* **51**, 1–10 (2014).

105. Kusek, M. E., Pazos, M. a., Pirzai, W. & Hurley, B. P. In vitro Coculture Assay to Assess Pathogen Induced Neutrophil Trans-epithelial Migration. *J. Vis. Exp.* 1–10 (2014). doi:10.3791/50823

106. Awatade, N. T. *et al.* Measurements of Functional Responses in Human Primary Lung Cells as a Basis for Personalized Therapy for Cystic Fibrosis. *EBioMedicine* **2**, 147–153 (2015).

107. Awatade, N. T. *et al.* Human Primary Epithelial Cell Models: Promising Tools in the Era of Cystic Fibrosis Personalized Medicine. *Front. Pharmacol.* **9**, 1–11 (2018).

108. Pollard, B. S. & Pollard, H. B. Induced pluripotent stem cells for treating cystic

fibrosis: State of the science. *Pediatr. Pulmonol.* **53**, S12–S29 (2018).

109. Kuehn, A. *et al.* Human alveolar epithelial cells expressing tight junctions to model the air-blood barrier. *ALTEX* **33**, 251–260 (2016).

110. Greene, C. M. *et al.* TLR-Induced Inflammation in Cystic Fibrosis and Non-Cystic Fibrosis Airway Epithelial Cells. *J. Immunol.* **174**, 1638–1646 (2014).

111. Dechecchi, M. C. *et al.* MPB-07 reduces the inflammatory response to Pseudomonas aeruginosa in cystic fibrosis bronchial cells. *Am. J. Respir. Cell Mol. Biol.* **36**, 615–624 (2007).

112. Lehmann, A. D. *et al.* An in vitro triple cell co-culture model with primary cells mimicking the human alveolar epithelial barrier. *Eur. J. Pharm. Biopharm.* **77**, 398–406 (2011).

113. Kletting, S. *et al.* Co-culture of human alveolar epithelial (hAELVi) and macrophage (THP-1) cell lines. *ALTEX* **35**, 211–222 (2018).

114. Moreau-Marquis, S., Redelman, C. V, Stanton, B. a & Anderson, G. G. Co-culture models of Pseudomonas aeruginosa biofilms grown on live human airway cells. *J. Vis. Exp.* 2–5 (2010). doi:10.3791/2186

115. Moreau-Marquis, S., O'Toole, G. A. & Stanton, B. A. Tobramycin and FDA-approved iron chelators eliminate Pseudomonas aeruginosa biofilms on cystic fibrosis cells. *Am. J. Respir. Cell Mol. Biol.* **41**, 305–313 (2009).

116. Juntke, J. A novel co-culture model of human bronchial epithelial cells and Pseudomonas aeruginosa biofilms to mimic chronic lung infections in cystic fibrosis. (University of Saarland, 2018). doi:10.22028/D291-27897

117. LaFayette, S. L. *et al.* Cystic fibrosis–adapted Pseudomonas aeruginosa quorum sensing lasR mutants cause hyperinflammatory responses . *Sci. Adv.* **1**, e1500199 (2015).

118. Orazi, G. & O'Toole, G. A. Pseudomonas aeruginosa alters Staphylococcus aureus sensitivity to vancomycin in a biofilm model of cystic fibrosis infection. *MBio* **8**, 1–17 (2017).

119. Castellani, S., Di Gioia, S., di Toma, L. & Conese, M. Human Cellular Models for the Investigation of Lung Inflammation and Mucus Production in Cystic Fibrosis. *Anal. Cell. Pathol. (Amst).* **2018**, 3839803 (2018).

120. Cozens, A. L. *et al.* CFTR Expression and Chloride Secretion in Polarized Immortal Human Bronchial Epithelial Cells. *Am J Respir Cell Mol. Bio.* **10**, 38–47 (1994).

121. Moreau-Marquis, S. *et al.* The DeltaF508-CFTR mutation results in increased biofilm formation by Pseudomonas aeruginosa by increasing iron availability. *Am. J. Physiol. Lung Cell. Mol. Physiol.* **295**, L25–L37 (2008).

122. Tsuchiya, S. *et al.* Establishment and characterization of a human acute monocytic leukemia cell line (THP-1). *Int. J. Cancer* **26**, 171–176 (1980).

123. Schwende, H., Fitzke, E., Ambs, P. & Dieter, P. Differences in the state of differentiation of THP-1 cells induced by phorbol ester and 1,25-dihydroxyvitamin D3. *J. Leukoc. Biol.* **59**, 555–561 (1996).

124. Susewind, J. *et al.* A 3D co-culture of three human cell lines to model the inflamed intestinal mucosa for safety testing of nanomaterials. *Nanotoxicology* **5390**, 1–10 (2015).

125. Montaudon M, Lederlin M, Reich S, Begueret H, Tunon-de-Lara JM, Marthan R, Berger P, L. F. Bronchial Measurements in Patients with Asthma : Comparison of Quantitative Thin-Section CT Findings with Those in Healthy Subjects and Correlation with Purpose : Methods : Results : Conclusion : *Radiology* **253**, (2009).

126. de Souza Carvalho, C. *et al.* Internalization, phagolysosomal biogenesis and killing of mycobacteria in enucleated epithelial cells. *Cell. Microbiol.* **13**, 1234–1249 (2011).

127. Chandorkar, P. *et al.* Fast-track development of an in vitro 3D lung/immune cell model to study Aspergillus infections. *Sci. Rep.* **7**, 1–13 (2017).

128. Lopes-Pacheco, M. CFTR modulators: Shedding light on precision medicine for cystic fibrosis. *Front. Pharmacol.* **7**, 1–20 (2016).

129. Schrier, S. B., Hill, A. S., Plana, D. & Lauffenburger, D. A. Synergistic Communication between CD4+ T Cells and Monocytes Impacts the Cytokine Environment. *Sci. Rep.* **6**, 1–11 (2016).

130. Nitta, C. F. & Orlando, R. A. Crosstalk between Immune Cells and Adipocytes Requires Both Paracrine Factors and Cell Contact to Modify Cytokine Secretion. *PLoS One* **8**, (2013).

131. Baum, M. M. *et al.* Characterization of structures in biofilms formed by a Pseudomonas fluorescens isolated from soil. *BMC Microbiol.* **9**, 103 (2009).

132. Roy, S., Bonfield, T. & Tartakoff, A. M. Non-Apoptotic Toxicity of Pseudomonas aeruginosa toward Murine Cells. *PLoS One* **8**, (2013).

133. Bucki, R. *et al.* Polyelectrolyte-mediated increase of biofilm mass formation. *BMC Microbiol.* **15**, (2015).

134. Fuxman Bass, J. I. *et al.* Extracellular DNA: A Major Proinflammatory Component of Pseudomonas aeruginosa Biofilms. *J. Immunol.* **184**, 6386–6395 (2010).

135. Adamali, H. *et al.* Macrophage migration inhibitory factor enzymatic activity, lung inflammation, and cystic fibrosis. *Am. J. Respir. Crit. Care Med.* **186**, 162–169 (2012).

136. Kämpfer, A. A. M. *et al.* Development of an in vitro co-culture model to mimic the human intestine in healthy and diseased state. *Toxicol. Vitr.* **45**, 31–43 (2017).

137. Kaja, S., Payne, A. J., Naumchuk, Y. & Koulen, P. Quantification of lactate dehydrogenase for cell viability testing using cell lines and primary cultured astrocytes. *Curr. Protoc. Toxicol.* **2017**, 1–10 (2017).

138. Crabbé, A. *et al.* Antimicrobial efficacy against Pseudomonas aeruginosa biofilm formation in a three-dimensional lung epithelial model and the influence of fetal bovine serum. *Sci. Rep.* **7**, 1–13 (2017).

139. Sagel, S. D., Chmiel, J. F. & Konstan, M. W. Sputum Biomarkers of Inflammation in Cystic Fibrosis Lung Disease. *Proc. Am. Thorac. Soc.* **4**, 406–417 (2007).

140. Husson, M. O., Wizla-Derambure, N., Turck, D., Gosset, P. & Wallaert, B. Effect of intermittent inhaled tobramycin on sputum cytokine profiles in cystic fibrosis. *J. Antimicrob. Chemother.* **56**, 247–249 (2005).

141. Gallagher, L. A., McKnight, S. L., Kuznetsova, M. S., Pesci, E. C. & Manoil, C. Functions required for extracellular quinolone signaling by Pseudomonas aeruginosa. *J. Bacteriol.* **184**, 6472–6480 (2002).

142. Mowat, E. *et al.* Pseudomonas aeruginosa population diversity and turnover in cystic fibrosis chronic infections. *Am. J. Respir. Crit. Care Med.* **183**, 1674–1679 (2011).

143. Danis-Wlodarczyk, K. *et al.* A proposed integrated approach for the preclinical evaluation of phage therapy in Pseudomonas infections. *Sci. Rep.* **6**, 28115 (2016).

144. Kamal, A. A. M., Petrera, L., Eberhard, J. & Hartmann, R. W. Structure-functionality relationship and pharmacological profiles of: Pseudomonas aeruginosa alkylquinolone quorum sensing modulators. *Org. Biomol. Chem.* **15**, 4620–4630 (2017).

145. Hurley, B. P., Siccardi, D., Mrsny, R. J. & McCormick, B. A. Polymorphonuclear cell transmigration induced by Pseudomonas aeruginosa requires the eicosanoid hepoxilin A3. *J. Immunol.* **173**, 5712–5720 (2004).

146. Ehrhardt, C. *et al.* Towards an in vitro model of cystic fibrosis small airway epithelium: characterisation of the human bronchial epithelial cell line CFBE41o-. *Cell Tissue Res.* **323**, 405–415 (2006).

147. Moreau-Marquis, S. *et al.* The F508-CFTR mutation results in increased biofilm formation by Pseudomonas aeruginosa by increasing iron availability. *AJP Lung Cell. Mol. Physiol.* **295**, L25–L37 (2008).

148. Kang, D., Turner, K. & Kirienko, N. PqsA Promotes Pyoverdine Production via Biofilm Formation. *Pathogens* **7**, 3 (2017).

149. John, G., Yildirim, A. Ö., Rubin, B. K., Gruenert, D. C. & Henke, M. O. TLR-4-mediated innate immunity is reduced in cystic fibrosis airway cells. *Am. J. Respir. Cell Mol. Biol.* **42**, 424–431 (2010).

150. Hampton, T. H. *et al.* Does the F508-CFTR mutation induce a proinflammatory response in human airway epithelial cells? *Am. J. Physiol. Lung Cell. Mol. Physiol.* **303**, L509-18 (2012).

151. Montgomery, S. T., Mall, M. A., Kicic, A. & Stick, S. M. Hypoxia and sterile inflammation in cystic fibrosis airways: Mechanisms and potential therapies. *Eur. Respir. J.* **49**, 1–13 (2017).

152. Johnston, B. L. & Conly, J. M. Tumour necrosis factor inhibitors and infection: What is there to know for infectious diseases physicians? *Can. J. Infect. Dis. Med. Microbiol.* **17**, 209–212 (2006).

153. Ali, T. *et al.* Clinical use of anti-TNF therapy and increased risk of infections. *Drug. Healthc. Patient Saf.* **5**, 79–99 (2013).

154. Bonfield, T. L., Konstan, M. W. & Berger, M. Altered respiratory epithelial cell cytokine production in cystic fibrosis. *J. Allergy Clin. Immunol.* **104**, 72–78 (1999).

155. Courtney, J. M., Ennis, M. & Elborn, J. S. Cytokines and inflammatory mediators in cystic fibrosis. *J. Cyst. Fibros.* **3**, 223–231 (2004).

156. Ballinger, M. N. *et al.* Role of granulocyte macrophage colony-stimulating factor during gram-negative lung infection with Pseudomonas aeruginosa. *Am. J. Respir. Cell Mol. Biol.* **34**, 766–774 (2006).

157. Cao, J. *et al.* IL-27 controls sepsis-induced impairment of lung antibacterial host defence. *Thorax* **69**, 926–937 (2014).

158. Nish, S. A. *et al.* T cell-intrinsic role of IL-6 signaling in primary and memory responses. *Elife* **2014**, 1–21 (2014).

159. Hams, E., Bermingham, R. & Fallon, P. G. Macrophage and innate lymphoid cell interplay in the genesis of fibrosis. *Front. Immunol.* **6**, 1–11 (2015).

160. Inoue, S. *et al.* IL-15 Prevents Apoptosis, Reverses Innate and Adaptive Immune

Dysfunction, and Improves Survival in Sepsis. *J. Immunol.* **184**, 1401–1409 (2009).

161. Opal, S. M. *et al.* Recombinant Human Interleukin-11 in Experimental Pseudomonas aeruginosa Sepsis in Immunocompromised Animals . *J. Infect. Dis.* **178**, 1205–1208 (2007).

162. Couper, K. N., Blount, D. G. & Riley, E. M. IL-10: The Master Regulator of Immunity to Infection. *J. Immunol.* **180**, 5771–5777 (2014).

163. Sun, L. *et al.* Effect of IL-10 on neutrophil recruitment and survival after Pseudomonas aeruginosa challenge. *Am. J. Respir. Cell Mol. Biol.* **41**, 76–84 (2009).

164. Anderson, G. G., Moreau-Marquis, S., Stanton, B. A. & O'Toole, G. A. In vitro analysis of tobramycin-treated Pseudomonas aeruginosa biofilms on cystic fibrosis-derived airway epithelial cells. *Infect. Immun.* **76**, 1423–1433 (2008).

165. Anderson, G. G., Kenney, T. F., Macleod, D. L., Henig, N. R. & O'Toole, G. A. Eradication of Pseudomonas aeruginosa biofilms on cultured airway cells by a fosfomycin/tobramycin antibiotic combination. *Pathog. Dis.* **67**, 39–45 (2013).

166. Fan, L. *et al.* Increased IL-8 production in human bronchial epithelial cells after exposure to azithromycin-pretreated *Pseudomonas aeruginosa in vitro*. *FEMS Microbiol. Lett.* **355**, 43–50 (2014).

167. Moraes, T. J. *et al.* Abnormalities in the pulmonary innate immune system in cystic fibrosis. *Am. J. Respir. Cell Mol. Biol.* **34**, 364–374 (2006).

168. Kennedy, A. D. & Deleo, F. R. Neutrophil apoptosis and the resolution of infection. *Immunol. Res.* **43**, 25–61 (2009).

169. Reid, D. W., Misso, N., Aggarwal, S., Thompson, P. J. & Walters, E. H. Oxidative

stress and lipid-derived inflammatory mediators during acute exacerbations of cystic fibrosis. *Respirology* **12**, 63–69 (2007).

170. Chmiel, J. F. & Davis, P. B. State of the art: why do the lungs of patients with cystic fibrosis become infected and why can't they clear the infection? *Respir. Res.* **4**, 8 (2003).

171. Kolpen, M. *et al.* Polymorphonuclear leucocytes consume oxygen in sputum from chronic Pseudomonas aeruginosa pneumonia in cystic fibrosis. *Thorax* **65**, 57–62 (2010).

172. Conese, M., Castellani, S., D'Oria, S., Di Gioia, S. & Montemurro, P. Role of Neutrophils in Cystic Fibrosis Lung Disease. *Intech* **i**, 13 (2017).

173. Rada, B. Interactions between Neutrophils and Pseudomonas aeruginosa in Cystic Fibrosis. *Pathogens* **6**, 10 (2017).

174. Chen, L.-Y. *et al.* Synergistic Induction of Inflammation by Bacterial Products Lipopolysaccharide and fMLP: An Important Microbial Pathogenic Mechanism. *J. Immunol.* **182**, 2518–2524 (2009).

175. Dagur, P. K. & McCoy, J. P. Collection, Storage, and Preparation of Human Blood Cells. *Curr. Protoc. Cytom.* **73**, 5.1.1-16 (2015).

176. Marcinkowska, E., Chrobak, A. & Wiedlocha, A. Evading apoptosis by calcitriol-differentiated human leukemic HL-60 cells is not mediated by changes in CD95 receptor system but by increased sensitivity of these cells to insulin. *Exp. Cell Res.* **270**, 119–127 (2001).

177. Drayson, M. T., Michell, R. H., Durham, J. & Brown, G. Cell proliferation and CD11b

expression are controlled independently during HL60 cell differentiation initiated by 1,25 alpha-dihydroxyvitamin D(3) or all-trans-retinoic acid. *Exp. Cell Res.* **266**, 126–134 (2001).

178. Carrigan, S. O., Weppler, A. L., Issekutz, A. C. & Stadnyk, A. W. Neutrophil differentiated HL-60 cells model Mac-1 (CD11b/CD18)-independent neutrophil transepithelial migration. *Immunology* **115**, 108–117 (2005).

179. Chu, D., Gao, J. & Wang, Z. Neutrophil-Mediated Delivery of Therapeutic Nanoparticles across Blood Vessel Barrier for Treatment of Inflammation and Infection. *ACS Nano* **9**, 11800–11811 (2015).

180. Hirako, N., Nakano, H. & Takahashi, S. A PU.1 suppressive target gene, metallothionein 1G, inhibits retinoic acid-induced NB4 cell differentiation. *PLoS One* **9**, 1–12 (2014).

181. Rastogi, R. P., Singh, S. P., Häder, D. P. & Sinha, R. P. Detection of reactive oxygen species (ROS) by the oxidant-sensing probe 2',7'-dichlorodihydrofluorescein diacetate in the cyanobacterium Anabaena variabilis PCC 7937. *Biochem. Biophys. Res. Commun.* **397**, 603–607 (2010).

182. Weirich, E. *et al.* Neutrophil CD11b expression as a diagnostic marker for early-onset neonatal infection. *J. Pediatr.* **132**, 445–451 (1998).

183. McIlroy, D. J. *et al.* Mitochondrial DNA neutrophil extracellular traps are formed after trauma and subsequent surgery. *J. Crit. Care* **29**, 1133.e1-1133.e5 (2014).

184. Yu, Z., Yu, M., Zhang, Z., Hong, G. & Xiong, Q. Bovine serum albumin nanoparticles as controlled release carrier for local drug delivery to the inner ear. *Nanoscale Res. Lett.* **9**, 1–7 (2014).

185.	Menina, S. *et al.* Invasin-functionalized liposome nanocarriers improve the intracellular delivery of anti-infective drugs. *RSC Adv.* **6**, 41622–41629 (2016).

186.	Roche Diagnostics International Ltd. *CASY Model TT – Cell Counter and Analyzer.* (2012).

187.	Chatterjee, D. *et al.* Monocytic differentiation of HL-60 promyelocytic leukemia cells correlates with the induction of Bcl-xL. *Cell Growth Differ.* **8**, 1083–1089 (1997).

188.	Baehner, R. & Nathan, D. Quantitative nitroblue tetrazolium test in chronic granulomatous disease. *Med. New Engl. J.* **307**, 205–211 (1982).

189.	Veda, P. Why are neutrophils polymorphonuclear? *Eur. J. Inflamm.* **9**, 85–93 (2011).

190.	Paiva, C. N. & Bozza, M. T. Are reactive oxygen species always detrimental to pathogens? *Antioxidants Redox Signal.* **20**, 1000–1034 (2014).

191.	Papayannopoulos, V. & Zychlinsky, A. NETs: a new strategy for using old weapons. *Trends Immunol.* **30**, 513–521 (2009).

192.	Khan, M. A. *et al.* Regulating NETosis: Increasing pH Promotes NADPH Oxidase-Dependent NETosis. *Front. Med.* **5**, (2018).

193.	Teimourian, S. & Moghanloo, E. Role of PTEN in neutrophil extracellular trap formation. *Mol. Immunol.* **66**, 319–324 (2015).

194.	Gray, R. D., McCullagh, B. N. & McCray, P. B. NETs and CF lung disease: Current status and future prospects. *Antibiotics* **4**, 62–75 (2015).

195.	Olins, A. L. & Olins, D. E. Cytoskeletal influences on nuclear shape in granulocytic HL-60 cells. *BMC Cell Biol.* **5**, 1–18 (2004).

196. Tasseff, R. *et al.* An Effective Model of the Retinoic Acid Induced HL-60 Differentiation Program. *Sci. Rep.* **7**, 1–21 (2017).

197. Jian, P. *et al.* Retinoic acid induces HL-60 cell differentiation via the upregulation of miR-663. *J. Hematol. Oncol.* **4**, 20 (2011).

198. Winterbourn, C. C., Kettle, A. J. & Hampton, M. B. Reactive Oxygen Species and Neutrophil Function. *Annu. Rev. Biochem.* **85**, 765–792 (2016).

199. Parkos, C. A., Delp, C., Amin Arnaout, M. & Madara, J. L. Neutrophil migration across a cultured intestinal epithelium: Dependence on a CD11b/CD18-mediated event and enhanced efficiency in physiological direction. *J. Clin. Invest.* **88**, 1605–1612 (1991).

200. Serikov, V. B., Choi, H., Chmiel, K. J., Wu, R. & Widdicombe, J. H. Activation of Extracellular Regulated Kinases Is Required for the Increase in Airway Epithelial Permeability during Leukocyte Transmigration. *Am. J. Respir. Cell Mol. Biol.* **30**, 261–270 (2004).

201. Zen, K., Liu, Y., Cairo, D. & Parkos, C. A. CD11b/CD18-Dependent Interactions of Neutrophils with Intestinal Epithelium Are Mediated by Fucosylated Proteoglycans. *J. Immunol.* **169**, 5270–5278 (2002).

202. Brinkmann, V. *et al.* Neutrophil Extracellular Traps Kill Bacteria. *Science (80-.).* **303**, 1532–1535 (2004).

203. Yaseen, R. *et al.* Antimicrobial activity of HL-60 cells compared to primary blood-derived neutrophils against Staphylococcus aureus. *J. Negat. Results Biomed.* **16**, 1–7 (2017).

204. Krachler, A. M. & Orth, K. Targeting the bacteria-host interface strategies in anti-adhesion therapy. *Virulence* **4**, 284–294 (2013).

205. Schütz, C. & Empting, M. Targeting the Pseudomonas quinolone signal quorum sensing system for the discovery of novel anti-infective pathoblockers. *Beilstein J. Org. Chem.* **14**, 2627–2645 (2018).

206. Gallo, J., Holinka, M. & Moucha, C. S. *Antibacterial surface treatment for orthopaedic implants*. *International Journal of Molecular Sciences* **15**, (2014).

207. Lallemand, F., Daull, P., Benita, S., Buggage, R. & Garrigue, J.-S. Successfully Improving Ocular Drug Delivery Using the Cationic Nanoemulsion, Novasorb. *J. Drug Deliv.* **2012**, 1–16 (2012).

208. Rizwana, N. The Role of Cetylpyridinium Chloride Mouthwash In The Treatment of Periodontitis. *Int. J. Pharm. Sci. Invent. ISSN* **2**, 36–37 (2013).

209. Gîfu, I. C. *et al.* Antimicrobial Activities of Hydrophobically Modified Poly(Acrylate) Films and Their Complexes with Different Chain Length Cationic Surfactants. *Coatings* **9**, 244 (2019).

210. Yang, S. C., Aljuffali, I. A., Sung, C. T., Lin, C. F. & Fang, J. Y. Antimicrobial activity of topically-applied soyaethyl morpholinium ethosulfate micelles against Staphylococcus species. *Nanomedicine* **11**, 657–671 (2016).

211. Hasan, J., Crawford, R. J. & Ivanova, E. P. Antibacterial surfaces: the quest for a new generation of biomaterials - ScienceDirect. *Trends Biotechnol.* **31**, 295–304 (2013).

212. Chamsaz, E. A., Mankoci, S., Barton, H. A. & Joy, A. Nontoxic Cationic Coumarin Polyester Coatings Prevent Pseudomonas aeruginosa Biofilm Formation. *ACS Appl.*

Mater. Interfaces **9**, 6704–6711 (2017).

213. Römling, U. *et al.* Microbial biofilm formation: A need to act. *J. Intern. Med.* **276**, 98–110 (2014).

214. Huh, A. J. & Kwon, Y. J. 'Nanoantibiotics': A new paradigm for treating infectious diseases using nanomaterials in the antibiotics resistant era. *J. Control. Release* **156**, 128–145 (2011).

215. Mi, G., Shi, D., Wang, M. & Webster, T. J. Reducing Bacterial Infections and Biofilm Formation Using Nanoparticles and Nanostructured Antibacterial Surfaces. *Adv. Healthc. Mater.* **7**, 1–23 (2018).

216. Tao, Y., Li, M. & Auguste, D. T. Pattern-based sensing of triple negative breast cancer cells with dual-ligand cofunctionalized gold nanoclusters. *Biomaterials* **116**, 21–33 (2017).

217. Mahmoud, N., Alkilany, A., Khalil, E. & Al-Bakri, A. Antibacterial activity of gold nanorods against Staphylococcus aureus and Propionibacterium acnes: misinterpretations and artifacts. *Int. J. Nanomedicine* **Volume 12**, 7311–7322 (2017).

218. Choi, I. *et al.* On-Demand Modulation of Bacterial Cell Fates on Multifunctional Dynamic Substrates. *ACS Appl. Mater. Interfaces* **10**, 4324–4332 (2018).

219. Salvati, E. *et al.* Liposomes functionalized to overcome the blood-brain barrier and to target amyloid-β peptide: The chemical design affects the permeability across an in vitro model. *Int. J. Nanomedicine* **8**, 1749–1758 (2013).

220. John Charles Marshali, S. Colorimetric determination of phospholipids with ammonium ferrothiocyanate. *Anal. Biochem.* **104**, 10–14 (1980).

221. Balouiri, M., Sadiki, M. & Ibnsouda, S. K. Methods for in vitro evaluating antimicrobial activity : A review. *J. Pharm. Anal.* **6**, 71–79 (2016).

222. Cho, J. *et al.* The antifungal activity and membrane-disruptive action of dioscin extracted from Dioscorea nipponica. *Biochim. Biophys. Acta - Biomembr.* **1828**, 1153–1158 (2013).

223. Freimoser, F. M., Jakob, C. A., Aebi, M. & Tuor, U. R. S. The MTT [3-(4,5-Dimethylthiazol-2-yl)-2,5-Diphenyltetrazolium Bromide] Assay Is a Fast and Reliable Method for Colorimetric Determination of Fungal Cell Densities. *Appl. Environ. Microbiol.* **65**, 3727–3729 (1999).

224. Simar, S., Sibley, D., Ashcraft, D. & Pankey, G. Colistin and Polymyxin B Minimal Inhibitory Concentrations Determined by Etest Found Unreliable for Gram-Negative Bacilli. *Ochsner J.* **17**, 239–242 (2017).

225. Kim, Y. M., Farrah, S. & Baney, R. H. Membrane damage of bacteria by silanols treatment. *Electron. J. Biotechnol.* **10**, 252–259 (2007).

226. Obłąk, E., Piecuch, A., Rewak-Soroczyńska, J. & Paluch, E. Activity of gemini quaternary ammonium salts against microorganisms. *Appl. Microbiol. Biotechnol.* 625–632 (2018). doi:10.1007/s00253-018-9523-2

227. Bieser, A. M. & Tiller, J. C. Mechanistic Considerations on Contact-Active Antimicrobial Surfaces with Controlled Functional Group Densities. *Macromol. Biosci.* **11**, 526–534 (2011).

228. Gao, J., White, E. M., Liu, Q. & Locklin, J. Evidence for the Phospholipid Sponge Effect as the Biocidal Mechanism in Surface-Bound Polyquaternary Ammonium Coatings with Variable Cross-Linking Density. *ACS Appl. Mater. Interfaces* **9**, 7745–

7751 (2017).

229. Hombach, M., Zbinden, R. & Böttger, E. C. Standardisation of disk diffusion results for antibiotic susceptibility testing using the sirscan automated zone reader. *BMC Microbiol.* **13**, (2013).

230. Wang, Z. *et al.* Fusion between fluid liposomes and intact bacteria: Study of driving parameters and in vitro bactericidal efficacy. *Int. J. Nanomedicine* **11**, 4025–4036 (2016).

231. Locatelli, E., Monaco, I. & Comes Franchini, M. Surface modifications of gold nanorods for applications in nanomedicine. *RSC Adv.* **5**, 21681–21699 (2015).

232. Marshall, L. J., Oguejiofor, W., Willetts, R. S., Griffiths, H. R. & Devitt, A. Developing accurate models of the human airways. *J. Pharm. Pharmacol.* **67**, 464–472 (2015).

233. Starkey, M. *et al.* Identification of Anti-virulence Compounds That Disrupt Quorum-Sensing Regulated Acute and Persistent Pathogenicity. *PLoS Pathog.* **10**, (2014).

VIII. Scientific Output

Research papers

- MONTEFUSCO-PEREIRA CV, Horstmann J, Ebensen T, Beisswenger C, Bals R, Guzmán CA, Schneider-Daum N, Carvalho-Wodarz C, Lehr CM. 3D air-liquid interface culture of Cystic Fibrosis bronchial epithelia, macrophages and *P. aeruginosa* for preclinical evaluation of inhaled antibiotics. In review to the Journal of Visualized Experiments.

- MONTEFUSCO-PEREIRA CV, Formicola B, Goes A, Re F, Marrano CA, Mantegazza F, Carvalho-Wodarz C, Fuhrmann G, Caneva E, Nicotra F, Lehr CM, Russo L. Surface-functionalized quaternary ammonium surfactants onto a new biocompatible liposomal formulation as a proposal against bacterial adherence and biofilm treatment. In review to European Journal of Biopharmaceutics.

- LABABIDI N, Montefusco-Pereira CV, Carvalho-Wodacz C, Lehr CM; Schneider M. Multifunctional inhalable microparticles combining antibiotics and a mucolytic with anti-inflammatory drug-loaded PLGA nanoparticles. Submitted to Journal of Controlled Release.

- FORMICOLA B, Dal Magro R, Montefusco-Pereira C, Lehr CM, Koch M, Russo L, Grasso G, Deriu MA, Danani A, Bourdoulous S, Re F. The synergistic efect of chlorotoxin-mApoE in boosting drug-loaded liposomes across the BBB. J Nanobiotechnol 17, 115 (2019) doi:10.1186/s12951-019-0546-3.

Oral presentations

- 3D in vitro model suitable for drug preclinical screening on the infected upper airways. NABBA meeting and 12th International Conference and Workshop on Biological Barriers, Saarbrucken, Germany, August 27-29 2018.

- Establishment of a 3D in vitro model of infected airways for the application of functional nanoparticles. NABBA 2nd Scientific & training meeting and summer school. Erice (Sicily), Centre of Scientific Culture Ettore Majorana, Italy, June 6-8 2016.

- Development of a 3D in vitro model of infected airways for the application of functional nanoparticles. NABBA ITN 1st Scientific & training meeting. Gif-sur-Yvette,CNRS castle, France, 25-27 November 2015.

Poster presentations

- *P. aeruginosa*-infected co-culture of human cystic fibrosis bronchial epithelial cells as a pre-clinical test system for anti-infectives. HIPS Symposium 2019, Saarbrucken, Germany.

- Monitoring the link inflammation/infection with a *P. aeruginosa*-infected co-culture of human cystic fibrosis bronchial epithelial cells and macrophages. 18th Scientific Meeting of the German Mukoviszidose Association. Bad Salzschlirf, 26-27 September 2018.

- 3D in vitro model of the cystic fibrosis infected upper airways: host-pathogen interaction, drug efficacy and inflammation. 12th International Conference and Workshop on Biological Barriers, Saarbrucken, Germany.

- Cystic fibrosis human bronchial epithelia combined with macrophages to evaluate host-pathogen response to *P. aeruginosa* infection. EMBL Symposium on Innate Immunity in Host-Pathogen Interactions, EMBL Heidelberg, Germany, 24 - 27 June 2018.

- Co-culture of cystic fibrosis human bronchial epithelia and macrophages to evaluate host-responses and efficacy of anti-infective formulations on *P. aeruginosa* infection. XII Spanish-Portuguese Conference on Controlled Drug Delivery: Tailoring drug delivery systems to the patients' needs. Coimbra, 14-16 January 2018.

- Cationic amino liposomes as proposal for broad spectrum formulation against bacteria adherence and biofilm treatment. BtBsDay 2017, Giornata del Dipartimento di Biotecnologie e Bioscienze – UNIMIB. Milan, 17th of December, 2017.

- Testing drug delivery systems and macrophage behavior on *P. aeruginosa*-infected cystic fibrosis human bronchial epithelia. HIPS Symposium 2017, Saarbrucken, Germany.

- Growth of *P. aeruginosa* on a 3D Model of Cystic Fibrosis Bronchial Epithelia and Macrophages. COMPACT consortium meeting, 2017, Saarbrucken, Germany.

IX. Curriculum Vitae

Personal information

Name: Carlos Victor Montefusco Pereira

Born: August 16, 1986 (Manaus/Brazil)

Address: Mainzer Str., 25, 1st floor. Saarbrücken, Germany

Email: cmontefusco@gmail.com

Education

2015 – 2020   **PhD Biopharmacy and Pharmaceutical Technology**. Saarland University, Saarbrücken, Germany.

2012 – 2014   **M.Sc. Forensic Sciences**. University of Lincoln, United Kingdom.

2005 – 2010   **B.Sc. Pharmacy and Biochemistry**. Universidade Paulista, Brazil.

Work Experience

09/2015 – 2019   **Researcher on Pharmaceutical Technology**. Helmholtz Institute for Pharmaceutical Research in Saarland (HIPS)

05/2018 – 06/2018   **Fellow on Cell and Molecular Biology**. Biotalentum Ltd (Hungary)

09/2017 – 01/2018   **Fellow on Nanotechnology and Organic Chemistry**. University of Milano-Bicocca

01/2015 – 07/2015   **Clinical Researcher on Fetal Medicine**. Maternitat del Hospital Clinic de Barcelona

08-12/2014   **External Consultant and Pharmacist Intern**. World Health Organization – Headquarters Geneva

03-06/2012   **Pharmacist**. Carrefour Group, Manaus, Brazil:

2007 - 2012   **Researcher on Drug Discovery**. Amazonas Federal University, Brazil

2006 - 2012   **Health Assistant**. Manaus Health City Office, SEMSA/MANAUS, Brazil

X. Acknowledgments